UNIVERSITÀ DEGLI STUDI DI PADOVA
DIPARTIMENTO DI INGEGNERIA CIVILE, EDILE E AMBIENTALE
Department Of Civil, Environmental and Architectural Engineering

Corso di Laurea Magistrale in Environmental Engineering

TESI DI LAUREA

ASSESSMENT OF THE AMMONIA NITROGEN REMOVAL EFFICIENCY FROM THE LIQUID FRACTION OF OFMSW DIGESTATE INTO A STRIPPING-ABSORPTION COMBINED PILOT PLANT

Supervisor:
PROF. ELENA BARBERA
Co-supervisor:
OMAR GATTO

Student: EDOARDO FRISON
2040625

ACADEMIC YEAR 2023-2024

Table Of Contents

Lists of Figure

Lists of Tables

Lists of Acronyms and Abbreviations

AD: Anaerobic Digestion
AR: Aspect Ratio
BAT: Best Available Techniques
Bcm: Billion Cubic Metres
BOD: Biological Oxygen Demand
CHP: Combined Heat and Power
COD: Chemical Oxygen Demand
EU: European Union
GHG: Green House Gases
HETP: height of each equivalent theoretical stage
HRT: Hydraulic Retention Time
IEA: International Energy Agency
NETP: number of equivalent theoretical stages
NF: Nanofiltration
OFMSW: Organic Fraction of Municipal Solid Waste
PP: polypropylene
RO: Reverse Osmosis
RSM: Response Surface Methodology
SS: Suspended solids
TOC: Total Organic Carbon
TS: Total Solids
TSS: Total Suspended Solids
UF: Ultrafiltration
VFA: Volatile Fatty Acids
VS: Volatile Solids
WWTP: Wastewater Treatment Plant

Abstract

The envisaged population growth challenges the entire food production chain, which clings to the need for circular alternatives. The traditional Haber-Bosch industrial process for synthetic ammonia production significantly consumes energy and natural resources, affecting humans and the planet's health. Sewage sludge, food waste, and animal manure represent optimal sustainable substrates for ammonia extraction, paving the way to close-the-loop thinking. This thesis analyses the performances of a pilot plant combining stripping and absorption to assess the achievement of a 70% ammonia removal efficiency threshold, with successful results. Several tests are performed by changing the operating variables, thus evaluating different conditions. The inlet solution of around 50 l/h consists of the liquid fraction retrieved from the OFMSW digestate. The Minitab application provides a statistical interpretation of the experimental data and the definition of the significant variables. Among all, pH and HRT were found to be relevant. The Response Surface Methodology leads to the evaluation of the combined interactions of the factors, highlighting the possible scenarios for the plant up-scaling procedure, validated through the solution of an optimization problem. Finally, the full-scale stripping and absorption reactors are designed based on the future flowrate of 100 m^3/d. Moreover, an evaluation of the heat requirements is reported for the stripping reactor, accounting for the seasonal variability of temperatures. Besides, the scrubber height and diameter design imply the McCabe-Thiele and Eckert graphical methods application, with the determination of the equilibrium and operating lines. Anyway, the outcomes outlined in this thesis should be corroborated by further studies, such as cost-benefit analysis, opening the discussion for future improvements.

Introduction

The population growth envisaged for the next years puts sustainability to the test, especially in the food sector. More intense food cultivations affect soil fertility, consequently asking for nutrient injection through fertilizers. The strongly industrialized world of mineral fertilizers contributes to greenhouse (GHG) emissions, having energy and emissions intensities above the levels of the highly impacting steel and cement sectors. The need to cling to more sustainable solutions hastens the search for alternatives. From the circular economy perspective, waste is considered a valuable resource. Nevertheless, legislative limitations hinder the end-of-waste process of sewage sludge, food waste, and animal manure. Furthermore, farmers still lack the technical and economic knowledge to benefit from such investments. However, researchers are trying to open the way in the field of nutrient recovery from waste and to support the development of innovative technologies. This thesis aims to get into this scenario, assessing the ammonium removal efficiency of a stripping-absorption combined pilot plant to treat liquid digestate. The technological readiness of these technologies makes them suitable to obtain effective results.

Chapter 1 introduces the context of the thesis. The crucial role of mineral fertilizers in food supply is highlighted, focusing on the traditional industrial nitrogen fertilizer production (Haber-Bosch process). The connected environmental impact evaluation shoves the need for more sustainable solutions. Nutrient recovery from waste is outlined as an opportunity to cope with the problem, at the same time valorising the waste from a circular economy perspective. The attention falls on the liquid fraction of digestate, describing the main properties and the technologies for its treatment. Advantages and disadvantages are reported, especially concentrating on the stripping and absorption processes.

Chapter 2 details the pilot plant and all the composing elements. Moreover, the characteristics of the inlet liquid fraction are explored and compared to real values and literature references. The identification of the principal operating variables allows the working strategy and testing conditions definition. Moreover, the analytical methods for the parameters' measurements are reported to ensure the scientific approach.

Chapter 3 reports the results obtained during the testing period. After discussing the laboratory analysis of the inlet solution, the Chapter compares the real *on-field* conditions to the set-point ones, contextualizing the differences. Then, the NH_4 and TN removal efficiencies for each test are

assessed and commented on, starting the analysis of the possible optimum conditions. Furthermore, the Chapter briefly discusses the specific electricity and soda consumption. The second part outlines a statistical model using the experimental dataset, and the goodness of the fitting is evaluated using Minitab. Both the effects of the single variables and their interactions on the removal efficiency are described by displaying the contour plots. Finally, the Chapter presents the solution of the optimization problem to reach the target efficiency of 70%.

Chapter 4 introduces the stripping and absorption reactors design for a large-scale plant, aiming to reach the target removal efficiency of 70%. The first part of the Chapter focuses on the optimum conditions found in Chapter 3 to define the geometrical features and to calculate the liquid and gas flowrates that interact with the plant. Once done, the power requirement is assessed, accounting for the seasonal variability. The second part of the Chapter deals with the scrubber unit design, evaluating the height as well as the diameter of each column.

Chapter 1

STATE OF THE ART

This chapter provides an overview of the framework on which this thesis has been developed. Starting from the importance of fertilizers to face future food demand, the attention falls on the industrial nitrogen fertilizer production (Haber-Bosch process) and the connected environmental impacts. In this context, wastes are presented as an opportunity to replace the current artificial production with more sustainable solutions. Among these, the focus is put on the liquid fraction of digestate, highlighting the main properties and the technologies for its valorisation. Each option is described exhaustively, reporting the main advantages and disadvantages. Moreover, the principal challenges hampering the spread of nutrient recovery technologies are briefly described. Finally, an overview of the EU project at the base of this thesis is depicted.

1.1. The Industrial N-Based Fertilizer Production Process

The demand for new commodities is commonplace in a continuously growing society, threatened by climate changes, economic and geopolitical crises. The ability to satisfy such needs represents one of the main challenges of the century. The United Nations estimates a global population of around 9.7 billion people in 2050 (United Nations, n.d.), with a consequent increase in food requests. One way to cope with that may be the destination of new land for agricultural purposes, with the loss of vegetation and ecosystems as a counter-effect. Moreover, it is reported that the changes in land use cause around 12% of GHGs emissions (Fertilizers Europe, 2018). With this in mind, the best choice becomes a better use of the available land. Indeed, in 1960 two people were fed from each hectare of land, whereas in 2025, the number will rise to five (Fertilizers Europe, 2018).

1.1.1. The Importance of N-based Fertilizers

To ensure crop efficiency, fertilizer application is a crucial complement to the natural processes that break down the organic matter in the soil and the crop residues. Taken singularly, these processes are not enough to ensure high soil fertility. Thus, organic and mineral fertilizers addition is unavoidable. The formers, including plant-derived matter, animal manure, and sludges, improve soil structure by introducing organic carbon and stimulating microbial activity. However, the main limitations are a difficultly-predictable composition and a slow-release rate in the soil. The first

may lead to nutrient losses, whereas the second is linked to the need for nutrients to be mineralized. On the other hand, mineral fertilizers guarantee a clearly-defined amount of nutrients in a way readily available for the plants (International Fertilizer Association, 2023-a). Thus, the widespread practice in agriculture implies the use of both forms.

By now, half of global food production relies on mineral fertilizers (Fertilizers Europe, 2023a), especially on the primary nutrients necessary for plant growth such as nitrogen N, phosphorus P, and potassium K. Considering a 3-year moving average, 9.8 million tons of N, 2.5 million tons of phosphate (P_2O_5), and 2.8 million tons of potash (K_2O) were applied to 123.8 million hectares of farmland in EU in 2019-2021, accounting for 65%, 17%, and 18% of the total, respectively (Fertilizer Europe, 2023b). Other secondary macronutrients and micronutrients are spread on the soil but generally in combination with the primary ones. In synthesis, the majority of the market relies on N-based fertilizers. Their production process evaluation helps highlighting the drawbacks, especially the need for more sustainable alternatives, becoming a helpful resource for industries and policymakers to reshape their strategies toward a greener future.

1.1.2. The Haber-Bosch Process

The core of nitrogen mineral fertilizers is ammonia. Indeed, regardless of the final products, the joint starting point is always the NH_3 synthesis. Ammonia production consists in the exploitation of the Haber-Bosch process, which artificially fixes atmospheric nitrogen to obtain a product with high fertilizing value. It dates back to 1907 and nowadays represents the largest source of synthetic ammonia fertilizer for agriculture (Kar et al., 2022). The first step is nitrogen isolation and hydrogen production to obtain the two main reagents of the ammonia reaction. The nitrogen comes from an air separation unit as the Pressure Swing Adsorption system, whereas pure H_2 derives mainly from steam methane reforming (SMR) or coal gasification. In particular, 72% of the whole ammonia produced in 2020 relied on natural gas steam reforming, 26% on coal gasification, and about 1% on oil products (International Energy Agency, 2021). The steam methane reforming process is endothermic, so CH_4 is used both as feedstock and external energy source. The steam addition leads to the production of syngas, which is a mixture composed of CO and H_2. The mixture enters a water–gas shift (WGS) reactor to maximize CO conversion, producing CO_2 and more H_2. Finally, the CO_2 can be removed through an amine-based or hot potassium carbonate absorption process, as it represents a poison for the subsequent ammonia synthesis catalyst. Once the nitrogen and the hydrogen have been extracted, the following step is their combination at a temperature of 400-500°C and a pressure of 15–25 MPa, with an iron-based catalyst. Equation (1) reports the equilibrium endothermic reaction. Since the single-pass conversion is low, the

unreacted hydrogen is recycled back upon ammonia condensation, thus decreasing the loss of reagents.

$$N_2 + 3H_2 \leftrightarrow 2NH_3 \quad (1)$$

Figure 1.1 shows the mass flow of the ammonia industrial production supply chain. About 70% of ammonia results in fertilisers, while the remainder is used for various industrial applications, such as plastics, explosives, and synthetic fibres. Fossil fuels consumption accounts for 136 Mt on year basis. Aside from natural gas and coal, secondary reactants comprising steam, oxygen, phosphoric and sulphuric acids are used (International Energy Agency, 2021). The nitrogen fertilizers produced in 2019 resulted in 216 Mt. It is worth noting that urea allows the consumption of carbon dioxide, lowering the carbon footprint of the process. However, urea is the N-based fertilizer with the highest ammonia emissions once spread on the soil (Fertilizer Europe, 2019).

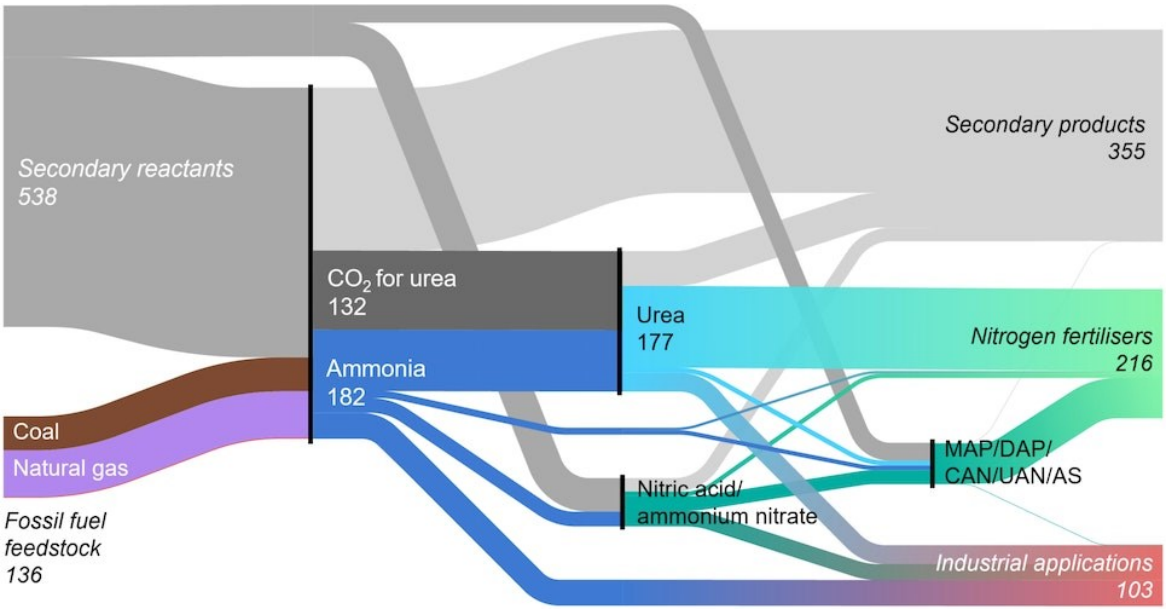

Figure 1.1: Mass flows in the ammonia supply chain: from fossil fuel feedstocks to nitrogen fertilizers and industrial products. Data based on the 2019 (International Energy Agency, 2021)

1.1.3. The Environmental Problem of Fossil-Based Ammonia

The ammonia production process is highly energy-intensive, accounting for 8.6 EJ on a yearly basis, 2% of the global energy consumption (International Fertilizer Association, 2023-b). The derived annual CO_2 amounts to 450 Mt per year, 1.3% of global energy sector emissions. To visualize this number, it is equivalent to the total energy emissions of South Africa, the 16th largest emitter in the world (International Energy Agency, 2021). However, this value is not encompassing as it states only the direct emissions. The IEA reports that when the indirect ones are included, a further 170 Mt CO_2 arises, mainly due to the energy generation and the emissions derived from

the fertilizer application on the soil. Figure 1.2 compares in specific terms the energy and emissions intensities of the ammonia process with steel and cement, highly environmentally impacting industries. The intriguing data is that ammonia production shows the highest value for both indicators, with an energy intensity of 46.2 GJ/t on a gross basis and a direct emission intensity of 2.4 t_{CO2}/t. The reason is that the steel and cement industries impact more as a whole, but when dealing with specific quantities, the environmental footprint decreases due to their production in far higher volumes. In the literature, studies report similar values to those presented in this paragraph, confirming the environmental effects caused by the ammonia production process.

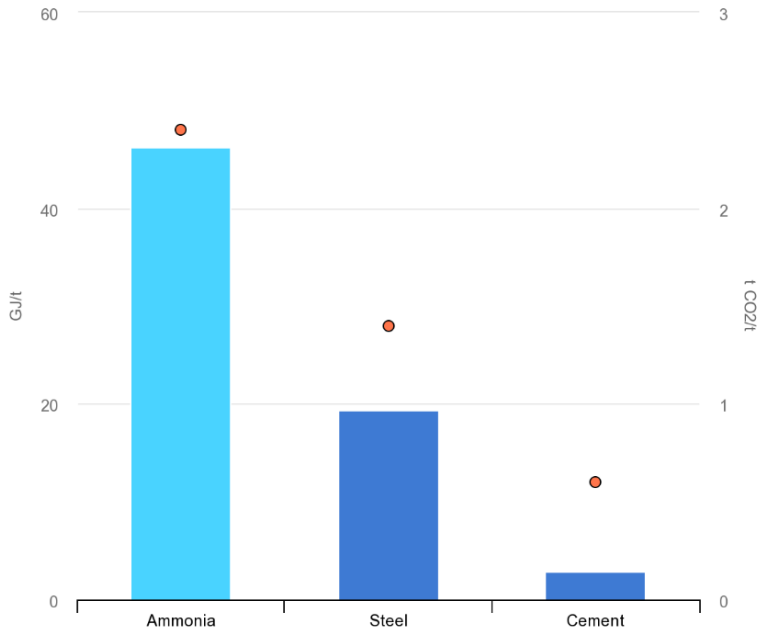

Figure 1.2: Energy intensity (bars) and emissions intensity (dots) for industrial ammonia, steel, and cement in 2021. The energy is expressed on a gross basis (i.e., excluding the energy of by-products), and the emissions refer only to direct ones (International Energy Agency, 2021)

The main current problem related to ammonia production is the strong dependency on fossil fuels. As said, natural gas covers over 70% of the ammonia production, with 170 bcm consumption representing 20% of industrial natural gas demand. Yang et al. (2022) describes a specific methane consumption of 0.6 $kg/kg_{NH3\text{-}N}$ in the Haber-Bosch process, which represents 3% to 5% of the global request. The situation in the EU is critical since natural gas is highly imported. The war between Ukraine and Russia witnessed the resources vulnerability of European countries, and Italy specifically, emphasizing the importance of self-reliance. The need for sustainable alternatives is also vital to cope with the increasing ammonia demand and the claim of environmental protection. These aspects lead to looking around and investigating innovative solutions.

The output obtained at the end of the Haber-Bosch process is defined as "grey ammonia" to recall the strong connection with fossil fuels. The first step towards near-zero-emission production is "blue ammonia", based on the same conventional process but integrated with carbon capture and storage systems (CSS). These latter require additional energy without decreasing the process emission intensity. Moreover, the CO_2 has to be transported through pipelines or ships to the sequestration basin, thus increasing costs. The operation's efficient result depends on many factors that make the real-scale implementation still slow. Besides, in a long-term perspective, the feasibility of storing becomes challenging due to the continuous need for new available sites. On the other hand, CO_2 utilization can help achieve a higher sustainability level. It is already happening in urea production, with the side-effect of high ammonia emissions when spread on soils. Carbon dioxide conversion to methane may represent an excellent path to reduce the consumption of raw natural gas, but not currently feasible since more hydrogen must be available as input for this process.

Another development direction is “green ammonia”, which involves renewable energy sources to generate hydrogen via water electrolysis. This perspective is the most attractive alternative to fossil fuels, with a saving of more than 60% of the natural gas inputs, corresponding to the feedstock of the steam methane reforming process. Moreover, energy requirements for ammonia synthesis could be completely fulfilled by renewables. Indeed, the request of energy for ammonia production is reported to be roughly 2,330 TWh yearly, completely covered by around 4,300 TWh from hydropower, 2,100 TWh from wind, and 1,300 TWh from solar energy in 2022 (Our World in Data, 2023). Obviously, the production from renewables cannot be destinated only to electrify the ammonia synthesis, but it is just to prove that efforts in this direction may be valuable. However, the main limitation is the use of water instead of methane for hydrogen production, which restrains the application in regions subjected to water scarcity.

1.2. A Resource from Waste: The Digestate

1.2.1. The Waste Opportunity in a Circular Economy Perspective

The presented scenario discussed ammonia production starting from raw inputs. However, the enthralling challenge of the circular economy is the ability to close the loop, transforming waste into new opportunities. The consequent beneficial effects for the environment lay on saved impacts from both avoided input extraction and emissions containment. The population increase will ensure continuous waste production from sewage, cattle manure, and food waste sectors. These represent the primary promising substrates for nutrient recovery to satisfy the increasing agricultural and food demand. In particular, Barreiro-Vescovo et al. (2020) reported a global

envisaged OFMSW production of 0.9-1.6 billion tons up to 2025. Currently, the lacking recovery of valuable nutrients from waste in Europe accounts for 2-5 Mt of N and around 0.6 Mt of P (RISE Foundation, 2016), roughly 20-50% and 43% of the mineral nitrogen and phosphorus applied to EU crops.

In the case of WWTP more or less 30% of the 118 Mt_N/y, which represents the 2020 global N-fertilizer production, ends up in sewage treatment plants. Of these, 60-65% are dissipated into the atmosphere during the treatments (Munasinghe-Arachchige & Nirmalakhandan, 2020). The production of WWTP sludge in the EU27 ranged around 10 Mt, containing 2.3-3.1 Mt of N and 0.3 Mt P. The sludge has several fates, such as its reuse in agriculture. Indeed, nearly half of it was applied on land directly or after composting in 2013 (RISE Foundation, 2016). However, governments have shown increasing attention to direct land application through the years to decrease phenomenon as overloading or environmental losses. Examples such as the European Nitrates Directive (91/676/EEC) and the European Farm-To-Fork strategy limit nitrogen addition to soils at a maximum of 170 kg/(ha*y) (EUR-Lex, 2023) and aim at least to halve the nutrient losses (European Commission, 2020), respectively.

1.2.2. The Anaerobic Digestion Process

The choice of anaerobic digestion as treatment method for WWTP sludge is a rewarding bio-based option for two main reasons: energy production and possible recovery of the outlet streams. It can be applied to raw organic substrates, such as manure and food waste, and even to sewage sludge. The inlet organic material to AD is degraded in an oxygen-free environment, producing biogas and digestate. The four steps of anaerobic digestion result in a gas composed mainly of CH_4 and CO_2, which can be upgraded to biomethane and used to partially fulfil the energy need of the plant or the digestor. The degradation of most of the volatile fatty acids (VFAs) leads to a pH increase, whereas the organic nitrogen is converted to ammonium, increasing the potential as a fertilizer. Studies report a 70% conversion of organic nitrogen to free ammonia (NH_3) and ammonium (NH_4^+) during hydrolysis (Yang et al., 2022; Shi et al., 2018). Finally, during thermophilic AD pathogens are killed, ensuring the safety of the derived digestate. All the presented reasons drive the diffusion of anaerobic digestion as a sustainable technology from both an energetic and nutrient perspective. Barampouti et al. (2020) reported 17,783 European installations in 2017, with a related installed electric capacity of 10,532 MWe. Specifically, 70% of total EU biogas plants were fed with agricultural substrates as plant residues and manure, leading to 6,631 MWe.

1.2.3. The Digestate Composition

The digestate composition changes depending on the substrate and the type of anaerobic digestion process. In these terms, a clear definition is a challenging task. Table 1.1 aims to summarize the parameters and their values. The main digestate composition is water, slowly- or non-biodegradable organic matter, and most micro and macronutrients. Heavy metals, trace metals, and antibiotics (especially in manure) are also present but in limited quantities. Besides, digestate shows high alkalinity and TKN values, whereas the biodegradation potential is limited. The direct application on land is well-established even if new pathways are becoming more convenient due to the increasingly more stringent regulations and the ongoing development of alternatives. As said, the digestate composition is fluctuating, with a concrete risk of nutrient overloading in the environment, especially in the most sensible areas, with consequences such as eutrophication phenomena or soil quality alteration. Furthermore, the digestate contains considerable amounts of water, implying higher costs for transportation as such. This latter can be difficulty avoided since the high volumes produced generally overcome the need of the area surrounding the plant. Facing these problems, digestate treatment can be seen as a beneficial method to close the loop with a more sustainable approach.

Table 1.1: Digestate composition: reference parameters and values

Parameter	Value	Reference
Dry weight (% on fresh weight)	8.70	Vaneeckhaute et al., 2016
	11.00 ± 1.00	Vaneeckhaute et al., 2013
Organic matter (% on fresh weight)	5.30	Vaneeckhaute et al., 2016
pH	8.10-8.60	Vaneeckhaute et al., 2016
	7.50 ± 0.60	Vaneeckhaute et al., 2013
Total N (% on fresh weight)	0.17-0.75	Vaneeckhaute et al., 2016
NH_4^+-N (g/l)	0.80-5.00	Shi et al., 2018
C:N-ratio	6.58	Vaneeckhaute et al., 2016
Total P (as P_2O_5, % on fresh weight)	0.14-0.65	Vaneeckhaute et al., 2016
Total K (as K_2O, % on fresh weight)	0.20-0.50	Vaneeckhaute et al., 2016

1.2.4. The Separation of the Liquid-Solid Fractions of Digestate

Separating a solid and a liquid fraction from the raw digestate is the first step after AD to create two streams with valuable potential. Sludge dewatering is a widespread practice in WWTP, performed through different technologies. The choice of the strategy is shaped by the local and

economic conditions of the user, with the preference for well-developed and easily applicable machinery. The main categories for fractions separation are physical, chemical, and thermal. Among the physical examples found in full-scale applications, screw presses, centrifuges, and belt presses are the most used. Barampouti et al. (2020) highlight the convenience of a screw press over a centrifuge, with a cost (capital and operational) of 0.54 €/$m^3_{digestate}$ and 3.68€/$m^3_{digestate}$, respectively. Flocculation is a typical case of chemical application, whereas dryers represent a thermal route especially suitable when well-dried solids are required.

Needless to say, the concentration of the components in the two fractions hinges on the technology used. However, some features can be highlighted. The solid fraction contains the recalcitrant organic matter and the nutrients that are bounded, such as organic N and P. This fraction encloses a large part of the phosphorus, with values around 40-90% of the total P, while just 20–25% of the N. Furthermore, the percentage of TS ranges around 20-25% (Barampouti et al., 2020). On the other hand, soluble nutrients and mineral salts accumulate in the liquid fraction. Here most of N and K can be found, especially ammonia. According to Vaneeckhaute et al. (2013), the N/P/K mass ratio accounts for 0.77/1/0.36 and 13/1/11 for the solid and liquid fractions, strengthening the concept explained. Instead, Peng & Pivato (2017) reports N/P/K ratios of 1.7/1.0/0.8 and 26.0/1.0/4.5 for the solid and the liquid fractions of OFMSW. Table 1.2 summarizes the values of the principal parameters found in literature. Since these streams are derived from the whole digestate, even in this case, the values can vary depending on the source and the treatment.

Table 1.2: Reference parameters and values of the solid and liquid fractions of the digestate

Parameter	Solid Fraction Value	Liquid Fraction Value	Reference
Dry weight	19.30-24.70	3.30-6.60	Barampouti et al., 2020
(% on fresh weight)	23.00 ± 1.00	2.50 ± 0.10	Vaneeckhaute et al., 2013
pH	7.70-8.50	7.80-7.90	Barampouti et al., 2020
	8.80 ± 0.00	8.34-8.80	Peng & Pivato, 2017
Total C (% dry matter)	9.00-10.1	2.64-3.15	Barampouti et al., 2020
Total N (% dry matter)	1.09	13.85	Peng & Pivato, 2017
NH_4^+ (% Total N)	26-50	40-80	Barampouti et al., 2020
Total P_2O_5 (% dry matter)	1.49	1.22	Peng & Pivato, 2017
Total K_2O (% dry matter)	0.78	3.64	Peng & Pivato, 2017

1.2.5. The Fate of the Different Fractions

Once separated, each fraction is managed to exploit its value. The dewatering process concentrates the solid fraction making the transportation easier than before, ready to be further treated. Composting is recommended if the solid fraction is targeted as fertilizer, with the side-effect of possible emissions during the process. Pelletizing might be a valuable market strategy, producing pellets with calorific values similar to softwood. In this case, moisture removal through tools such as belt dryers, mechanical drum dryers, or solar dryers becomes fundamental, with again the consequent risk of emissions into the environment. Another valorisation strategy is thermal treatment, such as pyrolysis, gasification, or hydrothermal carbonization. The obtained char stands as a promising advanced bio-based material used as fertilizer due to its high P content and nutrient slow release. Moreover, its high adsorption capacity does not exclude applications as nutrient adsorbent material (Barampouti et al., 2020; Sobhi et al., 2021). Finally, incineration represents another path for phosphorus recovery, but this approach is not at the top of the sustainability hierarchy.

Up to now, the solid fraction has always had the spotlight. However, the liquid fraction provides a valuable source of nutrients likewise. Generally, the liquid stream generated after the digestate dewatering is recycled back to the digestor or treated. In the specific case of WWTPs, the stream is sent to the plant headworks, thus increasing the inlet ammonia load. Kar et al. (2022) quantified this contribution to an additional 15-20% with respect to the feed stream of American WWTPs. This ammonia flow partially undergoes nitrification and denitrification, ending with an atmospheric release, consequently wasting its nutrient value. The liquid fraction could be even spread directly on soils, but the high water and low organic content decrease the market potential. To bring out the hidden potential by exploiting the nitrogen and the other nutrients present, the fraction requires further treatments. The interest in nutrient recovery to face the growing demand in agriculture pushes researchers to develop new innovative technologies that will be described in detail in the following section, enhancing the main pros and cons.

1.3. Technologies for ammonia recovery from liquid digestate

As said, the liquid fraction obtained after digestate dewatering is rich in ammonia, around 3.5 g_{NH3-N}/l as reported by Peng & Pivato (2017). The extraction of this nutrient must not rely on a single technology but rather be a function of the input conditions and the final target. Besides, the desired recovery efficiency, energy needs, and chemical consumption may influence the ending ranking of the options. The decision should pursue cost-effectiveness, simplicity, and, most importantly, create a product with a market value. Among the various physical, chemical, and biological

technologies, the most developed and recommended are ammonia stripping and struvite precipitation. Indeed, Vaneeckhaute et al. (2016) indicate them as Best Available Techniques (BAT) in the sector. Full-scale ammonia stripping plants operate in the U.S.A. and Europe, while struvite precipitation has been well demonstrated at pilot scale and in a few full-scale cases (Munasinghe-Arachchige & Nirmalakhandan, 2020). Furthermore, membranes, adsorption, and dryers represent emerging alternatives. The use of microalgae is more meant as a treatment, but novel studies are trying to increase the final value of the produced biomass in the pharmaceutical sectors or as biofuels (Chandrasekhar et al., 2021). Assessing the best technology is essential to strengthening the final choice, valorising the investment, and maximising the nutrient recovery.

1.3.1. Ammonia Stripping and Absorption

1.3.1.1. Ammonia Stripping Overview

Stripping is a physicochemical process based on the direct vaporization of components in a liquid phase when contacted with a gas. The mass transfer follows Fick's law, and the liquid mass transfer coefficient is generally the most influent on the final ammonia vaporization (Yang et al., 2022). Thus, generally tests and software help to get the values of the coefficients. The most widely applied configurations are packed tower and air bubble reactor, as presented in Figure 1.3. The former is generally run in counter-current mode to enhance the driving force represented by the difference of the species concentration in the phases with their equilibrium state. Inside the column, the liquid is sprayed from the top, flowing downwards due to gravity. Oppositely, the gas enters from the bottom, moving upward. This configuration ensures higher contact time between the phases, but fouling problems imply only low %SS feed solutions or cleaning cycles to remove the trapped particles. On the contrary, air bubble aeration involves a stationary liquid phase and continuous bubble aeration through the reactor. This treatment allows feed streams with SS up to 5%, limiting the risk of fouling (Baldi et al., 2018). However, foaming production is a counter-effect since the air is sparged through fine/medium diffusers.

In both cases, the ammonia-poor liquid outlet can be sent back to the headworks, whereas the gas exiting stream can flow towards other treatment units. Further configurations, such as water-sparged aerocyclone, rotating packed bed, and vacuum thermal stripping, seek to increase mass transfer. However, they are still under development and have never been tested at full scale.

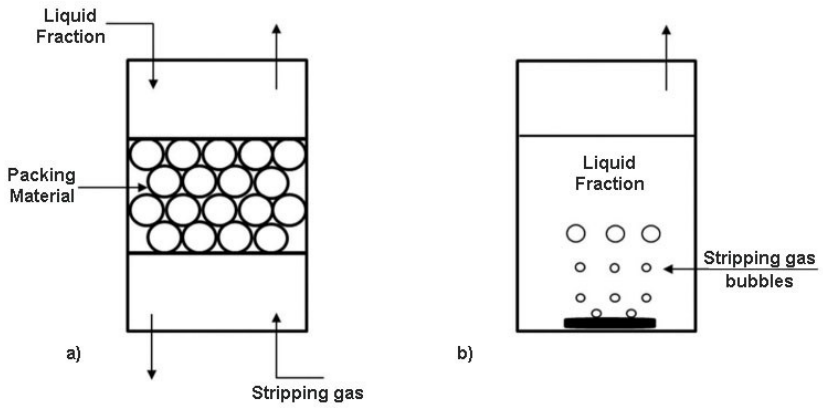

Figure 1.3: Typical stripping tower configurations: packed tower (a) and air bubble reactor (b) (Palakodeti et al., 2021)

It is worth noting that ammonia stripping is a versatile technology because applications to the whole digestate or raw waste are not excluded. Indeed, since AD is a biological process, an ammonia input overload may inhibit microbial activity. Thus, a decrease in the ammonia concentration becomes fundamental in this case. If this is done before the digestor, the process is called pre-AD stripping, whilst *in-situ* stripping results when performed inside the digestor using biogas as the stripping gas stream. However, these options are only convenient when inhibition may take place. The conventional stripping process, called post-AD stripping, ensued as the most flexible and efficient option, as the parameters inside the tower can be optimized regardless of the AD process conditions.

1.3.1.2. The Influence of the Process Parameters

Evaluating the process parameters is extremely important to maximize the final recovery efficiency. Below is a list of the most influent ones, together with the effects on the whole result.

a) pH

This parameter is considered the most affecting on the final removal efficiency. The equilibrium reaction between ammonia and ammonium ion in solution is reported in Equation (2) and strongly depends on the pH value. The higher the pH, the more the equilibrium shifts towards the left, producing free ammonia that tends to pass to the gaseous phase. Thus, high pH values have a beneficial effect on the removal efficiency. The pH increment is obtained through chemical addition before the stripping unit, particularly by sodium hydroxide NaOH.

$$NH_3 + H_2O \leftrightarrow NH_4^+ + OH^- \quad (2)$$

However, an optimal pH limit is outlined when considering the equilibrium graphical representation. As shown in Figure 1.4, for pH values higher than 10.5, the NH_3 percentage in the

liquid remains unchanged, only causing the use of more bases, increasing both costs and risk of scaling. Therefore, the NaOH dosage is restricted only to raise the pH of the liquid fraction from the initial value of 7.5-8 up to 10-10.5. It is important to note that novel approaches work without alkali addition, simply stripping the CO_2 into a column before the ammonia removal reactor. The idea is clearly shown in Equations 3 and 4, where CO_2 stripping induces the consumption of protons, with a consequent pH growth. This step minimizes the formation of carbonic sediments in the following stages. Moreover, the CO_2 volatilization tendency is about one thousand times the NH_3 one (Boehler et al., 2014), witnessing the valuable prospect of this approach to physically increase the pH without chemicals. Finally, in both cases, the NH_3 stripping leads to a pH decrease because of OH^- consumption.

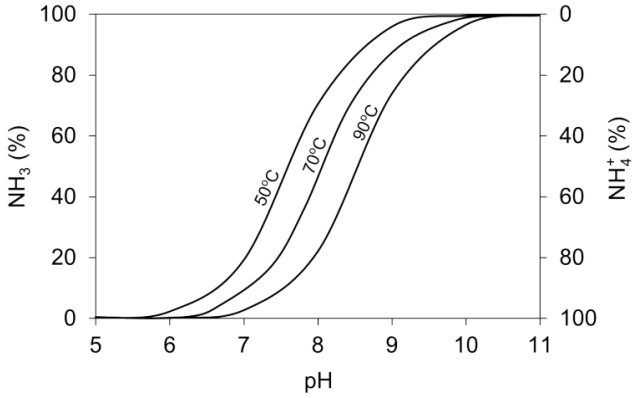

Figure 1.4: Effects of pH and temperature on the equilibrium of ammonia and ammonium ions (Jamaludin et al., 2018)

$$CO_2 + H_2O \leftrightarrow H_2CO_3 \leftrightarrow HCO_3^- + H^+ \quad (3)$$

$$HCO_3^- \leftrightarrow CO_3^{2-} + H^+ \quad (4)$$

b) Temperature

Temperature represents the second leading parameter after pH. An increase significantly improves the mass transfer coefficient and the driving force, reducing the surface tension and the pH needed for the removal. Provolo et al. (2017) reported the growth of the mass transfer coefficient by 7.25 times when the T passed from 20°C to 70°C. High working temperatures boost the removal efficiency but also the heat requirements. Thus, the smartest solution to contain the emissions generation is coupling the stripping tower with the heat generated by the AD process. Moreover, the need for heat supply is also limited by the high starting T of the liquid fraction. In conclusion, the best operating temperature ranges from the literature between 40-70 °C, with Barampouti et al. (2020) reporting that above 80°C ammonia can be fully recovered independently of pH.

c) Other parameters

Among the other parameters, the NH_4^+ concentration in the liquid fraction plays a significant role. The stripping input conditions inevitably influence the final removal efficiency, with higher values associated with higher ammonia input concentrations. Another contributing parameter is the air flowrate. High values stimulate the mass transfer and the ammonia removal, decreasing the resistance and the partial pressure. Nevertheless, excessive values produce foams, water evaporation, and temperature reduction, chiefly in air bubble reactors (Barampouti et al., 2020). Concerning the liquid, high flowrates lead to HRT reduction, dropping the overall efficiency. Hence, Provolo et al. (2017) claimed recommended volumetric gas-to-liquid flow ratios of 600-700:1 in industrial plants. Finally, other factors affecting the final process result in air bubble reactor applications are bubble size as well as liquid depth. Indeed, larger bubble diameters limit the air-liquid interface, thus decreasing the available surface for the transfer, and excessive depths lead to null or negative driving forces at the top with consequent worthless costs (Zhao et al., 2015).

1.3.1.3. Ammonia Absorption Overview

Absorption is the opposite process of stripping, simulating a direct condensation of components present in a gaseous phase contacted with a liquid phase. Even here, the mass transfer follows Fick's law. Besides the packed tower configuration typical of stripping, tray columns are also implemented in real applications, as shown in Figure 1.5. In the counter-current process, the gas enters from the bottom and flows upward, contacted with a liquid solution sprayed from the top of the reactor.

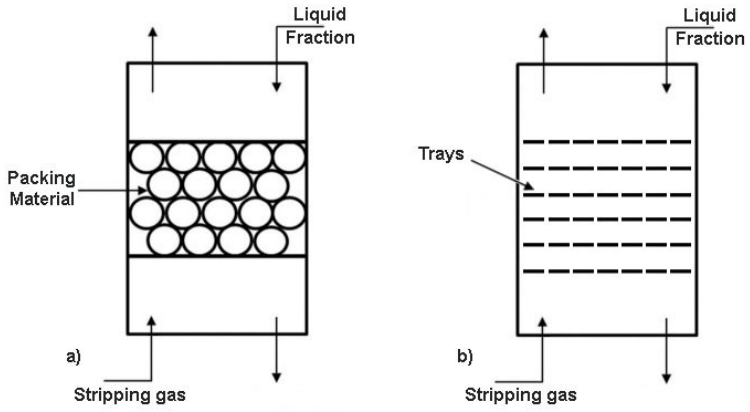

Figure 1.5: Typical scrubber configurations: packed tower (a) and tray column (b) (Adapted from Palakodeti et al., 2021)

The absorption process after stripping aims to form a valuable final product. The transfer efficiency depends on the solubility of the components in the liquid phase, which is enhanced by low T. Concerning ammonia equilibrium (Equation (2)), the soluble form is ammonium, favoured by low pH conditions. Typically, pH is around 4.5 (Boehler et al., 2014). To meet these requirements, an acidic solution is generally used as a scrubbing liquid. Sulphuric acid solutions are broadly diffused for that scope, with the consequent formation of ammonium sulphate after water dissociation, as stated in Equation (5).

$$2NH_4^+ + SO_4^{2-} \leftrightarrow (NH_4)_2SO_4 \quad (5)$$

Once purified, the gaseous stream can be sent back to the stripping column. On the other hand, the liquid is generally recycled again in the scrubber until it reaches an ammonium sulphate concentration of around 25-35%, below 40% to avoid salt crystallization (Kar et al., 2022). The outlet solution contains roughly 8% N and 8% S (Boehler et al., 2014; Baldi et al., 2018) and it may have beneficial effects as fertilizer, especially in S-lacking soils. The alternative use of nitric acid would produce a N-richer final output. However, the high ammonia feed needed for its production recalls all the environmental problems already presented, questioning the final sustainability of the process.

1.3.1.4. Pros and Cons of Stripping and Absorption

The reasons that make such technologies attractive are:

- The specificity in N removal, leaving the other nutrients mainly in the liquid fraction with the possibility of further implementation of other nutrient recovery technologies.
- The process's simplicity, capable of ensuring N removal efficiencies up to 98%.
- The ability and flexibility to work with different substrates, such as the liquid fraction of digestate or the whole digestate, derived from both manure, food waste, and sewage sludge.
- The technological maturity: in the USA 9-10 full-scale plants strip ammonia from digestate, whereas Germany counts 15 stripping plants (Shi et al., 2018).
- The contained emissions: 0.2-0.5 $kg_{CO2eq}/kg_{(NH4)2SO4}$ at 35%w/w, six times lower than the hydrocarbon-based Haber-Bosch process (Kar et al., 2022).

However, some limitations still persist:

- The low NH_3 volatilization implies medium energy consumption for the heat provisions and chemical requirement for pH adjustment.
- The need for liquid fraction separation equipment, increasing costs.

- The high specificity: since only ammonia can be removed, with low NH_3 feeds the efficiency may decrease.
- The risk of fouling, especially for packed columns, foaming, and scaling. The solution is a pretreatment improvement and a softening process with CaO (Vaneeckhaute et al., 2016).
- The risk of corrosion at low pH, and possible high salt content in the final solution. This latter may alter the soil salinity, lowering the crop efficiency, especially when NaOH is used to increase the pH (Barampouti et al., 2020).
- The solution with the ammonium sulphate has a lower N content than artificially produced fertilizers, 8% vs 20% (Bolzonella et al., 2017). Thus, the market penetration is still limited.

1.3.2. Struvite Precipitation

Struvite precipitation represents an alternative technology applicable to the alkaline liquid fraction of digestate. Even if full-scale installations are scarcer, some are reported treating wastewater-digested sludge. The most frequently used reactor configurations are fluidized bed and air-agitated reactors (Vaneeckhaute et al., 2016). The inlet solution is generally added in magnesium to increase its presence in traces (Barampouti et al., 2020). Indeed, the introduction of MgO, MgOH, $MgCl_2$, and $MgSO_4$ ensures the proper balance between the components, as expressed in Equation (6). N/P and Mg/P ratios above 3/1 and 1/1 are suggested (Shi et al., 2018). As a product, struvite precipitates as crystals, which can be dried to form a slow-release granular fertilizer.

$$Mg^{2+} + HPO_4^{2-} + NH_4^+ + 6H_2O \leftrightarrow MgNH_4PO_4 \cdot 6H_2O \downarrow + H^+ \quad (6)$$

The main influencing parameters are pH and ion concentration (Yang et al., 2022). The pH rise to optimal values of 8.5-9.5 can be done at ambient temperature through the NaOH addition, increasing the chemicals consumption, or by previous CO_2 stripping. In this last case, $CaCO_3$ sedimentation is prevented. The presence of calcium can pose a problem, competing with the magnesium and ammonia present. The recommended Mg/Ca ratio is above 2.25 (Shi et al., 2018). With higher Ca^{2+} concentrations, calcium phosphate recovery becomes more attractive. Indeed, calcium hydroxide ($Ca(OH)_2$) addition, coupled with a T of 70°C, invokes a pH rise over 10. The result is a fast precipitation (5 min) of phosphorus as hydroxyapatite ($Ca_5(PO_4)_3OH$) or brushite ($CaHPO_4 \cdot 2H_2O$). Finally, K struvite can be produced, particularly when potassium concentration exceeds the respective of ammonium (Barampouti et al., 2020).

The main advantages of this technologies can be summarized as:

- The slow-release nutrient capacity when applied to soils, limiting the nutrient overload.
- The low operational costs (Shi et al., 2018).

- The possibility to work at ambient T without a heat supply.

Unfortunately, struvite precipitation has still to face some problems:

- It is mainly suggested for phosphorus recovery. Vaneeckhaute et al. (2016) claimed removal efficiencies of up to 80-90% for the soluble P and only 10-40% for NH_4^+-N. The components in the struvite reaction are equimolar, and the stoichiometric N accounts for just 5.7%. Moreover, the nitrogen removal is a function of the phosphorus and magnesium compositions. Thus, struvite precipitation must be combined with other technologies to obtain high N recovery levels.
- It requires chemical consumption to raise the pH and ensure the correct Mg composition. In addition, since H^+ is produced during struvite formation, pH has to be kept in this optimal range by continuous alkali addition. As a support, Barampouti et al. (2020) stated that the contribution of chemicals may reach 75% of the production cost.
- Pretreatment is needed to limit ions interference and SS. Moreover, struvite may precipitate in pipes and equipment, increasing the maintenance costs (Hidalgo et al., 2015).

1.3.3. Membranes Treatment

The first thought concerning the membrane goal is the purification of water solutions rather than nutrient recovery, as proved by the well-developed installations for industrial wastewater treatment. However, the growing interest in the circular economy is triggering research on membranes for a new role in nutrient valorisation. Once the liquid fraction has been separated, the pre-treatment aims to retain the SS, reducing subsequent clogging. Horizontal centrifuges after polymer addition ensure a solution with SS lower than 2% (Bolzonella et al., 2017).

Considering pressure-driven membranes, ultrafiltration (UF) is generally implemented as a further liquid-solid separation, after which nanofiltration (NF) or reverse osmosis (RO) retains NH_4^+ and PO_4^{3-}, generating a clean output and a nutrient-rich stream. The permeate can be discharged into water courses or used for AD, whereas the retentate has a high fertilizer potential. Here, the nitrogen concentration reaches 7-10 g/l with RO, with a retention efficiency of up to 99-99.8% (Shi et al., 2018). The process is performed at ambient T and neutral pH, with increasing pressure required as the size of the pores decreases. A different mention goes to membrane distillation, which requires a heat supply to vaporize the ammonia in the liquid fraction. In addition to the high pH (>9.7), this condition (>45°C) shoves the NH_3 transfer to the gas phase that passes through a hydrophobic gas-permeable membrane. Shi et al. (2018) reported NH_4^+-N concentrations in the permeate up to 18.3 g/l. The gas stream crossing the hollow-fibre membrane is contacted with a

sulphuric acid solution to produce ammonium sulphate. Since only the gas can go through the membrane, this configuration is less prone to fouling (Yang et al., 2022), but as stripping, only N can be recovered.

On the other hand, electrodialysis (ED) and forward osmosis (FO) represent the principal technologies among the non-pressure membranes. The former allows N concentration up to 16-21 g/l (Barampouti et al., 2020) because of high current density, but also contributes to significant energy demand. Concerning FO, it consumes less energy than RO and leads to NH_4^+ concentration in the feed solution, opening further integrations with technologies such as ammonia stripping.

The use of membranes for nutrient recovery is not still mature. However, some advantages exist:

- One of the effluents after membrane treatment is rich in nutrients, highlighting the potential sustainable contribution to the fertilizer demand.
- Reduced transport costs since nutrients are concentrated. Moreover, RO produces a pure water stream, freely dischargeable.
- UF retains pathogens and bacteria, ensuring high safety of the following streams.
- The lack of a heat source does not limit the process, apart from membrane distillation.

On the contrary, some reasons currently hinder it from becoming a BAT for ammonia recovery:

- The full-scale development as nutrient recovery technology is still limited, especially for non-pressure membranes.
- High energy demand, particularly for RO and cleaning (Bolzonella et al., 2017).
- High investments and operational costs (Sobhi et al., 2021). Indeed, one or more pre-treatments are always required to remove SS. Anyway, cleaning becomes crucial against fouling and clogging to restore membrane properties. A backwash does not apply to all membranes, and chemicals are sometimes compulsory.
- Additional post-treatments may be necessary to extract N from the effluent as fertilizer (i.e., stripping and absorption after RO).

1.3.4. Adsorption and Ion Exchange

Adsorption and ion exchange share similar features, although the different nature. The former is driven by intermolecular forces, the latter by ionic forces, but both take place in a packed column using a solid material to retain the targeted components (Shi et al., 2018). Zeolite, clay, and resins represent the main sorbents used. Once the media is exhausted, it must be treated to restore the adsorption capacity and recover NH_4^+ and PO_4^{3-}. The regeneration may be performed thermally, chemically (through nitric acid washing or sodium chloride washing), and even biologically

(Barampouti et al., 2020). Finally, the process can be batch or continuous, depending on the columns available.

Adsorption and ion exchange are recommended when the pH of the liquid fraction is lower than 7 to avoid the high chemical consumption required by other treatments (Sobhi et al., 2021). Nevertheless, they have been studied predominantly at lab-scale. The combination with other technologies is a promising approach, with Vaneeckhaute et al. (2016) reporting 100% P and 83% N recoveries when zeolite adsorption and struvite precipitation are combined at lab-scale.

The advantages of these technologies can be summarized as:

- Slow-release fertilizer potential: the porosity of zeolite results in a slower nutrient release (desorption) than adsorption (Barampouti et al., 2020).
- Simplicity, with the lowest process energy demand as stand-alone technology (Sobhi et al., 2021). However, the need for combination and pre-treatment affects the final consumption.

On the other hand, the main challenges are:

- The application as a N recovery technology has still to be demonstrated (Sobhi et al., 2021).
- The adsorbing capacity decreases with time.
- One or more pre-treatments are needed. Anyway, fouling and ion competition decrease the efficiency.
- Higher cost than struvite precipitation and NH_3 stripping due to zeolite (Sobhi et al., 2021).

1.3.5. Drying and Vacuum Evaporation

These applications hinge on elevated temperatures to shove the NH_3 transfer to the gaseous phase, which is then recovered as ammonium sulphate or ammonium nitrate in the following absorption processes. Alternatively, the gas phase can be condensed and used for irrigation or other purposes. While dryers imply the use of hot air (70-80°C) (Bolzonella et al., 2017), vacuum evaporation works by applying negative pressure and keeping the boiling T at that pressure (Sobhi et al., 2021).

The application of these technologies can be beneficial because the volume of the input stream is strongly reduced by up to 50%, limiting transportation costs (Herbes et al., 2020).

Conversely, the major obstacle is represented by the high energy needs of the process. The 350 kWh/m^3 of evaporating water makes the implementation of this technology restricted to sites with waste thermal energy, such as some of the AD biogas plants (Sobhi et al., 2021). However, the derived heat may be not sufficient to cover the whole evaporation.

1.3.6. Main Challenges

The development of nutrient recovery technologies to sustain the circular economy is slowed by some challenges. Farmers may lack the financial confidence to make a critical investment decision, and the absence of clear shared regulations discourages users, threatened by possible sanctions. Moreover, the digestate composition is not constant, as it varies from the source of the waste and the working conditions. Wastewater acts as a stable feed for nutrient recovery, but the distance between plants and farmlands increases costs, hampering further reuse. Furthermore, the absence of complete knowledge of digestate derivatives intimidates farmers and hinders the application of these products on the soil. Indeed, concerns about pathogens, emerging contaminants, and heavy metals still limit the development of waste-derived fertilizers. All these barriers must be broken down by governments and administrators without further delay, promoting clean fertilizer production as an alternative to the increasingly scarce fossil-based resources.

1.4. The B-WaterSmart Project

Between the multiple options that seek to foster the transition to a circular economy, the B-WaterSmart project gathers six sites around Europe, with goals shaped on the water sector challenges of each territory. The six “Living Labs” are located in Venice (Italy), Alicante (Spain), Lisbon (Portugal), Bodo (Norway), Flanders (Belgium), and East Frisia (Germany). The project is funded by the European Union’s Horizon 2020 research and innovation programme under grant agreement No. 869171, for an investment of 15 million euros connecting 36 partners in 7 countries. Started in September 2020, the conclusion is set for August 2024 (ETRA, n.d.). In the specific case of Italy, Veritas is the leading company but other partners such as ETRA are involved. The goal is the valorisation of resource recovery opportunities in the wastewater field, looking for sustainable management models to break down the barriers that hamper the closing of the loop. Regarding nutrients, Veritas and ETRA test two pilot plants based on ammonia stripping and absorption to assess the potential recovery of fertilizers from wastewater. The locations of the plants are Fusina (Venice province) and Camposampiero (Padova province).

1.5. Aim of the Thesis

The current climate change situation shoves to disengage from scarce and impacting fossil fuels in favour of new sustainable approaches. The expected expansion of the population will lead to two remarkable results: on one hand, an increase in the food demand, and on the other, growth in waste production. Therefore, proper waste management can lead to a valuable and sustainable nutrient recovery, crucial in ensuring future food availability by safeguarding the environment. In

particular, the NH_3 contained in manure, food waste, and sewage sludge is a precious source for bio-based fertilizers, alternative to the high energy-intensive Haber-Bosch process. This thesis, which is carried out within the B-WaterSmart project, aims to test a pilot plant to recover ammonia as ammonium sulphate from the liquid fraction of digested food and green waste through a combination of ammonia stripping and absorption. The substrates are chosen as representatives of plants working in the wastewater field with extreme %TSS conditions.

After some initial tests to set the process, the plant is run changing the operating parameters to assess different scenarios and the related final recovery efficiency. However, this work also wants to provide helpful information for the upscaling of the pilot plant and to ease the comparative assessment with other technologies, as well as the realization of cost-benefit analysis.

Chapter 2

MATERIALS AND METHODS

Chapter 2 describes the pilot plant used for the study, with specific details on the combined stripping and absorption reactors. All the composing elements are presented, resulting in a clear explanation of the working framework. Moreover, the characteristics of the inlet liquid fraction are analysed and corroborated by real values and literature references. Additionally, this chapter presents the principal operating variables and analytical methods for measuring pH, total nitrogen, and ammonia nitrogen content. The existence of standard techniques for parameter assessment becomes fundamental to ensure the reproducibility of the obtained results, highlighting the scientific approach of the thesis. Finally, the working strategy and the testing conditions are outlined.

2.1. Plant Description

The pilot plant under investigation hinges on the combined stripping and absorption processes, specifically designed to recover N as ammonium sulphate from the liquid fraction obtained after digestate centrifugation. A schematic representation is reported in Figure 2.1. The pilot plant is located inside the WWTP of Camposampiero, within the Padova province, in the North-East of Italy. The provider is Renove Group, a company working in the sector of renewable energies. Since it is a pilot scale plant, the sizes allow to enclose the plant in a container, as shown in Figure 2.2.

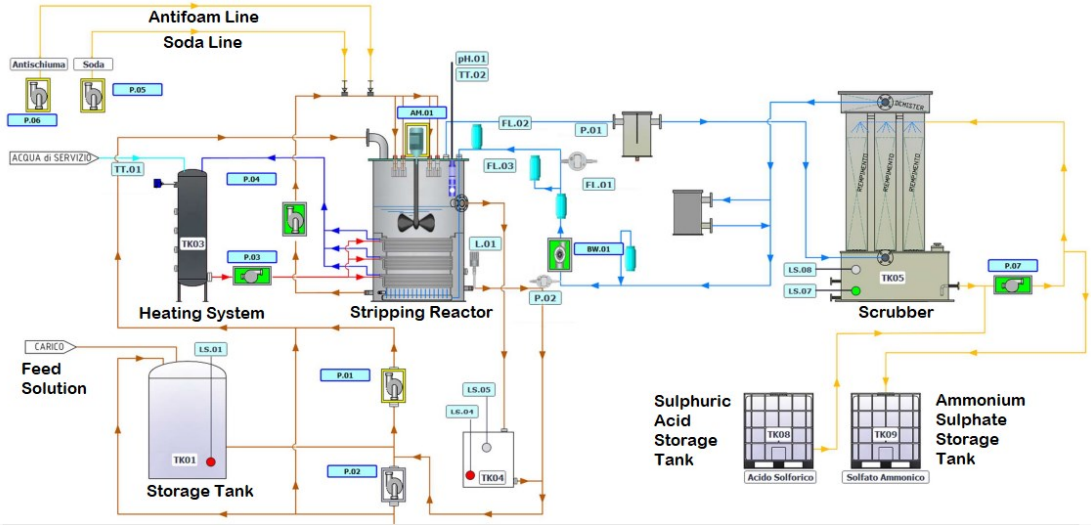

Figure 2.1: Schematic representation of the elements composing the pilot plant

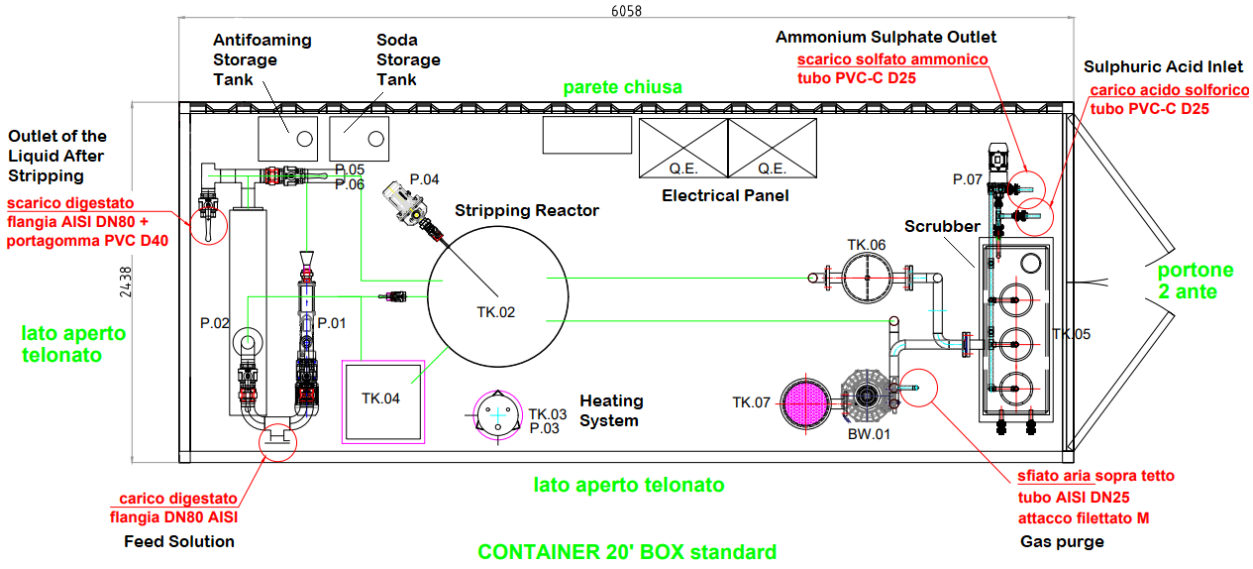

Figure 2.2: Layout of the pilot plant enclosed in the container at the WWTP in Camposampiero

2.1.1. Stripping Reactor

The stripping design recalls the air bubble configuration. The main reason is the inlet stream having a %TS larger than 2%, as will be explained in Chapter 2.2. Indeed, a packed column reactor system would have led to higher pre-treatment costs and the need for cleaning to cope with clogging. Moreover, the air bubble reactor allows to limit carbonates precipitation onto the packing surface, saving chemicals used for acid cleaning. In synthesis, the presented choice keeps the operative costs contained, ensuring the continuous run of the plant, and lowering the need for a shutdown.

The inlet stream is firstly stored in a bigger tank and then in a smaller one of 5 m^3, before being pushed through a progressing cavity pump to the stripping reactor (Figure 2.3). While the liquid phase enters from the top, the gas bubbles flow upward from the bottom, released by a diffuser. The presence of a mixer improves the mass transfer inside the reactor, forcing the ammonia to pass from the liquid to the gaseous phase. The volume of the cylindrical reactor made in AISI 304 is around 1.18 m^3 (D=1000 mm x H=1500 mm). Of this, nearly half (0.56 m^3) is occupied by liquid and half by gas. The free space for the air is crucial to efficiently manage the foam production typical of the air bubble reactor. Besides, the liquid is recirculated to prevent this formation, and a non-silicone antifoam agent is injected. Once reintroduced into the reactor, this stream hits some plates with consequent diffusion onto the liquid surface already present, thus preventing the foam formation.

Considering the process parameters and recalling what was described in Chapter 1.3.1.2., the regulation of pH and the temperature are fundamental for efficient ammonia removal. The former

can be controlled through caustic soda addition (NaOH at 32%,) in the recycled stream (Figure 2.3), while the latter is regulated by an adjustable heating system (Figure 2.4). The temperature inside the reactor remains constant due to a heat exchanger, where electrical resistors heat the utility water that enters the reactor into pipe coils and gets back cooled, creating a loop. It is worth noting that even if the reactor is thermally insulated, the heat supply becomes compulsory as the inlet liquid fraction is at ambient temperature. Indeed, the feed comes from another site managed by the ETRA company located in Bassano, in the Vicenza province. The reason for the importation of the liquid stream is the willingness to test the pilot plant in extreme conditions, represented here by the high inlet %TS and %TSS. Furthermore, the digestors of the WWTP in Camposampiero are temporarily out of service, confirming the need for feed importation.

Figure 2.3: Inlet liquid fraction and caustic soda storage tanks

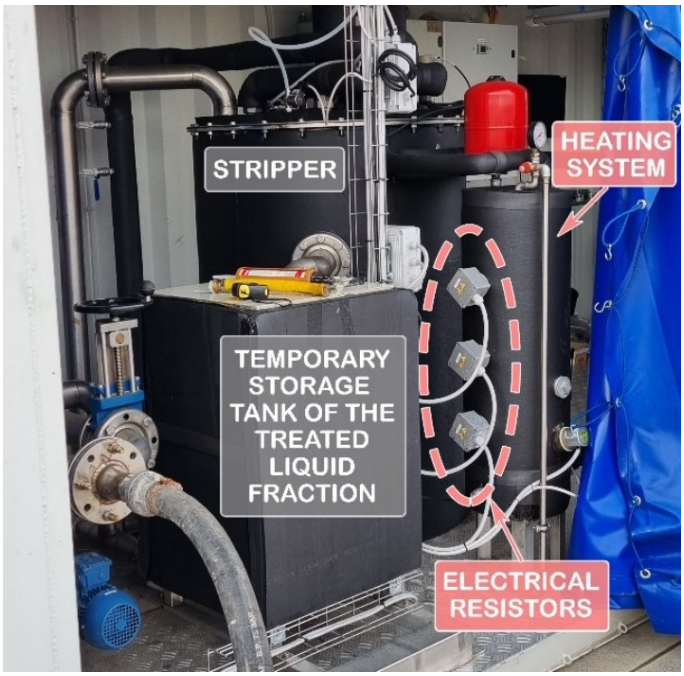

Figure 2.4: Front view of the stripping air bubble reactor, with the storage tank for the treated liquid and the heating system needed to keep the T set-point

The streams exiting the stripper have different fates. The treated liquid fraction is pumped out into a storage tank, to which also the reactor overflow is sent. Indeed, the level inside the stripping tank is controlled through an overfill put above the free liquid surface. When the volume overcomes the threshold, the liquid automatically flows out of the reactor and gets stored in a temporary tank before being pumped into the main storage tank. The liquid is then discharged into the WWTP to be further purified. Moreover, a valve placed at the bottom of the stripping reactor allows the removal of settled material if needed. On the other hand, the stripping gas flows across a foam trap once out from the reactor to remove the possible foams that may be dragged into the air pipe. Thus, the ammonia-rich air is ready to enter the scrubber to complete the second part of the process.

2.1.2. Absorption Reactor

The gas stream containing the ammonia removed in the stripper enters a scrubber composed of three columns working in parallel (Figure 2.5). These latter are packed with polypropylene (PP) pallets of 5/8", and the whole sizes are L=1500 mm x W=400 mm x H=2200 mm. The available volume is 185 litres. Inside the columns, the contacted streams flow counter-currently, with the air entering from the bottom moving upward and the liquid flowing in the opposite direction from the top. The scrubbing solution is pumped from a storage tank containing sulphuric acid in a concentration of 50%$_{w/w}$ (Figure 2.6) and recycled until the concentration of ammonium sulphate reaches values of around 30%. This ensures a %N (in weight) higher than the 6% required by the legislation to be used as a liquid fertilizer (MASAF, n.d.). Once obtained, the solution is accumulated into a tank (Figure 2.6).

Figure 2.5: Absorption reactor (scrubber) and air flow path

Figure 2.6: Sulphuric acid solution (scrubbing solution) and ammonium sulphate solution (final product) storage tanks

Finally, recalling what presented in Figure 2.5, the poor-ammonia air stream is sent back to the stripping reactor in an internal loop prior to a demister that retains the water droplets. The plant is equipped with a purge and make-up system, and the released gas contains CO_2, NH_3, and VFA. Anyway, the flow is so minimal that the emissions can be neglected.

2.2. Composition of the Digestate Liquid Fraction

The characterization of the plant feed represents the first strategic step to calculate the final removal efficiency. Considering the specific case presented in this thesis, the inlet stream is obtained from an external site managed by ETRA and located in Bassano del Grappa. Here, the organic fraction of municipal solid waste (OFMSW) is mixed with shredded green waste until the proportions reach 93% and 7%, respectively. Indeed, this condition seemed to be the most suitable for the anaerobic digestion into a thermophilic Valorga dry reactor, preventing the packing and easing the mixing. The obtained digestate is then separated through a centrifuge into a solid and liquid fraction, with this latter transported to the pilot plant inside the WWTP in Camposampiero for further treatments. The liquid after the transport is at ambient temperature, requiring a heating system to reach the desired set-point. Table 2.1 reports the main analysed parameters concerning the liquid fraction to highlight the characteristics of the stream entering the plant. However, as previously said, the composition depends on the type of digested substrate as well as the separation method used after the process, besides the working conditions at which the anaerobic digestion is performed. This aspect, added to the fact that the research is focused preferentially on whole digestate applications, makes it difficult to compare this stream with the others from the literature.

Observing Table 2.1, most of the results are aligned with the reference values. In particular, the pH is around neutrality, weakly basic (range of 7.80-8.20), and the TS content recalls the high dilution derived from the centrifugation process. What strongly differs from the literature is the high amount of TSS, with mean values of 10.85 g/l, compared to 4.2 ± 2.3 g/l reported by Barreiro-Vescovo et al (2020). The reason is attributable to the AD feedstock and the lack of any coagulant or flocculant dosage before the centrifugation. However, chemical usage is intentionally avoided to simulate extreme working conditions in a WWTP. Indeed, even if the inlet substrate to the pilot plant comes from municipal solid waste, the thesis is carried out within the B-WaterSmart project, which aims to assess new opportunities for the valorisation of the wastewater sector.

Table 2.1: Main parameters and values about the liquid fraction composition representing the pilot plant inlet stream, and comparison with literature

Parameter	Unit of Measurement	Mean Value	Minimum Value	Maximum Value	Standard Deviation	Literature Reference Value
pH	-	7.60	6.50	8.40	0.30	8.34-8.80[a]
Total Solids (TS)	% fresh weight	2.50	0.90	4.70	0.70	3.90[a]
Volatile Solids (VS)	% TS	60.70	59.50	61.90	0.90	64.04[a]
Total Suspended Solids (TSS)	g/l	10.85	4.90	24.44	4.30	4.2 ± 2.3[c]
Volatile Fatty Acids (VFA)	g/l (as acetic acid)	8.08	5.95	2.25	11.88	-
Alkalinity	g_{CaCO3}/l	18.91	15.80	23.09	2.91	14.1-16.5[d]
Conductivity	mS/cm	20.68	13.81	31.92	3.45	22[e]
Total N	g_N/l	3.62	2.30	4.93	0.85	1.5-6.5[f]
Ammonia N	g_{NH4}/l	2.82	1.15	5.29	0.94	2.93 ± 0.14 $g_{NH3–N}$/l[c]
Total P	g_P/l	0.15	0.10	0.23	0.04	0.051[c]
Chlorides	g_{Cl}/l	2.79	1.65	4.80	1.06	2.25-2.30[b,e]
Sulphates	g_{SO4}/l	2.10	1.11	3.24	0.62	0.1[b]
Calcium	g_{Ca}/l	0.36	0.20	0.45	0.1	0.42[e]
Total COD	g_{O2}/l	35.05	6.60	72.70	15.03	39.5-40.2[b,d]
BOD_5	g_{O2}/l	15.32	12.00	18.00	2.88	4.5-7.3[b,d]
Total TOC	g_C/l	6.63	4.60	9.48	1.95	-

a: Peng & Pivato, 2017
b: Akhiar et al., 2021, (plant I)
c: Barreiro-Vescovo et al., 2020
d: Systemic, n.d.

e: Agnieszka & Małgorzata, 2022
f: Akhiar et al., 2017

The liquid fraction beyond TSS content is rich in alkalinity, nitrogen, and COD. Proper management is necessary to prevent complications during the process, even if these values do not diverge significantly from the literature, apart from the TSS content. Indeed, as said, this latter has played a crucial role in the choice of the stripping reactor, opting for an air bubble reactor instead of a packed column. Concerning alkalinity, high values may lead to scaling and precipitates, whilst high COD increase the costs for further treatments to comply with legislation limits at the discharge point. It is worth noting that the BOD_5 seems to be higher than expected, leading to BOD_5/COD ratios of 44%, quite higher than the average 20% (Chuda et al., 2022) and the typical range of 10-30% (Systemic, n.d.; Agnieszka & Małgorzata, 2022). In terms of nutrients, the mass ratio of nitrogen to phosphorus, which is approximately 24:1, is slightly similar to the 13:1 ratio reported by Vaneeckhaute et al. (2013). Additionally, the ratio of ammonia to total nitrogen is 78%, which falls within the range of 40-80% reported in Table 1.2. This indicates promising removal efficiencies in the pilot plant treatment, with the consequent valorisation of the waste.

2.3. Working Strategy and On-Field Conditions

After analysing the composition of the input stream, the core of the testing process involves managing multiple variables and measuring various parameters. Monitoring is crucial as a change in the setting conditions affects not only the final nitrogen removal but also the total energy consumption and the dosage of chemicals, influencing the operative costs. Therefore, the chosen strategy must balance contained expenses and maximized recovery efficiency. This subchapter will cover the main variables controlled in the plant, along with the necessary analytical techniques and operating strategies to achieve the desired goals.

2.3.1. Operating Variables

Flowrates represent the majority of the variables controlled in the plant because of the essential interactions of the closed loop with external elements, such as chemicals and purge, which adjustments allow the definition of the best conditions to raise the process performances.

a) Hydraulic Retention Time – HRT

The inlet liquid flow rate Q_{LF} is related to the Hydraulic Retention Time (HRT). The former is set through a control panel, after which the HRT is calculated by dividing the reactor volume by the Q_{LF}. Using the HRT ratio as an operating variable becomes fundamental when approaching the up-scaling process. Indeed, the HRT remains constant from pilot to full-scale since it represents

the process, that is independent from the plant scale. Hence, once the inlet flow rate is defined in full-scale, it is immediate to calculate the reactor volume.

In particular, higher inlet flowrates result in a reduction of the HRT, and the consequent drop of the removal efficiency. A reduced removal efficiency is also obtained applying too low flowrates, leading to null or low driving forces. The plant is designed to work with a maximum inlet load of 100 l/h and the regulation is done though a pump that shoves the liquid fraction from the inlet storing tank into the stripping reactor.

b) Air Flowrate – Q_A

The air flows pushed by a blower into a closed loop between the stripping reactor and the scrubber. The flowrate is set through the control panel. Low values produce effects similar to those of liquid fraction, thus decreasing the driving force. On the contrary, higher flowrates reduce the mass transfer resistance, favouring the ammonia transfer into the gas phase. However, excessive values lead to foam formation and introduce the need for an antifoam.

c) Ratio of Purge and Air Flowrates – R_{PA}

Controlling the make-up and purge flowrates (Q_{MU} and Q_P) is fundamental to avoid air saturation and efficiency decrease. Indeed, the air exiting the scrubber contains CO_2, NH_3, VFA, and traces of sulphuric acid and ammonium sulphate, which are transported into the air bubble reactor if not removed. The presence of these compounds in the stream entering the stripper would lower the quantity of ammonia that can volatilize into the gas phase, reducing the NH_3 available for absorption in the scrubber. Hence, purge and make-up are unavoidable to purify continuously the air through the partial release into the atmosphere and the equal replacement with fresh air. However, excessive flowrates increase the heat needed to maintain the temperature constant inside the stripping reactor since the atmospheric air has a lower T than the one flowing in the loop. With these considerations, the choice of the proper purge and make-up flowrates becomes a trade-off between higher driving forces and lower electricity costs. After being set by the operator, the calculation of the ratio between the Q_P and the Q_A defines a useful operating variable. Indeed, as for the HRT, this ratio eases the up-scaling procedure, representing the process independently from the plant scale.

d) Antifoam Flowrate – Q_{AF}

As previously mentioned, the primary disadvantage of air bubble reactors is the occurrence of foams, which accumulate on the top of the liquid fraction and may enter the pipe conducing to the scrubber, consequently stressing the sensors placed in this second reactor. To address this issue, a

non-silicone antifoam is introduced into the liquid portion of the recycling stream surrounding the stripping reactor.

The elevated temperatures inside the stripper force the release of CO_2 and the volatilization of NH_3. During the start-up phase of the process, the evaporation affects both the liquid filling the reactor body and the one entering the reactor, leading to high foam production. On the other hand, when the process reaches the regime conditions, the ions and CO_2 evaporation contribution are mainly attributable to the liquid approaching the reactor, limiting the dosage of antifoam. Thus, the dosage is contained and kept constant through a pump.

The flowrate of the dosed antifoam is kept almost constant among the different conditions tested and set through the control panel.

e) pH

By recalling Chapter 1.3.1.2., pH represents the key parameter to enhance nitrogen removal. Basic conditions foster ammonia evaporation in the stripper up to limit pH values of around 10.5, above which the effects of chemical addition become negligible. The desired pH in the pilot plant is set through the control panel, and a sensor inside the air bubble reactor measures the difference between the real value and the set-point to regulate the soda dosage. As for the antifoam, the caustic soda flowrate is dosed automatically through a pump in the recycled stream surrounding the stripper.

f) T and Electrical Resistors

The temperature is regulated through the heat provision by the electrical resistors. As introduced in Chapter 2.1.1., the electrical energy warms the utility water, which flows in a closed loop and enters the stripper into coil pipes, thus exchanging the heat with the liquid fraction up to the desired set-point. As for the pH, the desired temperature is set, and a sensor measures the difference between the real and set-point values. Once the theoretical testing conditions are established, the heating system switches off. The operating choice is to work below 70°C since excessive temperatures would hasten the evaporation and consequently lead to higher condensation in the blower. The effects could be damage and scaling problems. It is important to note that while this thesis focuses on electricity as the primary source, the plant could potentially utilize residual heat from the Combined Heat and Power (CHP) system when scaled up.

2.3.2. Analytical Techniques

The selection of the parameters to be measured reflects the role they play in the final ammonia recovery. In the case of this thesis, pH, TN, and ammonia N are analysed. These parameters are monitored through laboratory tests on samples from both the input and output streams from the stripping reactor to assess the variation of the parameters along the testing period. In particular, the ammonia N is a fundamental factor for calculating the removal efficiency η, as described in Equation (7), where $C_{OUT,NH4+}$ and $C_{IN,NH4+}$ are the ammonia concentrations in the solutions leaving and entering the stripping reactor, respectively. The lab-measured pH differs from the pH presented as an operating variable since, in this case, it simply represents a value and cannot be manipulated.

$$\eta = 1 - \frac{C_{OUT,NH_4^+}}{C_{IN,NH_4^+}} \quad (7)$$

Standard references of analysis crucially guide laboratories during the test, providing harmonized procedures to ensure the reproducibility of the results. This section briefly describes the analytical techniques used to assess the above-mentioned parameters for the liquid fractions entering and exiting the stripping reactor. The measuring frequency is 2 and 5 samples per day, respectively. Moreover, other tests on parameters such as TS, TSS, total phosphorus (TP), and alkalinity are performed once every two weeks for the inlet liquid fraction. Instead, once treated, the TP in the liquid solution is measured only once a week. Finally, the ammonium sulphate solution is tested once every two weeks.

a) pH Test

The procedure for this test is “APAT CNR IRSA 2060 Man 29 2003”. Based on the potentiometric principle, a couple of electrodes compose the measurement system, and the pH is derived from a difference in voltage. Figure 2.7 gives a graphical explanation of the equipment. The pH-sensitive glass electrode is bulb-shaped at the end, whereas the reference electrode has a junction to complete the electrical circuit. Both electrodes are filled with a neutral solution of potassium chloride KCl at 3.5M (IRSA, n.d.-a) and a suspended metal wire. After an initial calibration with pH-known solutions, the system is inserted into the sample. The difference in H^+ concentrations across the glass bulb determines a positive or negative voltage, which provides the pH value when subtracting it from the steady reference of the other electrode.

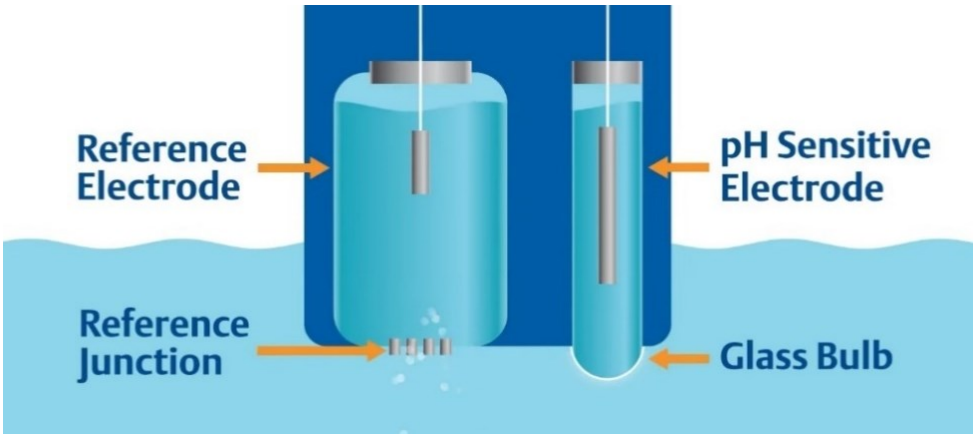

Figure 2.7: Schematic representation of a potentiometric pH meter (Rosemount, 2022)

b) Total Nitrogen Test

The reference procedure for this test is the standard "UNI 11759:2019". The oxidative digestion with sodium persulphate ($Na_2S_2O_8$) represents the first step of the process. The elevated temperature and pressure, coupled with basic conditions, provoke ammonia, nitrites, and organic N oxidation to nitrates. Then, the NO_3^- concentration is measured through UV spectrometry after acidification. Finally, the total nitrogen content is calculated proportionally based on the resulting absorbance at 210 nm wavelength. (UNI, n.d.).

c) Ammonia Nitrogen Test

The reference procedure to assess the ammonia nitrogen content is "APAT CNR IRSA 4030 C Man 29 2003". The test begins with a distillation since ammonia is a weak basis and shows high volatility at pH around 9.5. The presence of ammonia in the lab or inside the equipment must be carefully evaluated as it may be a source of interference. Once the NH_3 has been collected into the distillate, it can be further determined through spectrophotometry with Nessler's reagent or by titration with a strong acid solution and turning point at pH=5 (IRSA, n.d.-b). In particular, these methods are recommended for lower and higher ammonia values, respectively.

2.3.3. Running Mode and Working Conditions

The pilot plant is designed to continuously run after the definition of the working conditions. A batch mode was initially considered but definitely abandoned as the reaction velocities can be extrapolated from the period between the start-up and the steady regime conditions. The latter is established after 2.5-3 folds the HRT value.

The continuous working mode includes the following steps. From the start-up:

i. After filling the tank that stores the inlet liquid fraction, a sensor provides positive feedback, and the loading process begins. The progressing cavity pump shoves the stream into the stripping reactor until it reaches the desired level, monitored by a sensor.
ii. The electrical resistors switch on and heat the process water until the set-point T is reached. Once done, a pump puts the water into circulation to heat the liquid fraction inside the air bubble reactor.
iii. The blower activates, providing the air to the diffusers placed at the bottom of the stripper.
iv. The mixer and the pump for the liquid recycling start working, and the antifoam is injected from the corresponding storage tank. Moreover, the pH is regulated through another pump up to the set-point.
v. A pump charges the sulphuric acid solution into the scrubber.
vi. When the temporary storage tank containing the treated liquid fraction reaches the maximum level, a sensor provides a signal, and a pump sends the liquid into the final storage tank.

The working strategy involves testing periods that last for a week or longer, during which the process parameters are kept constant, and no variables are modified. This approach allows for testing multiple scenarios and collecting data from different conditions, thus providing a wide data set for the final efficiency value assessment. Hence, Table 2.2 reports the values of the tested variables and parameters, plus some other information.

Finally, it is worth underlining that the conditions at the scrubber are kept constant for the entire testing period and that the mixing is constantly working to enhance the transfer inside the stripping process.

Table 2.2: Testing conditions for the ammonia nitrogen removal efficiency evaluation

Tested Operating Variable/Parameter	Unit of Measurement	Tested Values
Inlet Flowrate - Q_F	l/h	39.51; 43.50
Liquid Available Volume Inside the Stripper	l	560; 630
HRT	h	14.17; 14.48
Air Flowrate - Q_A	m^3/h	50; 55; 60
Make-Up and Purge Flowrates - Q_P	m^3/h	20; 30

Ratio Q_P/Q_A – R_{PA}	-	0.36; 0.4; 0.5
Antifoam Flowrate - Q_{AF}	l/h	0.04
pH Stripper	-	Unaltered State; 10.5
Mixing	-	ON
T of the Inlet Liquid Fraction	°C	22
T Stripper	°C	55; 60; 65
Concentration of the Outlet Ammonium	%w/w	35
Sulphate Solution	%N	6
pH of the Outlet Ammonium Sulphate	-	3-3.5
Solution		

Table 2.2 expresses all the tested values. However, Table 2.3 shows their combination, defining the conditions in which the plant was run. The whole analysis encompasses roughly two months. Only one test out of six was conducted with an increased pH level. This was due to the desire to maintain the pH at the raw level, minimizing the costs associated with caustic soda consumption. Each test is performed by keeping the single working values constant, varying them at the end of the testing period. All the presented tests lasted for at least one week. However, more conditions were tried, but too briefly to provide significant validity of the results. For this reason, they are omitted. Finally, it is important to underline that the HRT associated with a Q_F of 43.50 l/h is larger than the one related to 39.51 l/h. The reason is the difference in the liquid volume inside the stripping reactor in the two cases (630 l and 560 l, respectively). This confirms the choice of the HRT rather than the inlet flowrate as an operating variable.

Table 2.3: Testing periods and relative set conditions

	Q_F	HRT	Q_A	Q_P	R_{PA}	$T_{stripper}$	$pH_{stripper}$
Unit	l/h	h	m^3/h	m^3/h	-	°C	-
Test 1	43.50	14.48	60	30	0.50	60	Unaltered
Test 2	43.50	14.48	60	30	0.50	65	Unaltered
Test 3	39.51	14.17	50	20	0.40	60	Unaltered
Test 4	39.51	14.17	55	20	0.36	65	Unaltered
Test 5	39.51	14.17	50	20	0.40	55	Unaltered
Test 6	39.51	14.17	50	20	0.40	60	10.5

2.4. Data Elaboration

The procedure for the analysis of the results exploits different tools to provide a valid and accurate interpretation of the experimental data, which crucially affects the future development of the plant. In the case of this thesis, the presented graphs are obtained through Excel and Minitab, a software for statistical analysis. The willingness to optimize the process prior to the upscaling procedure leads to the use of the so-called "Response Surface Methodology" (RSM). This collection of statistical and mathematical techniques is particularly useful when several input variables potentially influence some performance. The variables that are manipulated are defined as "predictors" or "factors", whereas the measured output is called "response" (Myers, 2009). Generally, the function connecting the independent variables and the outcome is unknown. The RSM creates an empirical model through regression and allows a graphical representation of the response as the factor varies. The generated surface eases the optimization procedure, defining regions where the response can be maximized or targeted. One of the main advantages of the RSM is the ability to catch the combined effect of the factors on the response. Moreover, the RSM procedure asks for the design of the experiment, suggesting specific testing conditions to maximize the fitting of the regression model on the data. However, in this thesis, the testing conditions were already set by the company. Thus, the model accuracy will be lower than a tailored approach, but anyway, consistent to obtain noteworthy results.

The statistical analysis in Minitab firstly provides an information about the goodness of the fitted model on the experimental data, through the coefficient R^2. Values higher than 90% would describe an accurate fitting of the model. However, due to the lack of any experimental design procedure, values above 70% can be accepted. Minitab also shows the p-value for the different terms considered in the model. The p-value is the probability that measures the evidence against the null hypothesis, here stating that no association persist between the term and the response. Lower values provide stronger evidence against the null hypothesis. For the analysis, a significance level (α level) of 0.05 is chosen as a threshold to evaluate significance of the terms. If the p-value is less than or equal to the significance level, it is possible to conclude that there is a statistically significant association between the response variable and the term.

Chapter 3

EXPERIMENTAL RESULTS AND DISCUSSION

The Chapter is divided into two parts. The first presents and discusses the main results obtained during the testing period. The second aims to create a statistical model for the data interpretation. The discussion starts by reporting the laboratory analysis on the inlet solution, providing a table with mean values and a chart to evaluate the composition of NH_4, TN, and pH over time. Moreover, the real *on-field* conditions are compared to the set ones, contextualizing the differences. Then, the NH_4 and TN removal efficiencies for each test are assessed and commented on through tables and plots, starting the analysis of the possible optimum conditions. Furthermore, the Chapter briefly discusses the specific electricity and soda consumption. In the second part, a statistical model is outlined using the experimental dataset, and the goodness of the fitting is evaluated using Minitab. Both the effects of the single variables and their interactions on the removal efficiency are described by displaying the contour plots. Finally, the Chapter shows the solution of the optimization problem to reach the target removal efficiency of 70%.

3.1. Experimental Data from the Plant

3.1.1. Results on the Samples from the Inlet Solution

The laboratory tests conducted on the samples taken from the input liquid solution claimed a difference between the expected values of the parameters and the measured results. The main reason is the excessive storage of the liquid in the tank before entering the stripping plant. Indeed, the stream was brought to Camposampiero before the plant started. The storage lasted a few months due to some technical problems. This, coupled with the high summer temperature, favoured the digestion of the organic matter and the consequent increase of the pH and ammonia content. Table 3.1 presents the results of the laboratory tests on the samples associated with the inlet stream, compared to the expected inlet composition, already presented in Table 2.1. Moreover, Figure 3.1 reports the trend of the inlet pH, TN, and NH_4-N concentrations over the testing period. The choice to express the ammonia concentration in terms of nitrogen is meant to ease the comparison between the nitrogen present as NH_4 and the total one, neglecting the hydrogen contribution.

Table 3.1: Mean, maximum, and minimum values of the inlet liquid samples tested, compared with the values measured in the original liquid fraction in Bassano del Grappa

Parameter	Mean Value	Minimum Value	Maximum Value	Expected Value (from Table 2.1)
pH (at 20°C)	8.00	7.79	9.75	7.60
NH_4-N (mg/l)	3448.25	2542.17	4534.44	2820.00
TN (mg/l)	4395.86	3270.00	5850.00	3620.00

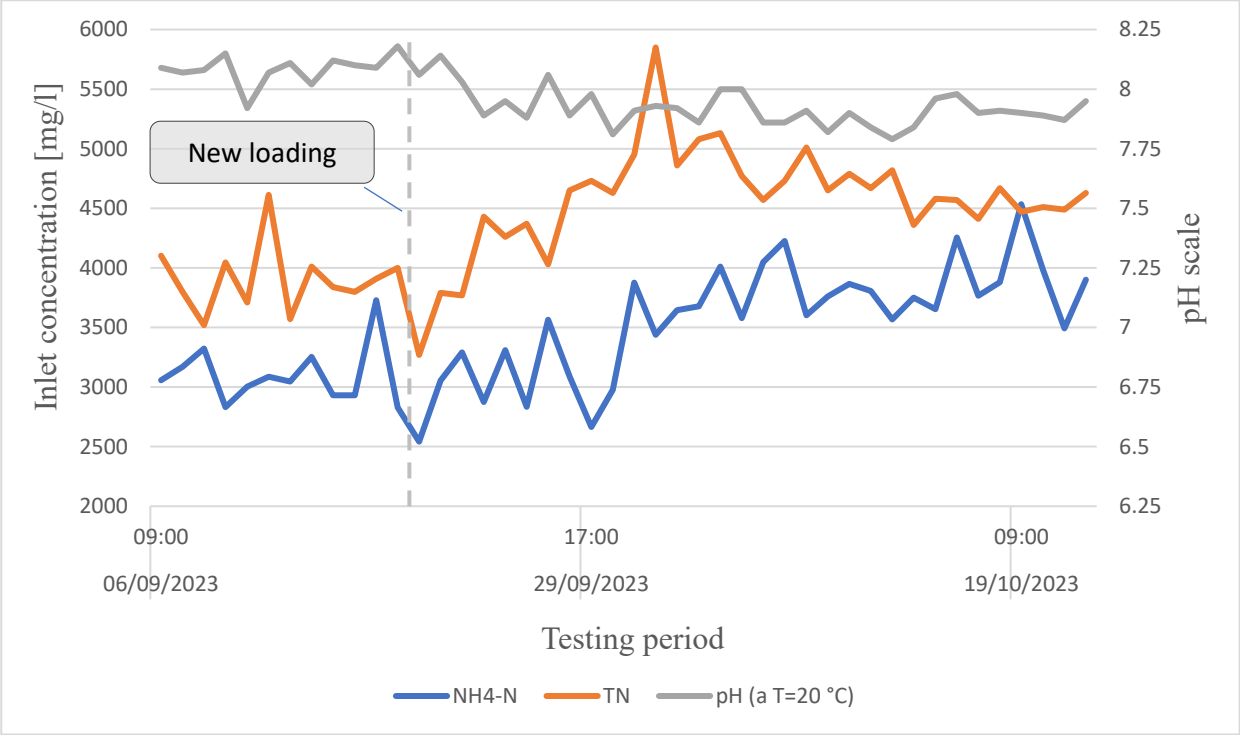

Figure 3.1: Trends of pH, NH_4-N, and TN along the testing period. Values obtained from laboratory tests on the inlet liquid samples

The first comment on the figure is the high fluctuance of the input concentrations for both NH_4 and TN. This behaviour looks unusual, especially considering that the inlet matrix does not change or undergo any treatment. The main explanation is connected to lab inaccuracies. Since the solution is highly concentrated, a strong dilution or a small interference may seriously alter the final result. Even if the concentrations fluctuate along the testing period, the mean ratio between the NH_4-N and TN is 79%, still consistent with expectations. However, in the right part of the chart, a point of the ammonia concentration exceeds the TN one. This is impossible and again attributable to a measurement error.

It is interesting to observe the change in concentrations after the main temporary storage tank reloading. The new liquid solution coming from the plant located in Bassano del Grappa should contain less NH_4 than the initial fill, as the lower residence time inside the tank does not permit the digestion of the organic nitrogen to ammonium. Despite that, the reason may rely on the lower ambient temperature. Indeed, the higher values typical of the summer period increase the ammonia volatilization in the tank, decreasing the remaining quantity in the liquid. On the contrary, during the milder autumn weather, less ammonia passes in the gaseous phase. This effect is surely less important than the volatilization in the stripping reactor, but nevertheless significant to change the amount of ammonia that enters the process. Similarly, the trend of the pH value can be explained. The higher tendency of the CO_2 to be transferred into the gaseous phase pushed the consumption of H^+ to form new carbonic acid, increasing the pH over 8. On the other hand, after the refilling, the pH settles to values below 8 due to lower ambient temperature and storage time.

3.1.2. On-Field Values vs Set Values

Before exploring the obtained efficiencies, it is crucial to underline the *on-field* working conditions. Indeed, the real values taken by the operating variables differ from what is reported in Table 2.3, mainly due to the uncertainty typical of each measurement device. These contributions may significantly alter the expectations, especially when dealing with pilot or full-scale plants. Table 3.2 and Table 3.3 report the real average working conditions of each testing period and also the deviations from the values reported in Table 2.3.

Table 3.2: Real average working conditions

	Q_F	HRT	Q_A	Q_P	R_{PA}	$T_{stripper}$	$pH_{stripper}$
Unit	l/h	h	m^3/h	m^3/h	-	°C	-
Test 1	43.50	14.48	43.09	13.40	0.31	61.57	9.19
Test 2	43.50	14.48	36.61	14.04	0.38	65.61	9.18
Test 3	39.51	14.17	52.81	29.06	0.55	60.92	9.05
Test 4	39.61	14.14	50.29	28.44	0.56	65.78	9.05
Test 5	39.51	14.17	49.12	28.77	0.58	55.26	9.10
Test 6	39.51	14.17	51.07	11.55	0.23	60.42	10.32

Table 3.3: Percentual deviations of the *on-field* values from the set values of Table 2.3

	Q_F	HRT	Q_A	Q_P	R_{PA}	$T_{stripper}$	$pH_{stripper}$
Test 1	0.00%	0.00%	-28.18%	-55.33%	-38.00%	2.62%	0.62%
Test 2	0.00%	0.00%	-38.98%	-53.20%	-24.00%	0.94%	0.51%
Test 3	0.00%	0.00%	5.62%	45.30%	37.50%	1.53%	-0.92%
Test 4	0.25%	-0.21%	-8.56%	42.20%	54.00%	1.20%	-0.92%
Test 5	0.00%	0.00%	-1.76%	43.85%	45.00%	0.47%	-0.37%
Test 6	0.00%	0.00%	2.14%	-42.25%	-42.50%	0.70%	-1.71%

What emerges from the tables is the strong difference of the *on-field* air and purge flowrates, and consequently the R_{PA}. One reason to explain such a trend is that after Test 2, the blower was substituted with a new one, reducing Q_A deviations from more than 25% to less than 10%. The remaining fluctuance, from Test 3 to Test 6, can be attributed to the uncertainty of the Pitot pipe sensor used for the airflow measurement. However, the main effects on the R_{PA} are generated by the purge flowrate variability, mainly related to the uncertainty of the Pitot pipe sensor. On the other hand, the deviations of the HRT, temperature, and pH, are contained and completely in the range of the experience on pilot plants. Anyway, due to the large deviations from set values, the situation shown in Table 3.2 will be considered as the new reference condition from now on.

An interesting observation is the correlation between the R_{PA} and the pH level inside the stripping reactor. Specifically, low R_{PA} values (0.31 and 0.38 of Test 1 and Test 2, respectively) are linked to high pH values (9.19 and 9.18). The opposite tendency happens in Test 3, Test 4, and Test 5 with R_{PA} values of 0.55, 0.56, 0.58, and pH of 9.05 and 9.10. This is probably caused by the high concentration of carbonates in the liquid stream. In fact, the CO_2 volatilization in the stripping reactor leads to the H^+ consumption, increasing the pH. When the air entering the reactor is poorer in CO_2, as in the case of noticeable purge flowrate, the room for carbon dioxide volatilization is larger, consequently resulting in a higher pH increase.

3.1.3. Results of The Removal Efficiency

The measurement of the NH_4 concentrations in the samples taken from the input and the output allows the calculation of the removal efficiency, as expressed in Equation (7) in Chapter 2. Figure 3.2 focuses on the mean removal efficiencies for NH_4 and TN. Indeed, even if the main target is ammonia removal, the total nitrogen evaluation over time can complete the assessment. The two profiles should follow the same trend, as nitrogen residence time in the cycle is too contained for

the mineralization process. Surely, the mean values change from test to test, representing a first glimpse of the optimum situation that could be implemented in full-scale. Table 3.4 reports the mean, maximum, and minimum values for each test to enlarge the assessment, also focusing on the variability of the results inside each period. Finally, Figure 3.3 graphically shows the trends of the NH_4 and TN removal efficiencies over time, with the standard deviations included.

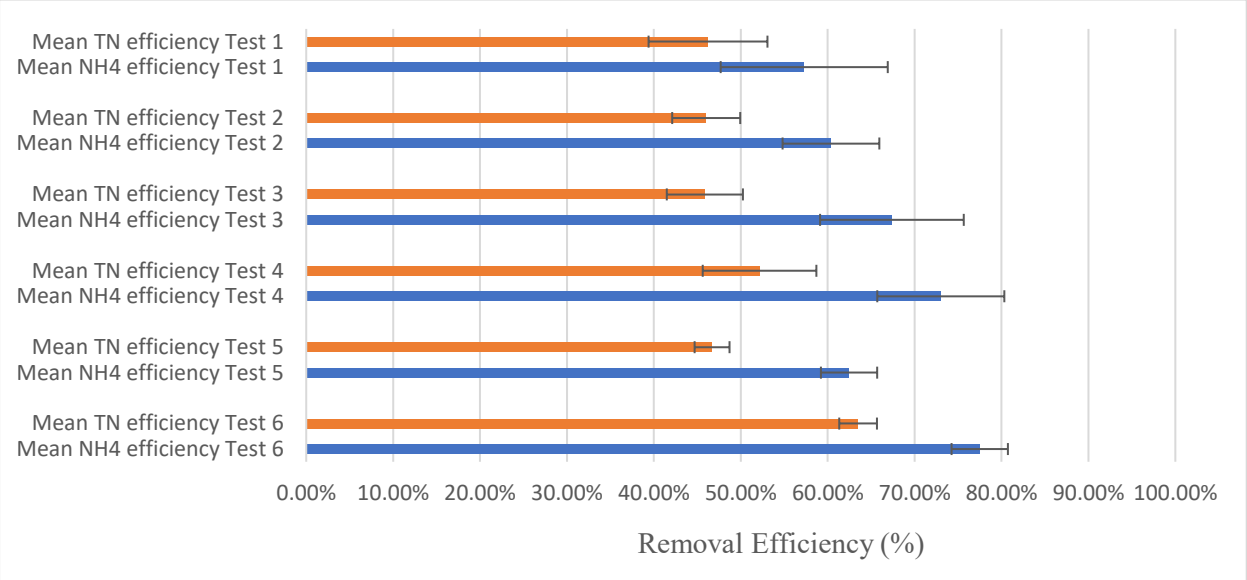

Figure 3.2: Mean NH_4 and TN percentage removal efficiencies for each test, with standard deviations

Table 3.4: Mean, minimum, and maximum values of the NH_4 and TN removal efficiencies for each test

	NH_4 Mean Removal Efficiency	NH_4 Min. Removal Efficiency	NH_4 Max. Removal Efficiency	TN Mean Removal Efficiency	TN Min. Removal Efficiency	TN Max. Removal Efficiency
Test 1	57.30%	28.55%	66.37%	46.23%	28.77%	59.45%
Test 2	60.38%	48.71%	66.98%	46.02%	37.91%	51.62%
Test 3	67.39%	43.63%	77.25%	45.87%	37.00%	51.49%
Test 4	73.01%	49.70%	79.56%	52.16%	41.30%	61.40%
Test 5	62.46%	54.96%	68.03%	46.69%	43.76%	49.89%
Test 6	77.49%	69.88%	83.53%	63.50%	58.73%	67.11%

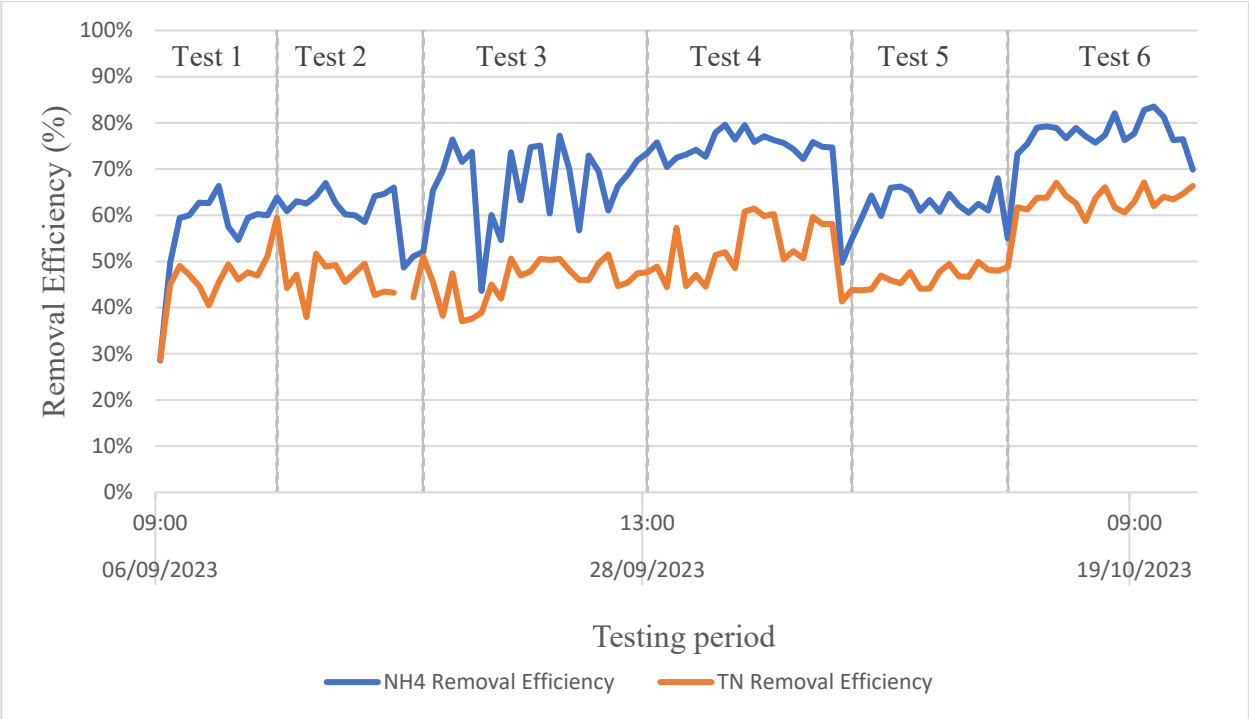

Figure 3.3: NH_4 and TN removal efficiencies for each test over time, in percentage

Starting from Figure 3.2, it is firstly noticeable to highlight that all the tested periods meanly overcome an ammonia removal efficiency level of 50%. This strengthens the effectiveness of the range chosen for the variables. Moreover, Test 4 and Test 6 attain an average ammonia efficiency of over 70% (73.01% and 77.49%, respectively), which is considered a significant threshold. In particular, Test 6 draws near 80%. This value is obtained with a high pH level (10.32 on average), stressing the influence of this parameter on the final result. Test 4 was characterized by the lowest HRT (14.14 h), joined to the highest temperature level of 65.78°C. Looking at the worst results, Test 1 is the only period where the average ammonia removal efficiency does not reach 60% (57.30%). Test 1 and Test 2 share high HRT (14.48 h), and the difference in temperature of 5°C slightly affects the result. On the contrary, the temperature influences Test 5 and Test 3, where the same gap as before leads to an efficiency variation of 5% (62.46% and 67.39%). Finally, the mean TN removal efficiency is less variable among the tests than the NH4 values. Indeed, apart from Test 4 and Test 6, all the efficiencies gather around 46%.

Table 3.4 reports maximum and minimum values in more detail with respect to Figure 3.2. The interesting point is that the minimum ammonia removal efficiency of Test 6 (69.88%) overcomes the maximum values of Test 1, Test 2, and Test 5 (66.37%, 66.98%, 68.03%, respectively), witnessing the strength of the working conditions of Test 6. Moreover, the maximum value for the ammonia removal in Test 6 is higher than 80% (83.53%). This behaviour is similar for the TN.

Considering the difference between maximum and minimum values for the ammonia removal efficiencies, some tests stand out among the others. Indeed, 37.82% of Test 1, 33.62% of Test 3, and 29.86% of Test 4 strongly differ from 18.27% of Test 2, 13.07% of Test 5, and 13.65% of Test 6. The reason for such gaps lies in the minimum values of the first tests aforementioned (28.55%, 43.63%, 49.70% for Test 1, Test 3, and Test 4), probably caused by plant malfunctions. The presence of these points is clearly visible in Figure 3.3, where the NH_4 and TN removal efficiencies are reported over the testing period. The chart confirms the increase of the efficiency in Test 4 and Test 6. Moreover, it describes a large variability of the results in Test 3, mainly attributed to the change of the blower. It is important to note that the TN trend presents some discontinuities, because of some missing data.

3.1.4. Specific Consumption of Electricity and Soda

The energy consumption affects the final operative costs of the plant. The analysis of the kWh consumed during each testing period supports the optimum strategy determination. Indeed, the conditions ensuring the highest removal efficiency may not be economically sustainable for the plant, as in the case of extreme temperatures or pH values. The energy consumption should be expressed as a specific quantity, to account for the differences in the inlet flowrates. Furthermore, the result should hinge on a single hour of testing since the periods lasted differently. Thus, the recorded consumption for each test is divided by the inlet flowrate and the working hours, providing the result in kWh/m^3. The energy absorbed by the plant is in the form of electrical energy, as the reactor heating system is based on the resistors. The total consumption is reported in Figure 3.4, where even the single plant and resistors contributions are included. The whole consumption splitting into two parts aims to highlight the different pumping and heating needs. This latter represents functional information in the upscaling procedure to understand the more sustainable mix of energy providers.

Figure 3.4 displays similar trends between the whole, resistors, and plant consumptions. The rises in the reactor temperature of around 5 °C (meanly from 61.57 °C to 65.61 °C in Test 1 and Test 2, from 60.92 °C to 65.75 °C in Test 3 and Test 4, and from 55.26 °C to 60.42 °C in Test 5 and Test 6) require electrical energy, provided by the resistors. The increases are visible in the chart, with an average consumption of 40-50 kWh/m^3. The gap between Test 5 and Test 6 is 50 kWh/m^3 due to the lower working temperature of Test 5. The energy leveraged to maintain the temperature at constant levels, keeping the water warm, does not particularly affect the results. Thus, the resistor consumption mainly derives from the heating process.

Inspecting the plant trend, Test 3, Test 4, and Test 5 share similar inlet, air, and purge flowrates (39.51 l/h, around 50 m^3/h, and 29 m^3/h, respectively). However, Test 5 consumes significantly less energy. Anyway, the result seems consistent with the plant variability. Test 2 consumes the highest amount of energy (78.35 kWh) even though the Q_F level is the same as Test 1 (43.50 l/h). Moreover, both the air and purge flowrates are lower than Test 3, Test 4, and Test 5. The obtained results may be caused by the old blower installed in the plant. Finally, Test 6 consumption (77.95 kWh) reflects the increased pH level, achieved through the soda addition.

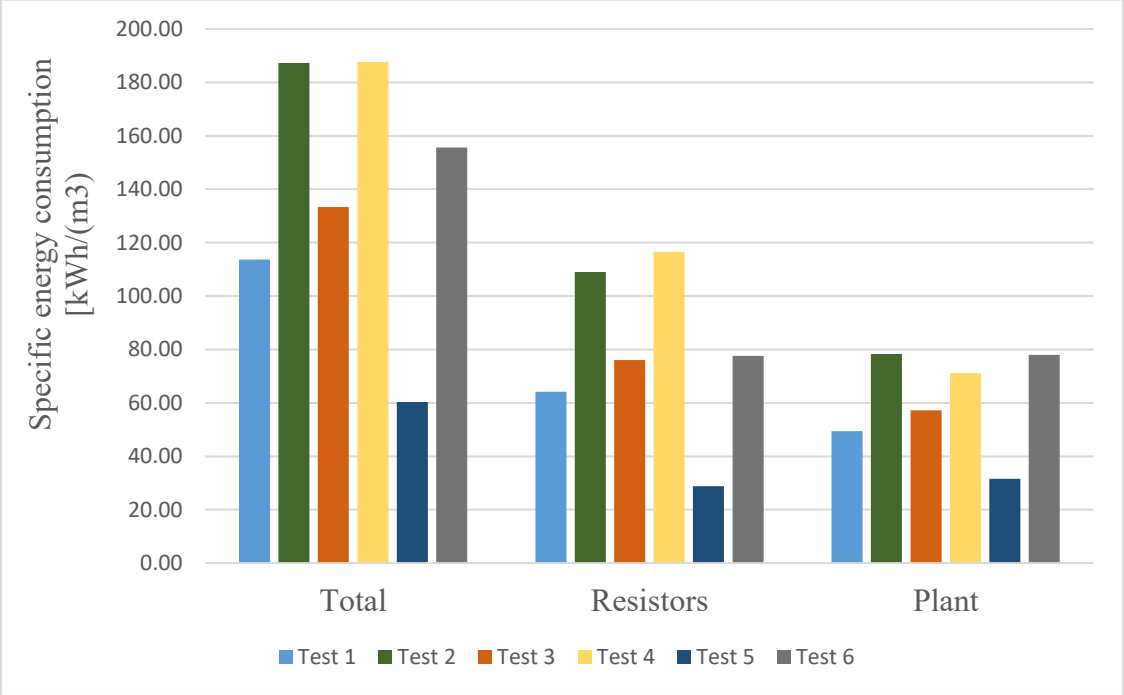

Figure 3.4: Total specific hourly energy consumption and single contributions of the resistors and the plant

The increased pH condition was only tested in Test 6. The connected soda consumption is 2.04 l/h, or 51 l/m^3_{inlet}. As known, the caustic soda solution is expensive, costing even more than 2 €/kg. In these conditions, the choice of pH containment becomes paramount. Besides, a lower pH positively affects the sulphuric acid consumption since the need for pH acidification is reduced. However, the sulphuric acid consumption can be hardly evaluated in each test due to the batch filling of the scrubber columns.

3.2. Statistical Modelling

3.2.1. Significance of the Variables

The analysis of the experimental data highlighted that the solution to achieve the highest removal efficiency hinges on the pH rise. However, as said, the costs associated with the process hinder the possibility of replicating the same strategy in a full-scale plant, especially in the case of a lacking CO_2 stripper that would naturally lead to a pH increase. The formulation of a model that considers the effects of the operating variables on the final efficiency would help the designer to define the optimum set of conditions and simulate new scenarios by simply adjusting the input levels. For this purpose, Minitab allows the statistical modelling of the experimental data. As already explained in Chapter 2.4, the procedure relies on the Response Surface Methodology, which is also used to evaluate the interactions between the variables.

As a first trial, all the experimental data are included in the model creation. Table 3.5 reports the main results obtained. By using the complete dataset, all the interactions can be estimated, outlining the system's complexity. Table 3.5 indicates the p-value of the single factors and their interactions, as well as the R^2 of the model. Furthermore, it shows the standard error S, the average distance that the observed values fall with respect to the regression line.

Table 3.5: Results of the statistical analysis for the complete dataset

Factor	P-Value	R^2	S
HRT	0.00	63.52%	0.060
R_{PA}	0.81		
Tstripping	0.27		
pHstripping	0.01		
HRT*R_{PA}	0.75		
HRT*Tstripping	1.00		
HRT*pHstripping	0.00		
R_{PA}*Tstripping	0.67		
R_{PA}*pHstripping	0.01		
Tstripping*pHstripping	0.24		

Looking at the table, the significant contributions have a p-value lower than 0.05, corresponding to the significance level α. The single terms going under this level are the HRT (p-value of 0.00)

and the pH (p-value of 0.01). Curiously, the former was revealed as the most influential parameter, changing literature expectations that appointed the pH as the main contributor to the final efficiency, followed by the temperature. The ranking obtained from the software is confirmed by the results, having Test 1 and Test 2 the highest HRT (14.48 h) and the lowest average efficiencies (57.30% and 60.38%, respectively). Moreover, Test 4 is characterized by the highest efficiency (73.01%) and the minimum HRT (14.14 h) among the tests without an increased pH. Test 6 is the only condition with a raised pH (10.5), guaranteeing the best average removal efficiency (77.49%). To improve the quality of the results, other experiments with high pH should be carried out. Regarding the temperature, it becomes the third single factor of importance, widely far from the p-value threshold of 0.05 (p-value of 0.27). Finally, the ratio of the air flowrates R_{AP} seemed to be not significant (p-value of 0.81). It is important to remember that for the sake of simplicity, the preferred choice fell on the ratio between the purge and air flowrates. However, the two variables may affect singularly and differently the removal efficiency, and these contributions are not considered.

In terms of interactions, the combined effect of the HRT and pH resulted in the most influential (p-value of 0.00), on par with the HRT. Moreover, the interaction between the R_{PA} and the pH (p-value of 0.01) slightly stays below the p-value of the threshold, witnessing that the R_{PA} may contribute more in combination with other factors than alone. All the remaining interactions are not significant, with a p-value above 0.05.

Assessing the model adequacy, an R^2 of around 63% is a good starting point for the first trial. The standard error S indicates a mean deviation of the experimental data from the fitted model of 6%. The R^2 value is not far from the 70% considered as an acceptable threshold. To increase the model fitting accuracy, Minitab provides a warning table, reported in Table 3.6, with the points that ask for more investigations.

Table 3.6: Fits and Diagnostics for Unusual Observations

Test Condition	Efficiency value	Residue
Test 1	28.55%	-0.23
Test 3	43.63%	-0.20
Test 3	56.68%	-0.13
Test 4	49.70%	-0.19
Test 4	54.87%	-0.13

The table reports the removal efficiency of single samples even belonging to the same test condition, as for Test 3 and Test 4. In these points the efficiency falls, strongly contributing to the average removal of each Test, as reported in Figure 3.2. Most of them have already been introduced in Subchapter 3.1.3. and clearly visible in Figure 3.3, representing the lower peaks of the trend. The efficiencies of these points strongly deviate from both the mean of their reference testing period (Table 3.4) and the fitted model. The residue, which expresses the differences between an observed value and its corresponding fitted value, shows that the efficiencies of the aforementioned points are robustly below the fitted model. The residue ranges from -23% of Test 1 to -13% of Test 4, far from the 6% of the standard error. Investigating the nature of these low values is crucial to strengthen the fitting model. Indeed, understanding if the points are due to plant/process malfunctions or if they are a valid part of the dataset influences the final interpretation. Fortunately, the presented situation falls over the first option, connected to problems with the scrubber or other anomalies. This result led to considering these points as outliers, confirming the possibility of removing them from the dataset to increase the fitting accuracy. The only exception is the third point in the table (removal efficiency of 56.68%), which remains in the dataset. In this scenario, the process has been run again, and the new results are reported in Table 3.7.

Table 3.7: Results of the statistical analysis for data without outliers

Term	P-Value	R^2	S
HRT	0.00		
R_{PA}	0.56		
Tstripping	0.53		
pHstripping	0.00		
HRT*R_{PA}	0.49		
HRT*Tstripping	0.68	74.84%	0.043
HRT*pHstripping	0.00		
R_{PA}*Tstripping	0.37		
R_{PA}*pHstripping	0.46		
Tstripping*pHstripping	0.64		

The updated model shows higher accuracy of the fitting procedure, with an R^2 value of 74.84%, above the threshold fixed at 70%. The standard error S decreases by 0.017 from the value in Table

3.5 (0.060). This means that the experimental points are closer by 1.7% to the fitting line than before, concluding that the model can almost properly approximate the data. According to the p-values, the presented results claim the significance of the HRT and pH (p-values of 0.00). The p-value associated with the pH lowers, nearly reaching zero. Besides, the temperature and the R_{PA} continue to produce negligible effects on the final response. Interestingly, the p-value associated with the R_{PA} lowers (from 0.81 to 0.56), whereas the T one increases (from 0.27 to 0.53), meaning that the two contributions are still not significant but more similar. Dealing with interactions, all the combined effects involving the HRT show a decreased p-value (0.49, 0.68, with R_{PA} and Tstripping, respectively), apart from the interaction with the pH that was already at zero. Moreover, the interaction of the R_{PA} with the T decreases from a p-value of 0.67 to 0.37. On the contrary, a weaker relation between R_{PA} and pH was observed (p-value from 0.01 to 0.46), consequently losing the significance. A rise in the p-value (from 0.24 to 0.64) also resulted from the interaction between the temperature and the pH.

The magnitude and the importance of the effects are confirmed in Figure 3.5, representing the Pareto chart of the standardized effects. The significance level α is 0.05, which combined with the degrees of freedom of the error, provides the value of the reference line for statistical significance, represented as a red vertical line. All the standardized effects that cross the reference line are statistically significant, corroborating the analysis results.

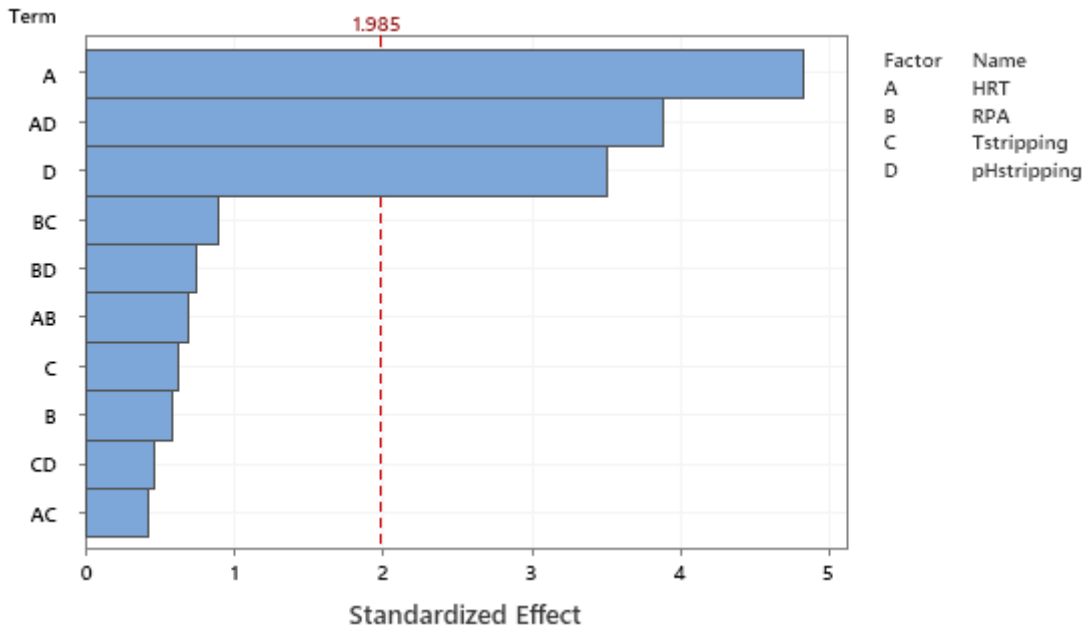

Figure 3.5: Pareto chart of the standardized effects, with significance level α of 0.05

To validate the respect of the assumptions for the regression model, Figure 3.6, Figure 3.7, and Figure 3.8 are reported. The first figure shows the normal probability plot of the residuals, which

displays the residuals versus their expected values with a normal distribution. Since the trend of the points almost follows the red straight line, the assumption that the residuals are normally distributed is verified. However, some points at the top and the bottom of the chart differ from the line. The removal of these points would increase the fitting model adequacy, but they cannot be eliminated from the dataset as they are not linked to plant malfunctions but rather to errors in the measurements. Figure 3.7 introduces the residuals versus fits graph, which plots the residuals on the y-axis and the fitted values on the x-axis. Ideally, the points should fall randomly on both sides of 0, with no recognizable patterns. The points in the graph satisfy this condition, validating the assumption that the residuals are randomly distributed and have constant variance. Finally, Figure 3.8 presents the residuals versus order plot and reports the residuals in the order that the data were collected. As the residuals show no trends or patterns and they fall quite randomly around the centre line, the assumption of residuals' independence of one another is confirmed.

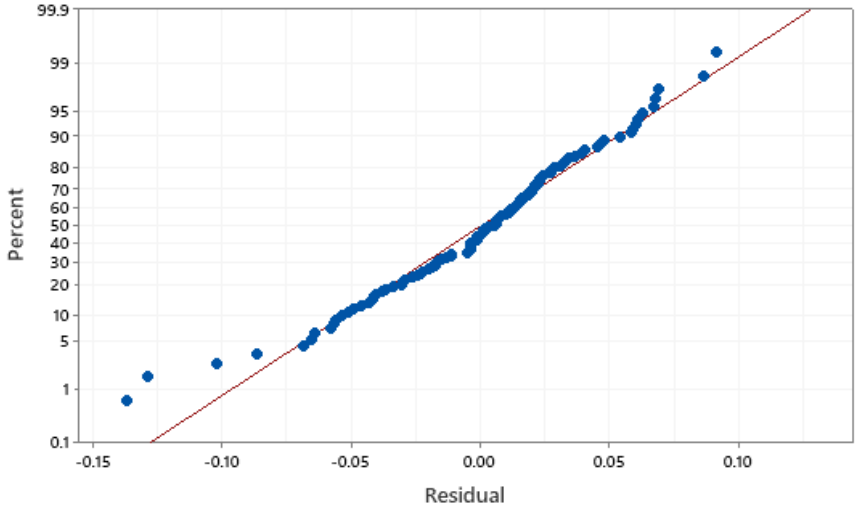

Figure 3.6: Normal probability plot of the residuals

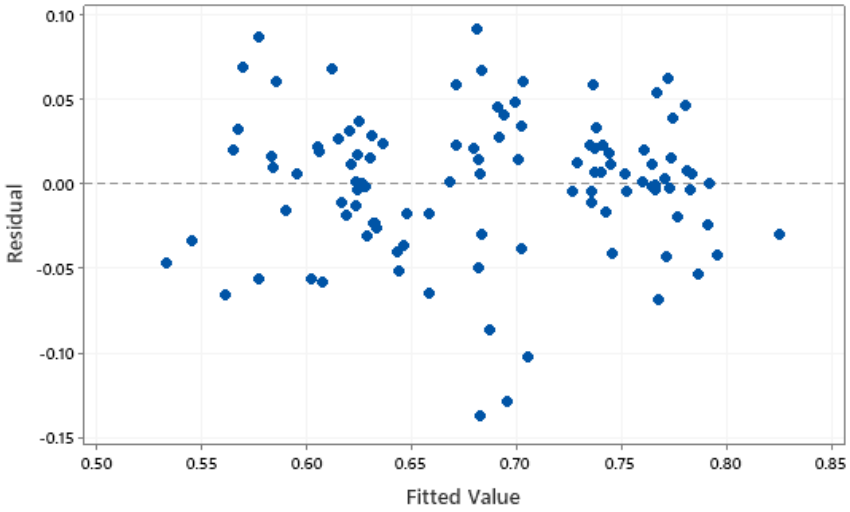

Figure 3.7: Residuals versus fits plot

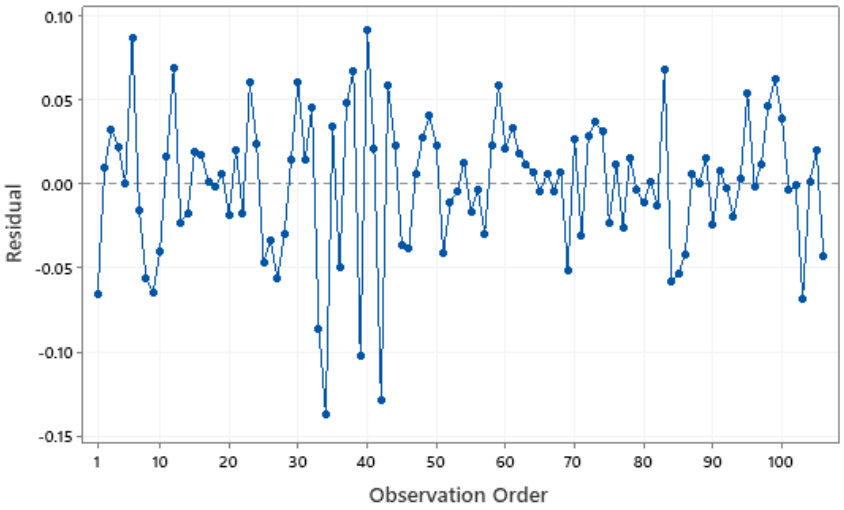

Figure 3.8: Residuals versus order plot

3.2.2. Influence of the Single Factors, Interactions, and Contour Plots

Figure 3.5 showed which factors could be considered significant. However, no information was given on how they singularly influence the removal efficiency. To this purpose, Minitab provides a clear assessment, which is depicted in Figure 3.9. Understanding the single impacts on the response guides the setting of the variables to values that satisfy both process efficiency and cost containment.

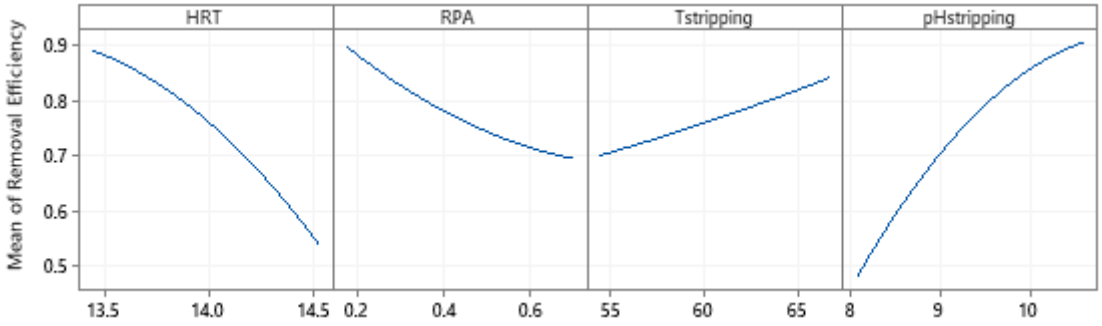

Figure 3.9: Main effects plot for removal efficiency

The trends reported in Figure 3.9 are based on the fitted data. Starting from the HRT, lower values lead to higher removal efficiency. Smaller HRT at constant volume imply greater inlet flowrates, providing fresh solution and an ammonia load higher than the one already present inside the reactor. This favoured efficiency. From the experimental data, the best working conditions result in an HRT value of 14.17 h or even lower. Indeed, the anomalous value of 13.49 h recorded in Test 4 led to a removal efficiency of 79.56%, the maximum in these conditions. However, more energy is needed with lower HRT, as the flowrate to be pumped is more.

About the R_{PA}, the graphical trend resembles the one of the HRT, even if with a different curvature and concavity. Contained R_{PA} with fixed air flowrate means lower purge flowrate and less pH increase in the stripping reactor, as explained in Subchapter 3.1.2. An R_{PA} of 0.23 was found in Test 6. This, coupled with the high pH level due to the soda additions, produced an efficiency of 77.49% on average. However, removals of 67.39% and 73.01% were observed with R_{PA} of around 0.55 in Test 3 and Test 4, but also of 57.30% and 60.38% for values of around 0.35 in Test 1 and Test 2. The lack of a clear connection between the R_{PA} and the efficiency confirms the low significance of this variable. As previously mentioned, it would be interesting to assess the purge and air flowrates effects separately, but for the sake of simplicity, it is left out of the thesis.

The temperature trend for the removal efficiency resulted in the reversal of the R_{PA}. Logically, higher temperatures boost the efficiency, stimulating the volatilization. Indeed, passing from the average T of 55.26 °C of Test 5 to the 60.92 °C of Test 3 and 65.78 °C of Test 4, the removal efficiency increased from 62.46% to 67.39% and 73.01%, respectively. However, the change from 61.57 °C of Test 1 to 65.61 °C of Test 2 raises the efficiency of just 3%, from 57.30% to 60.38%, respectively. This means that even if the temperature is an important operating variable, other factors affect more the final result. This is confirmed by the curve slope, where the steepest curves reflect higher significance.

Finally, as expected, raised pH positively influences the final response. Apart from the result obtained in Test 4 (73.01%), which was characterized by the minimum HRT level (14.14 h), the difference in the average efficiency from Test 6 and Test 3 is around 10% (77.49% and 67.39%, respectively). This shows the importance of pH as an operating variable. Nevertheless, high pH means other investment costs (CO_2 stripping column) or operative costs (soda addition). Moreover, increased pH led to higher foam formation. Thus, the ability to ensure acceptable efficiencies while maintaining the natural pH is worth of interest.

As previously said, understanding the influence of single factors on the final target is extremely important. However, due to the process complexity, the interactions between the variables may alter the magnitude of the effects of each single variable. For example, the reasoning that the growth of the removal efficiency is always verified by increasing the pH may be misleading in a complex system. To cope with that, Minitab provides the contour plots. These latter estimate the removal efficiency ordered by isolines based on the fitted model. Besides, the pattern is exactly the 3-D response surface on a 2-D plane, reflecting the change in the efficiency by varying two factors per time. The chosen efficiency values for the isolines range from 60% to 75%, with a gap of 2.5%. The green colour refers to high removals, and the blue to low. The vertical and horizontal

boundaries are set according to the initial conditions designed for the experiments (Table 2.3) and not to the *on-field* values (Table 3.2). Finally, the other two fixed factors are held at average values to avoid influences on the efficiency pattern. The first presented situation, reported in Figure 3.10, displays the response variation depending on the pH and the HRT levels.

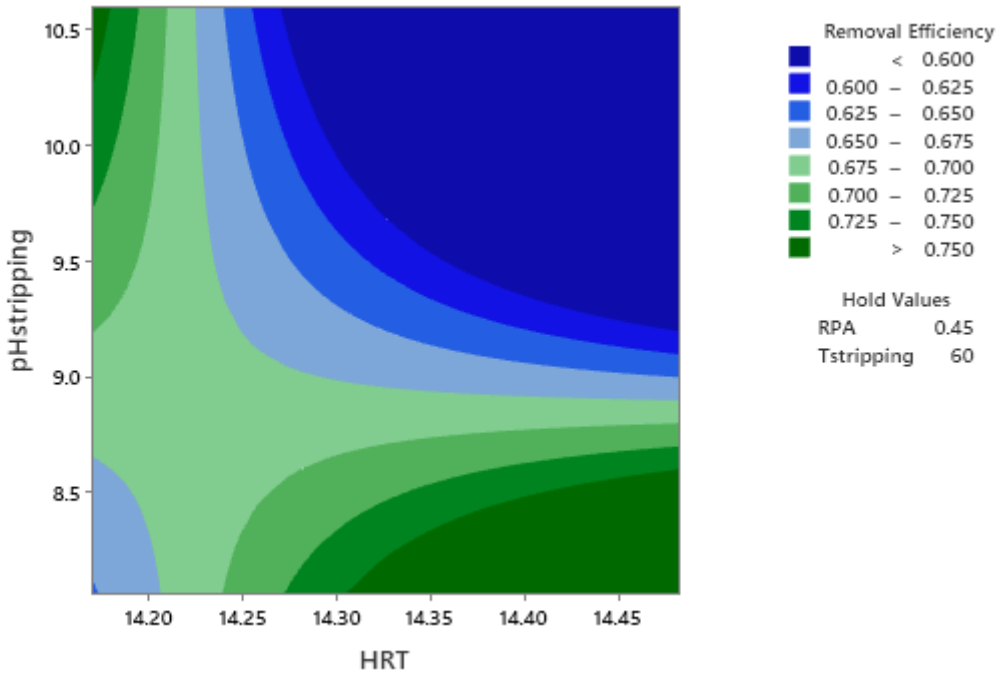

Figure 3.10: Contour plot of removal efficiency based on different values of HRT and pH

What immediately appears from the figure is the lack of a linear correspondence between each single factor and the response. Recalling the expected trends of Figure 3.9, the removal efficiency should be directly influenced by the pH and inversely by the HRT. However, these trends are satisfied only in the region of high pH and low HRT. For the upper part of the graph, the efficiency improves when decreasing the HRT at a fixed pH. Conversely, in the lower part, the behaviour is reversed. Similarly, on the left part of the chart, increasing the pH raises the efficiency, with a flipped effect on the right part. Two imaginary lines at pH of around 8.8 and HRT of around 14.15 h define the inversion of the trends for the two factors. The result seems surprising and probably derived from the significant interaction between the pH and the HRT.

The second contour plot, presented in Figure 3.11, shows the ratio of the purge and air flowrates R_{PA} on the abscissa and the temperature on the ordinate. The HRT and the pH are fixed at the average values of 14.32 h and 9.13. This latter does not consider the contribution of Test 6 (average pH of 10.32) since the goal is pH containment, possibly avoiding the high costs of soda. Even in this chart, the expectations are just partially fulfilled. A temperature improvement positively affects the removal efficiency, with values above 70% in the case of T above 65 °C. However,

Figure 3.9 indicated a beneficial effect of low R_{PA} values, here denied by the plot. By decreasing the R_{PA}, the removal efficiency remains constant or decreases. A possible cause can be attributed to the interaction effect, but it more probably derives from the HRT influence. To this purpose, Figure 3.12 is depicted, where the HRT value is set to the optimum theoretical condition of 14.17 h. The pH is intentionally kept constant and not increased to respect cost limitations.

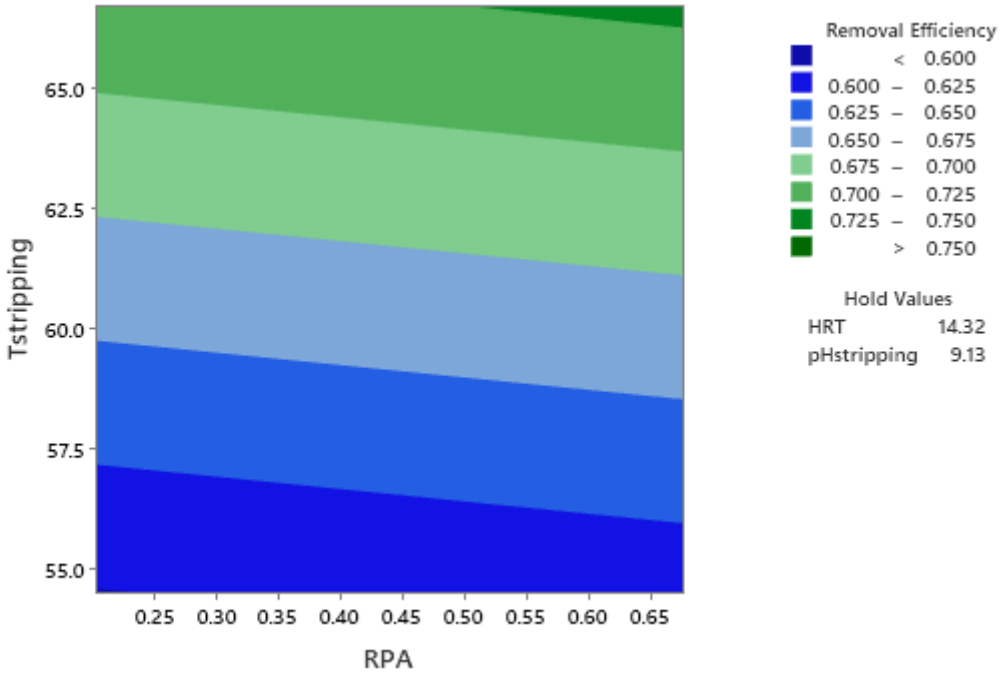

Figure 3.11: Contour plot of removal efficiency based on different values of R_{PA} and T

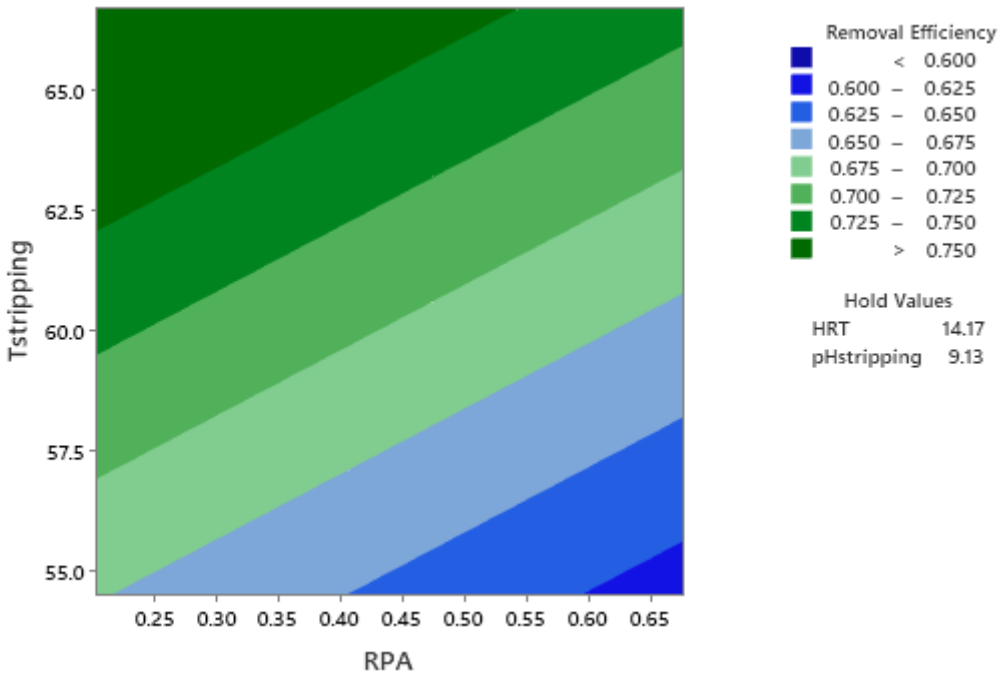

Figure 3.12: Contour plot of removal efficiency based on different values of R_{PA} and T, with an HRT of 14.17 h

The HRT setting to optimum conditions creates the envisaged pattern of the response. Indeed, a growth of the removal efficiency is observed with low R_{PA} values and elevated temperatures, up to values higher than 75%. The obtained chart strengthens the influence of the HRT on the final response, validating the outcome of the Pareto chart.

Another focus is the removal efficiency evaluation as the R_{PA} and the pH vary. The HRT is initially set at the average value of 14.32 h and the temperature at 60 °C. Figure 3.13 displays the isolines. Similarly to Figure 3.11, by reducing the values of the R_{PA}, the efficiency lowers too. In this case, the isolines are narrower than before, meaning that the R_{PA} effect on the response is more contained. Moreover, the main surprising result is the lowest efficiency above pH values of 9.7. This strongly differs from expectations and may lead to wonder about the validity of the model. However, it reflects the system complexity, outlined by all the interactions between the factors. To understand the HRT influence, the contour plot depicted in Figure 3.14 is presented, with the optimum theoretical condition of 14.17 h.

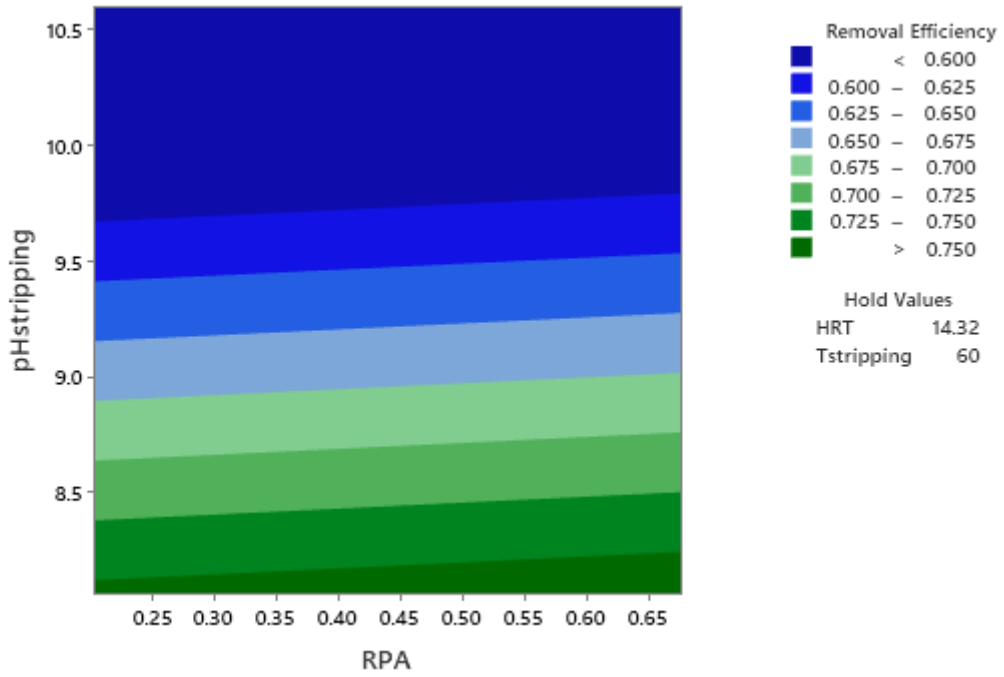

Figure 3.13: Contour plot of removal efficiency based on different values of R_{PA} and pH

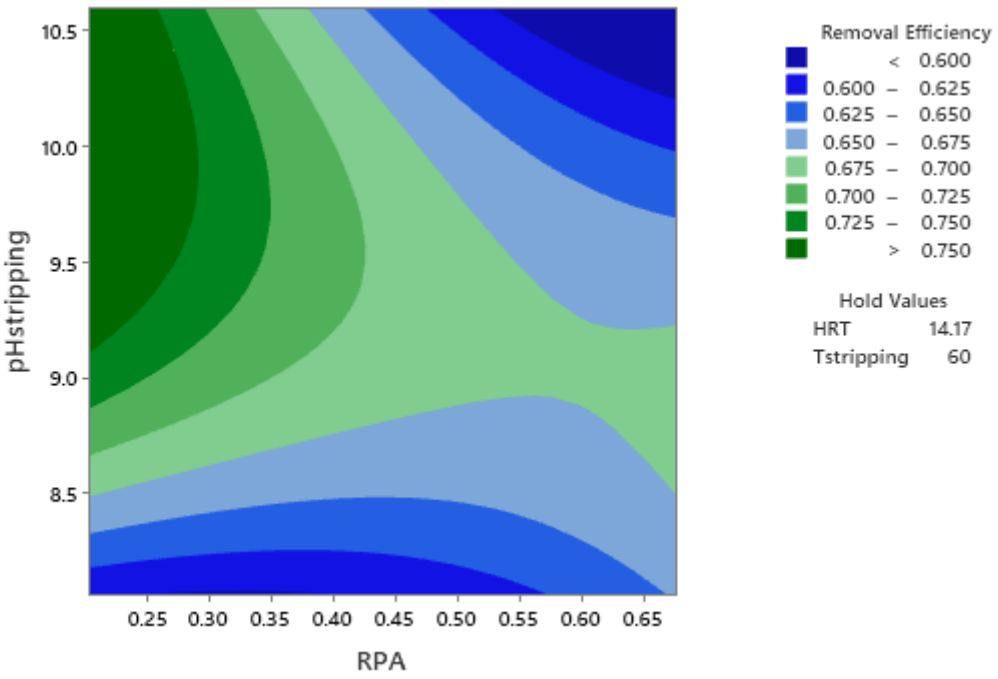

Figure 3.14: Contour plot of removal efficiency based on different values of R_{PA} and pH, with an HRT of 14.17 h

Figure 3.14 shows a different trend from Figure 3.13. The temperature is kept constant between the two charts to evaluate the HRT impact only. Here, the efficiency attains values above 75% by combining low R_{PA} with high pH levels, confirming what emerged from Figure 3.9. However, increasing removals are linked to decreasing R_{PA} only in the case of high pH. For pH levels below 8.5, the efficiency falls or remains constant at most. When dealing with low R_{PA} values, a pH rise guarantees an improvement of the response, whereas, for higher R_{PA} values, the result is mirrored around a pH value of 9.0. Summarizing, the main upshot of this chart is the evidence of the strong HRT significance.

The fourth situation presented through the contour plot is the R_{PA} and HRT combination. The temperature is kept at the average value of 60 °C, as well as the pH of 9.13. Looking at the plot reported in Figure 3.15, the expected trend is immediately matched. Indeed, by working at low HRT and R_{PA} conditions, the efficiency reaches its maximum of above 72.5%. The enthralling observation is the wide presence of efficiency isolines below 70% inside the selected domain. A plausible reason may rely in the need for higher T and pH levels, or even on a particular effect created by the interactions between the factors. Thus, it would be worth further investigation. However, a reduction in the R_{PA} increases the removal by 5% in the lower part and decreases by more than 5% in the upper part. For an average HRT value of 14.32 h, the efficiency is not affected by the R_{PA}. When the ratio between the purge and air flowrate is fixed, the HRT inversely

influences the efficiency, apart from R_{PA} values higher than 0.61, where the response is independent from the HRT level.

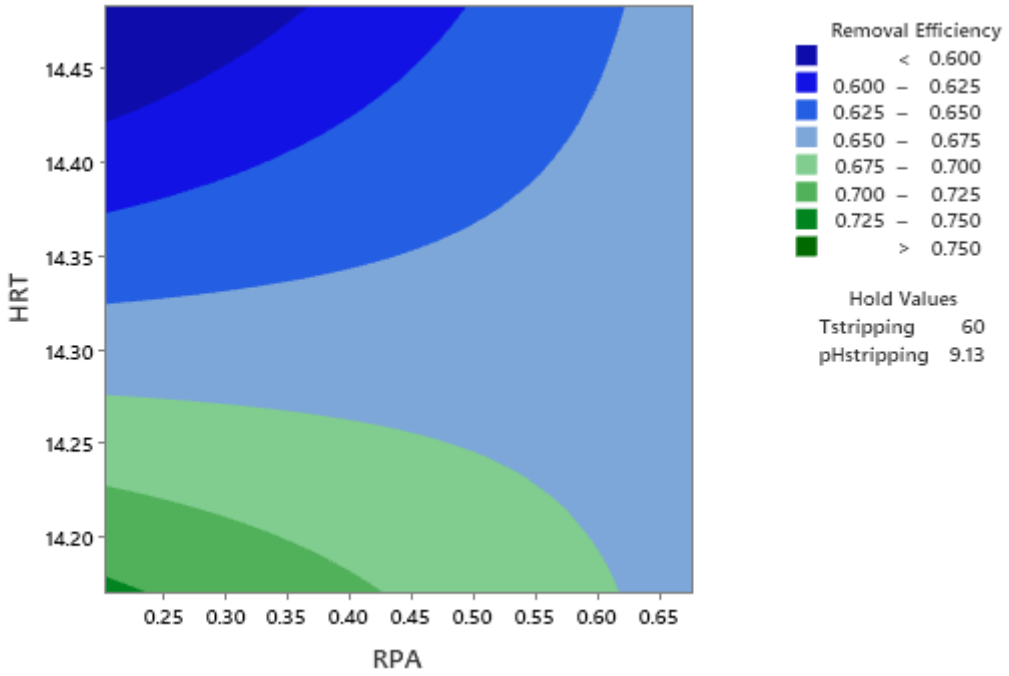

Figure 3.15: Contour plot of removal efficiency based on different values of R_{PA} and HRT

The evaluation of the contour plot with isolines as a function of the temperature and the pH represents an interesting situation, especially because these two factors were considered the most influential by the literature. The pattern presented in Figure 3.16 recalls Figure 3.13, not for the shape of the isolines but rather for their width. Indeed, narrow profiles appear, quickly switching from efficiencies below 60% to ones higher than 75%. In both cases, the top part of the plot is characterized by a wide portion of the lowest removals. This means that the temperature does not influence the removal for a pH above 9.7, respecting the expected trend just below that level. As known, a pH rise must increase the removal, and the result of the chart is completely opposite. To cope with that, as in the previous cases, the HRT influence is examined by lowering the factor to the optimum theoretical condition of 14.17 h. The outcome is displayed in Figure 3.17. The R_{PA} is fixed at the average value of 0.45 and kept constant among the two figures.

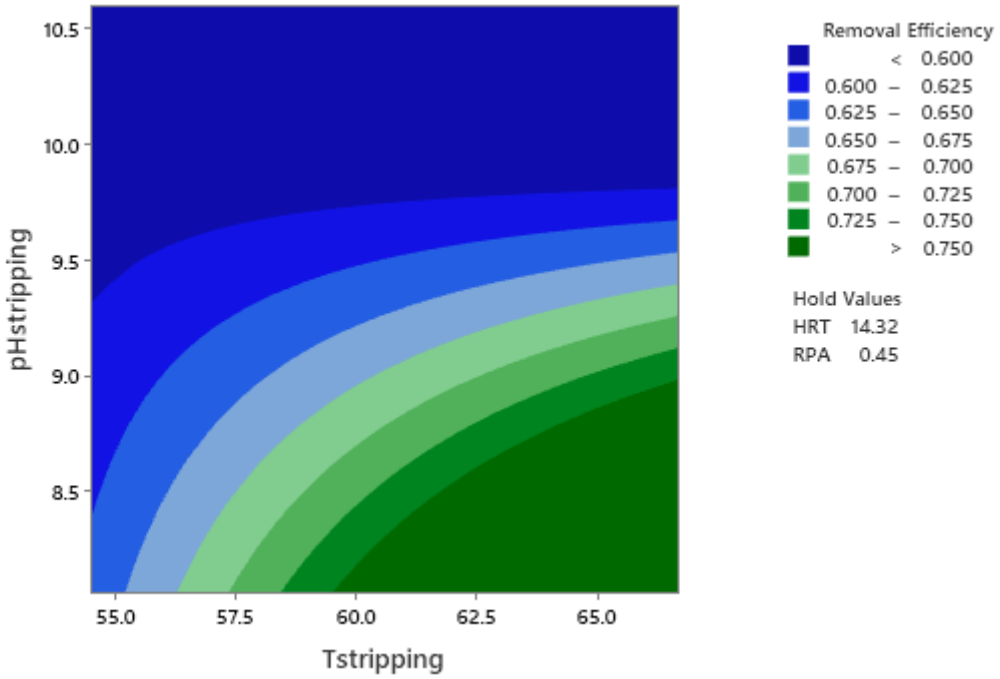

Figure 3.16: Contour plot of removal efficiency based on different values of T and pH

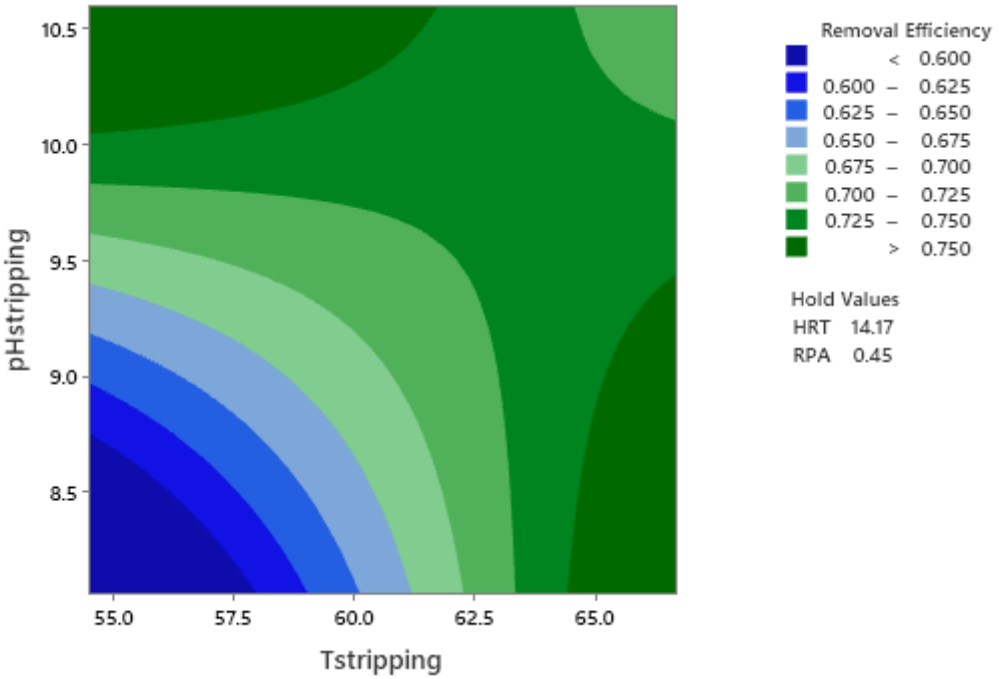

Figure 3.17: Contour plot of removal efficiency based on different values of T and pH, with an HRT of 14.17 h

The pattern resulting from Figure 3.17 strongly differs from the one reported in Figure 3.16, corroborating the strong influence of the HRT. Indeed, the trend now becomes similar to the first case presented (Figure 3.10). A removal improvement is observed through the pH growth at low temperatures, reversing the trend in the case of values close to 65 °C. On the contrary, an increase in the temperature positively affects the efficiency for low pH, switching the effect for values

above 10. However, the response changes in the top and right parts of the chart of just 5% or slightly more, different from more than 15%, resulted in the bottom and left part of the plot. As in the case of Figure 3.10, two imaginary lines at pH 10 and T of 64 °C define the inversion of the influence of the two factors. It is interesting to note that the maximum levels of pH and T do not lead to the highest removal efficiency. This may be the result of the complex interacting effects of all the factors and should be verified on the plant with a new test. If the result presented in the plot is confirmed by the experimental test, it would allow reaching efficiencies above 75% by raising the temperature above 65 °C saving chemicals for the pH basification or by increasing the pH value up to 10.5, without particularly heating the liquid fraction.

The last situation presented describes the removal efficiency variation by changing the temperature and the HRT. The R_{PA} and the pH levels are set at the average of 0.45 and 9.13, respectively. The result displayed in Figure 3.18 respects the expected trend of Figure 3.9. Indeed, a temperature increase, and an HRT reduction, beneficially reflect on an efficiency improvement, attaining maximum values higher than 75%. What emerges is the bands' steepness, suggesting an influential effect of the temperature for the reported set of conditions.

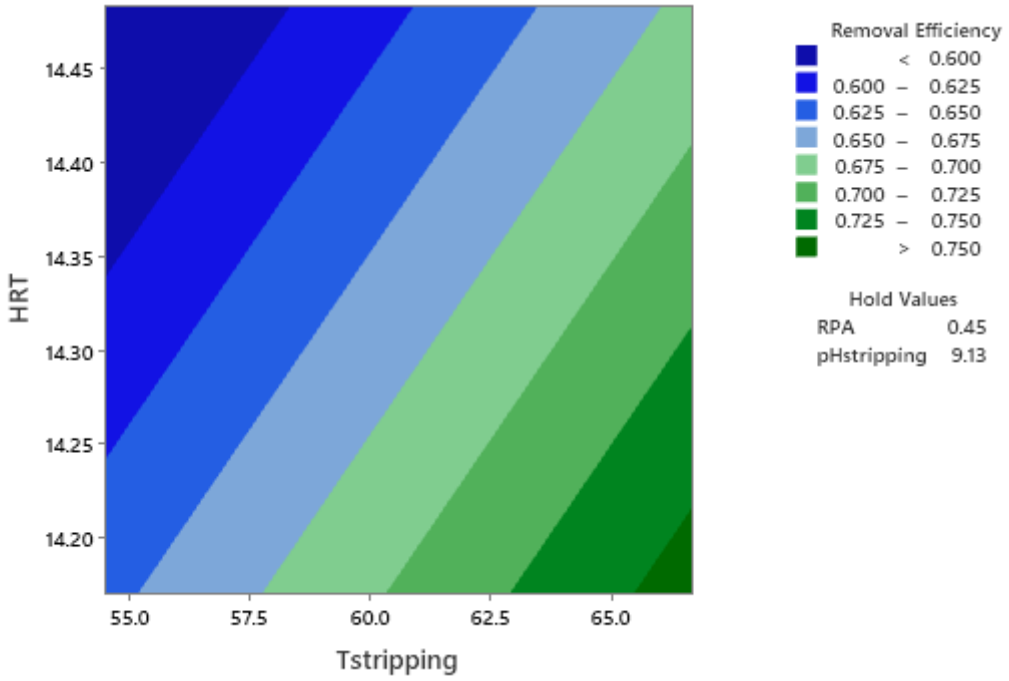

Figure 3.18: Contour plot of removal efficiency based on different values of T and HRT

Summarizing the key outcomes of all the presented cases, the contour plots strongly display the huge complexity of the system, especially caused by the multiple effects of the factors' interactions. Indeed, in the situation described, the removal efficiency was influenced not only by the couple of varying factors and their combined effect, but also by the levels of the fixed factors and their

interaction with each variable reported in the axis. The HRT influence on the response claimed the significance of this operating variable. However, the upshot derived from this statistical analysis should be verified *on-field* with other sets of experiments to better understand the accuracy of the fitted model and to corroborate the adequacy of the results.

3.2.3. Optimization Problem

As explained in the previous subchapter, the interactions between the factors strongly change the envisaged effect of each single factor on the response. The contour plots help the designer to graphically reveal the efficiency pattern and the connected subsets of factors. However, a variation in one factor may completely upset the interpretation, making an optimization process difficult. In this context, the removal efficiency targeting or maximization procedure needs an *ad-hoc* tool that considers the combination of all the variables and their mutual effects. To this purpose, Minitab offers the possibility to cope with that. The idea is to highlight the conditions that attains a target removal efficiency threshold to evaluate the economic feasibility as well as the basic design of the full-scale plant. The features of the optimization problem are reported in Table 3.8, together with the values of the factors composing the solution. The threshold efficiency is assumed at 70%, as an acceptable result from the economic and process perspectives. The graphical solution is presented in Figure 3.19.

Table 3.8: Features and solution of the response optimization procedure

Response	Removal Efficiency
Goal	Target value
Target	70%
Factors and Optimum Levels	
HRT [h]	14.17
R_{PA} [-]	0.39
T stripping [°C]	60.00
pH stripping [-]	9.13

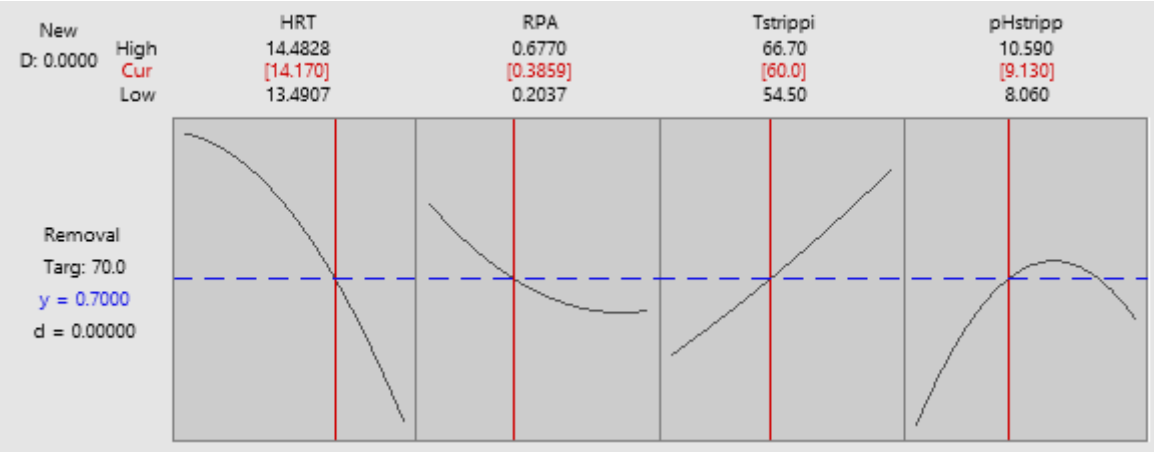

Figure 3.19: Set of factors for the response optimization to the target value of 70%

The trends reported in Figure 3.19 are slightly different from the main effects plot of Figure 3.9. The reason is the Minitab ability to consider, in this case, the combined effects of the factors. The HRT is set at 14.17 h as it is one of the most influential variables. Higher values would have reduced the efficiency but decreased the pumping energy requirements. However, since the HRT is extremely significant, the choice to set it at low values is preferred to obtain the target efficiency. The temperature and the pH are fixed at 60 °C and 9.13 as average initial values. A pH containment is the first requirement to be satisfied, avoiding high costs for chemicals. With these limitations, an efficiency of 70% is obtained with an R_{PA} value of 0.39. This solution is easily achievable in the plant and should be evaluated to confirm the result. However, as second trial, the temperature can be lowered to 55 °C, reducing the need for heating. The result is an efficiency decrease that must be balanced through an HRT and R_{PA} reduction. As reported in Figure 3.20, by setting HRT and R_{PA} values of 14 h and 0.3 respectively, the efficiency is close to 72%. The two presented solutions witness the possibility of reaching the threshold response value with contained costs, corroborating the goodness of the plant design and of the carried test.

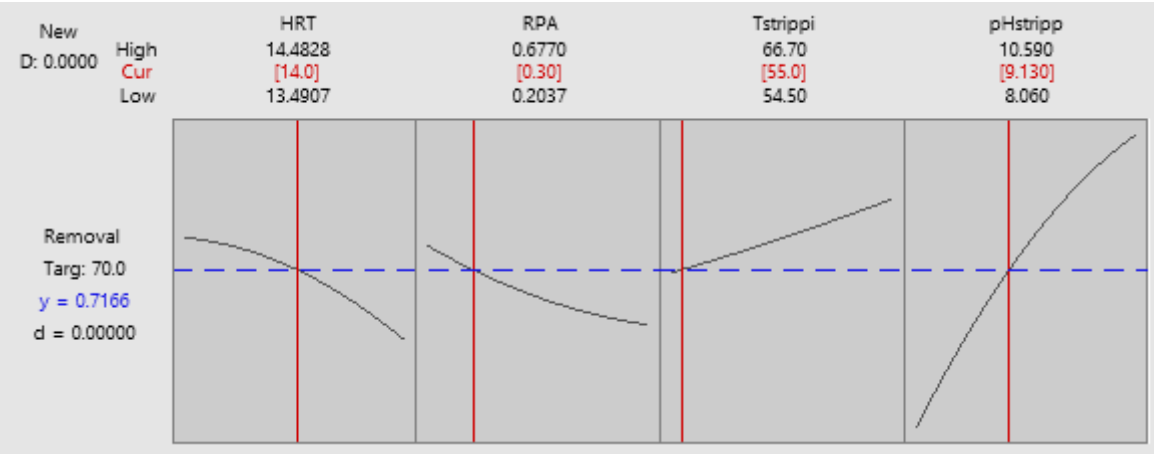

Figure 3.20: Set of improved factors for the response optimization to the target value of 70%

Chapter 4

PLANT UPSCALING

Chapter 4 aims to design the stripping and absorption reactors to reach the target removal efficiency of 70%. The optimum conditions found in Chapter 3 are exploited to define the geometrical features and to calculate the liquid and gas streams that interact with the plant. The diameter of the air bubble reactor is derived by the use of the aspect ratio. Moreover, the specific air flowrate introduction allows the obtaining of the air and purge flowrates. Once done, the power requirement to heat the inlet liquid and air is assessed, accounting for the seasonal variability. However, the energy mix definition to meet the plant demand is not considered. Looking at the scrubber unit, three columns in parallel are assumed. Furthermore, the equilibrium and operating lines are displayed to find the number of theoretical stages needed to satisfy the process through the McCabe-Thiele graphical construction. The height of each packed column is then calculated through the height of the theoretical stages. Finally, the evaluation of the liquid volume entering the scrubber, coupled with the Eckert diagram for packed columns, lead to the diameter estimation. It is worth precising that the outcomes from this chapter should be studied under a cost-benefit perspective to discover possible improvements by containing the costs.

4.1. Air Bubble Stripping Reactor

The stripping reactor represents the first part of the ammonia removal process. However, before designing, it is crucial to define the inlet conditions. The full-scale plant is intended to operate continuously with a liquid inlet flowrate of 100 m^3/d, characterized by the conditions presented in Table 2.1. Since the flowrate is roughly 100 folds the pilot plant one, the strong presence of the TSS may pose some problems in the up-scaling process, requiring separation improvement. Moreover, to cope with the high carbonate concentration, the realization of a CO_2 stripping reactor prior to ammonia removal may be necessary, especially to generate a CO_2 stream reusable in the chemical industry or stored underground in a long-term perspective. Despite this, the CO_2 stripping realization would require a cost-benefit analysis, and for this reason, it is left outside of the thesis. The operative conditions of the air bubble stripping reactor for the ammonia removal are chosen as the ones in Table 3.8, able to ensure an efficiency of 70%. Another possible set of parameters is reported in Figure 3.20, with a temperature of 55 °C, but the lack of any experimental test in these conditions forces to maintain the values of Figure 3.19. Indeed, a temperature of 55 °C was only

tested in Test 5, but with different R_{PA} values. A pH of 9.13 is sufficient to attain high removals, even without soda addition or CO_2 stripping. The design HRT, R_{PA}, and T values are set at 14.17 h, 0.39, and 60 °C, respectively. It is highlighted that the best design solution from the experience would suggest creating two reactors in series. With this configuration, the residence time of the liquid would match the real set HRT. Indeed, in the case of one single reactor, part of the liquid may remain in the reactor for less or more than the set time due to the recirculation. Nevertheless, the presented design considers one single reactor for the sake of simplicity.

The inlet flowrate of 100 m^3/d (4.17 m^3/h) and an HRT of 14.17 h lead to an estimated liquid volume V_L of 59.04 m^3. To define the geometrical features of the air bubble reactor, the aspect ratio (AR) is introduced. It is defined as the height-to-diameter ratio of the liquid filled in the reactor (H_L/D). The set value is 1.2, below 1.5 to contain the pressure drops. By replacing Equation (8) into Equation (9) and solving with respect to D, the diameter results as 3.97 m, approximated to 4 m as the closest commercial diameter.

$$H_L = \frac{V_L}{A} = \frac{V_L}{\left(\frac{\pi \cdot D^2}{4}\right)} \tag{8}$$

$$D = \frac{H_L}{AR} \tag{9}$$

The area obtained with a diameter of 4 m is 12.57 m^2. The calculation of the H_L easily results by dividing the liquid volume for the area and accounts for 4.70 m. However, the product of the diameter and the AR value is 4.80 m. Even if the two values are close, 4.80 m is chosen as a factor of safety. To determine the total height H of the reactor, it is worth remembering that the volume occupied by the air and the liquid in the pilot plant was equal. For this reason, the total height is simply calculated by doubling the height of the liquid, thus reaching 9.60 m. The corresponding total volume of the reactor is 120.64 m^3. The results are summarized in Table 4.1.

Table 4.1: Geometrical features of the full-scale air bubble reactor for ammonia stripping

Plant feature	Value
Liquid Flowrate [m^3/d]	100
HRT [h]	14.17
Liquid Volume V_L [m^3]	59.04
Aspect Ratio (AR)	1.2

Diameter [m]	4.00
Liquid Height H_L [m]	4.80
Total Height H [m]	9.60
Area A [m^2]	12.57
Total Volume [m^3]	120.64

After defining the reactor volume, the specific air flowrate can be calculated. It is expressed as the volume of air added to a unit volume of liquid per minute [$m^3_{air}/(m^3_{liq}\cdot min)$] (Kang et al., 2017). In other words, it represents the air flowrate per unit of liquid volume in the reactor. The value is assumed of around 1.50, equal to the pilot scale case, having a Q_A of 50 m^3/h and a liquid volume of 0.56 m^3. The full-scale V_L in the air bubble reactor is 59.04 m^3, leading to an air flowrate of 5314 m^3/h. With a set purge-to-air flowrate ratio R_{AP} of 0.39, the corresponding purge flowrate Q_P is 2072 m^3/h.

About the power needed for liquid heating, the heat requirement is determined by considering the inlet solution mass flowrate, and not the volume inside the reactor. Thus, the contribution of the mass kept warm inside the reactor is not considered. The liquid density is chosen as 970 kg/m^3, according to Kang et al. (2017), leading to a mass flowrate of 4041.67 kg/h. The temperature gap to be covered seasonally varies. The digestors located in Bassano del Grappa work in mesophilic conditions. During winter, it is assumed a T drop to 30 °C after the liquid-solid digestate separation, whereas in the summer period, the temperature falls to 40 °C. Equation (10) provides the formula to obtain the power needed, where $\dot{m}$ is the mass flowrate, c_p the water specific heat of 4186 J/(kg·°C), T_s and T_{in} the stripping and inlet temperatures. This latter differs from winter to summer, and for this reason, two contributions are calculated, leading to 141 kW and 94 kW, respectively.

$$P = \dot{m} \cdot C_p \cdot (T_s - T_{in}) \tag{10}$$

Moreover, the result should be increased to account for the pre-heating of the make-up air from the ambient to the process temperature. Equation (10) can be used once more, replacing T_s and T_{in} with the air stripping and air inlet temperatures. An air mass flowrate of 2528 kg/h is derived by considering the Q_P of 2072 m^3/h and a density of 1.22 kg/m^3 at 15 °C and 1 atmosphere (Wikipedia, 2023). The dry air specific heat at 25 °C and 1 bar is 1006 J/(kg·°C) (Engineering ToolBox, 2023a). The temperature of the air inside the loop is assumed to be 60 °C, whilst the ambient condition is averaged at 15 °C. The result of the calculation is 31.72 kW, which must be added to the previous

consumption for the inlet heating. The outcomes are summarised in Table 4.2, Table 4.3, and Table 4.4.

Table 4.2: Air flowrates of the full-scale air bubble reactor for ammonia stripping

Plant feature	Value
Specific Air Flowrate [$m^3_{air}/(m^3_{liq} \cdot min)$]	1.50
Air Flowrate Q_A (m^3_{air}/h)	5313.75
R_{AP}	0.39
Purge Flowrate Q_P (m^3_{air}/h]	2072.36

Table 4.3: Power demand for the liquid heating in the full-scale air bubble reactor for ammonia stripping

Plant feature	Value
Liquid Density [kg/m^3]	970
Liquid Mass Flowrate [kg/h]	4041.67
Water Specific Heat at 25 °C and 1 bar [J/(kg·°C)]	4186
Winter Inlet Liquid Temperature Tin [°C]	30
Summer Inlet Liquid Temperature Tin [°C]	40
T stripping [°C]	60
Winter power required [kW]	140.99
Summer power required [kW]	93.99

Table 4.4: Power demand for the air heating in the full-scale air bubble reactor for ammonia stripping

Plant feature	Value
Air Density at 15 °C and 1 atm [kg/m^3]	1.22
Air Mass Flowrate [kg/h]	2528.28
Air Specific Heat at 25 °C and 1 bar [J/(kg·°C)]	1006
Average Inlet Temperature Tin [°C]	15
T air stripping [°C]	60
Power required [kW]	31.72

The power requirement to meet the plant demand may involve different technologies. Surely, the biogas produced in the anaerobic digestion process could be theoretically used in a Combined Heat and Power (CHP) system. However, it is more economically convenient to put the biogas into the grid due to national incentives, by consuming natural gas. Looking at other renewable sources, a group of photovoltaic system could be implemented. Anyway, the calculation of the needed photovoltaic surface is left out of the thesis.

4.2. Packed Column Scrubber for Ammonia Absorption

The height and diameter determinations of the packed columns are two essential features of the full-scale plant design. Many other factors, such as gas and liquid velocities, pressure drops, and mass transfer, should be investigated. However, they are left outside of this thesis for the sake of simplicity. In this case, the aim is to introduce the column design, providing effective information for further studies.

4.2.1. Height Calculation

The height of a packed column strongly relies on the number of equivalent theoretical stages (NETP) and the height of each equivalent theoretical stage (HETP). In this context, the definition of the equilibrium and operating lines is of primary importance. Equation (11) reports the general expression of the equilibrium line, where y_{NH3} and x_{NH3} indicate the ammonia molar fraction in the

gas and the liquid at equilibrium, H_{NH3} the Henry's law constant, and p the working pressure. Equation (12) describes the material balance (i.e., the operating line on a y vs x graph), where y_{NH3} and $y_{NH3,u}$ express the ammonia molar fractions in the gas inside the column and in the outlet, L and G the liquid and vapor molar flowrates, x_{NH3} and $x_{NH3,e}$ the ammonia molar fraction in the liquid inside the column and in the inlet. The scrubber is designed to work with three packed columns in parallel to manage maintenance problems or malfunctions.

$$y_{NH3} = \frac{H_{NH3}}{p} x_{NH3} \tag{11}$$

$$y_{NH3} = y_{NH3,u} + \frac{L}{G}(x_{NH3} - x_{NH3,e}) \tag{12}$$

The equilibrium line is defined once the H and p values, representing the slope of the straight line in the y vs x graph, are set. For this study, Henry's constant is 0.93 atm/(mole fraction) at 25°C (Sander, 2023), whereas the scrubbing pressure corresponds to 1 atm. The operating line requires the knowledge of $y_{NH3,e}$, i.e., the NH_3 molar fraction in the gas phase at the scrubber inlet. To cope with that, the molar flowrate of the ammonia removed in the stripping reactor is derived from Equation (13), corresponding to the one approaching the scrubber. The value is then divided by the total air molar flowrate that enters the packed columns, retrieved from Equation (14)), leading to a $y_{NH3,e}$ value of $2.48 \cdot 10^{-3}$. The temperature and the pressure are 331 K and 1 atm, respectively. The fact that $y_{NH3,e}$ is below $5 \cdot 10^{-3}$ indicates that the system can be assumed as diluted. However, the calculations will be referred to the inert liquid and gas molar flowrates ($\bar{L}, \bar{G}$) to consider any possible uncertainty. In this case, molar ratios must be used instead of molar fractions, but the amounts are so small that the two expressions coincide. For the sake of simplicity, the gas mixture is assumed to contain NH_3 and air only, neglecting the CO_2, VFA, and other contributions. Finally, supposing a full-scale scrubbing efficiency of 85%, the NH_3 molar ratio in the gas phase at the outlet $Y_{NH3,u}$ results in $3.72 \cdot 10^{-4}$. The low value witnesses the goodness of the treatment.

$$\dot{n}_{NH3,gas} = Q_{in,stripper} \cdot C_{NH3,in,stripper} \cdot \eta_{stripper} \cdot \frac{1}{MM_{NH3}} = \tag{13}$$

$$= 100 \frac{m^3}{d} \cdot 2825 \frac{g_{NH3}}{m^3} \cdot 0.70 \cdot \frac{1}{17} \frac{mol_{NH3}}{g_{NH3}} \cdot \frac{1}{24} \frac{d}{h} \cdot \frac{1}{1000} \frac{kmol}{mol} = 0.48 \frac{mol_{NH3}}{h}$$

$$\dot{n}_{air,gas} = \frac{Q_{air} \cdot p}{R \cdot T} = \frac{5313.75 \frac{m^3}{h} \cdot 1\ atm}{8.02 \cdot 10^{-5} \frac{m^3 \cdot atm}{mol \cdot K} \cdot 331\ K} \cdot \frac{1}{1000} \frac{kmol}{mol} = 195.64 \frac{kmol_{air}}{h} \tag{14}$$

Regarding the single-column inert gas molar flowrate $\bar{G}$ of 65.21 kmol/h, it is exactly the result of Equation (14) divided by 3, which is the total number of packed columns. On the other hand, the liquid stream entering the scrubber consists of a solution made up of 50%$_{w/w}$ sulphuric acid from a tank, plus the recycled portion from the scrubber outlet. To better understand, Figure 4.1 illustrates the situation.

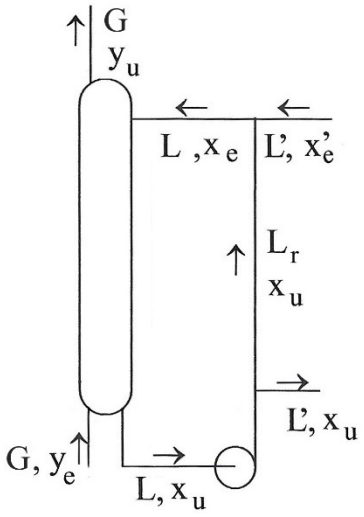

Figure 4.1: Schematic representation of the streams in the scrubber (Adapted from Bertucco et al., 2023)

Assuming the single-column flowrate of the sulphuric acid 50%$_{w/w}$ solution equal to 3 m^3/h, the related mass flowrate is 4173.00 kg/h due to a density of 1391.00 kg/m^3 at 25 °C (Handymath, 2023). Since the solution contains H_2SO_4 in 50%$_{w/w}$, both the acid and water mass flowrates account for 2086.50 kg/h. In molar terms, 21.28 and 115.92 kmol/h, respectively. However, it is important to note that not all moles of the acid can be considered to be inert. Indeed, part of the H_2SO_4 reacts with the ammonium to form ammonium sulphate. As shown in Equation (5) from Chapter 1, one mole of sulfuric acid reacts with two moles of ammonia. Therefore, the amount of acid consumed is half of the moles removed in the packed tower. With a scrubbing efficiency of 85% and an inlet single-column ammonia gas molar flowrate of 0.16 kmol/h (0.48 kmol/h divided in the three columns), the acidic consumption flowrate ranges around 0.07 kmol/h. Thus, the inert acidic flowrate in the 50%$_{w/w}$ solution is 21.21 kmol/h, leading to a total $\bar{L}'$ of 137.13 kmol/h when added to the water. Lower values would reduce the costs due to contained injection, while higher values would limit capital costs by reducing the number of necessary stages and the total column height. Thus, the chosen single-column flowrate of 3 m^3/h is considered a compromise and a reasonable value for the full-scale plant.

With reference to the total mass balance around the splitter, Equation (15) allows to calculate the inert molar flowrate of the liquid entering the scrubber. The recycle ratio R, expressing the ratio between the recycled and total inert molar flowrates ($\bar{L}_r/\bar{L}$) is set at 10%. Hence, the result of the balance is $\bar{L}_r$ and $\bar{L}$ values of 15.23 kmol/h and 152.36 kmol/h, respectively.

$$1 = \frac{\bar{L}'}{\bar{L}} + R \tag{15}$$

To complete the data needed to display the operating line, the ammonia liquid molar ratios at the inlet (X_e) and the outlet (X_u) must be derived. An iterative process is performed based on the ammonia material balance around the mixer, reported in Equation (16), and the operating line of Equation (12). Since the ammonia absence in the sulphuric acid 50%$_{w/w}$ solution, X_e' is null, deleting the $\bar{L}'$ contribution. After a couple of iterations started with X_e=0, the obtained X_e and the X_u are $1.00 \cdot 10^{-4}$ and $1.00 \cdot 10^{-3}$, respectively. The key outcomes thus far are summarized in Table 4.5. It is important to note that, in reality, the X_u value is likely lower as ammonia reacts with sulphuric acid to form ammonium sulphate. However, for reasons of simplification, this process is not evaluated due to the strong dependence of the reaction kinetics on the temperature and interactions with the other elements in the system.

$$\bar{L} \cdot X_e = \bar{L}_r \cdot X_u + \bar{L}' \cdot X_e' \tag{16}$$

Table 4.5: Values of the parameters required in the equilibrium and operating lines per each packed column

Equilibrium Line	
Henry's Constant H [atm/mole fraction]	0.93
Scrubber Pressure p [atm]	1
Operating Line	
NH_3 Molar Ratio in the Inlet Gas Ye [-]	$2.48 \cdot 10^{-3}$
NH_3 Molar Ratio in the Outlet Gas Yu [-]	$3.72 \cdot 10^{-4}$
Inert Gas Molar Flowrate $\bar{G}$ [kmol/h]	65.21
NH_3 Molar Ratio in the Inlet Liquid Xe [-]	$1.00 \cdot 10^{-4}$
NH_3 Molar Ratio in the Outlet Liquid Xu [-]	$1.00 \cdot 10^{-3}$
Inert Liquid Molar Flowrate $\bar{L}$ [kmol/h]	152.36

Once defined all the necessary elements, the equilibrium and the operating line expressed in Equation (11) and Equation (12) can be graphically displayed. The operating line alternately links points associated with the inlet/outlet gas and outlet/inlet liquid conditions from each stage, as for the couple (X_e, Y_u) or (X_u, Y_e). On the other hand, the equilibrium line hinges on the assumption that the outlet gas molar ratio is in equilibrium with the outlet liquid molar ratio of the same stage. In other words, Y_u*(X_u). These concepts are inbuilt inside the McCabe-Thiele graphical method, presented in Figure 4.2. Starting from the point (X_u, Y_e) that lies on the operating line, two stages (NETP) are enough to reach the minimum outlet gas molar ratio Y_u, satisfying process needs. The condition for the process to proceed is that the operating line always stays above the equilibrium line, ensuring the driving force. As shown in the graph, this is clearly respected.

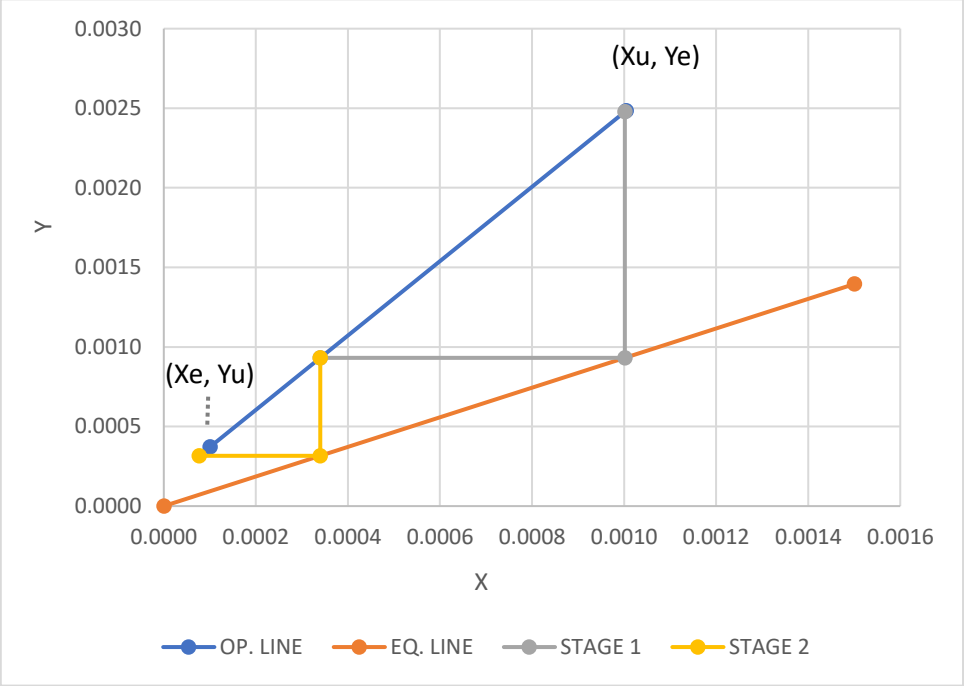

Figure 4.2: Calculation of the number of ideal stages according to the McCabe-Thiele method

Once the number of equivalent theoretical stages (NETP) is obtained, the height of the packed column Z results from the expression reported in Equation (17). Moreover, Bertucco et al. (2023) indicate a height of each equivalent theoretical stage (HETP) of 1 m in the case of random-packed columns, implying a total height of 2 m.

$$Z = NETP \cdot HETP \tag{17}$$

4.2.2. Diameter Calculation

To determine the diameter of each packed column, the inlet liquid flowrate definition becomes crucial. In the previous subchapter, all the flowrates were indicated in molar terms, apart from $\bar{L}'$, assumed of 3 m^3/h for each column. In particular, the molar flowrates of water and acid serve as effective tools for evaluating the liquid composition. By recalling what was already explained in Chapter 4.2.1., the two aforementioned contributions in $\bar{L}'$ account for 115.92 kmol/h and 21.21 kmol/h, respectively. Since these represent inert quantities, the ratio remains constant even in the stream $\bar{L}$ after the mixing, as well as in the recycled stream $\bar{L}_r$. By dividing the two flowrates, the result is 5.46, meaning that for each mole of acid, there are 5.46 moles of water. Thus, the inert liquid molar flowrate $\bar{L}$ entering the scrubber (152.36 kmol/h) consists of 23.56 kmol/h of sulphuric acid and 128.80 kmol/h of water. In mass terms, 2311.27 kg/h and 2318.11 kg/h, respectively. The values align with a 1:1 acid-to-water ratio, except for acid mass used in ammonium sulphate formation. Finally, by summing the acid and water volumetric flowrates obtained through the densities (1830 kg/m^3 and 1000 kg/m^3, respectively), the total liquid entering the scrubber results in 3.58 m^3/h. In this last case, separate densities for individual volumes are used instead of the whole mixture density (1391 kg/m^3).

The liquid volumetric flowrate entering the scrubber is essential in the diameter calculation. The Eckert diagram, displayed in Figure 4.3, is used to derive the area of each packed column. In the abscissa, the flow parameter F_{lv} is indicated, whereas in the ordinate, the dimensionless group K is synthesized. The two terms expressions are reported in Equation (18) and Equation (19). Q_L and Q_A represent the liquid and air volumetric flowrates per column, ρ_L and ρ_A the related densities. The Q_A term in this formula refers to the single-column flowrate of 1771.25 m^3/h, obtained by dividing the total 5313.75 m^3/h of Table 4.2 by three. Regarding K, $\dot{m}_A$ describes the air mass flowrate entering each column (0.58 kg/s), A the area, ρ_{H2O} the water density. The values chosen for the liquid and water viscosities μ_L and μ_{H2O} are $5.42 \cdot 10^{-3}$ Pa·s (LabChem, 2012) and $0.89 \cdot 10^{-3}$ Pa·s (Engineering Toolbox, 2023b), respectively. C_f is the packing parameter, experimentally determined, and function of packing shape, size, and material. For this thesis, it is chosen as 130 m^{-1}, related to a plastic Pall Rings packing of 1.5” (38 mm) (Bertucco et al., 2023).

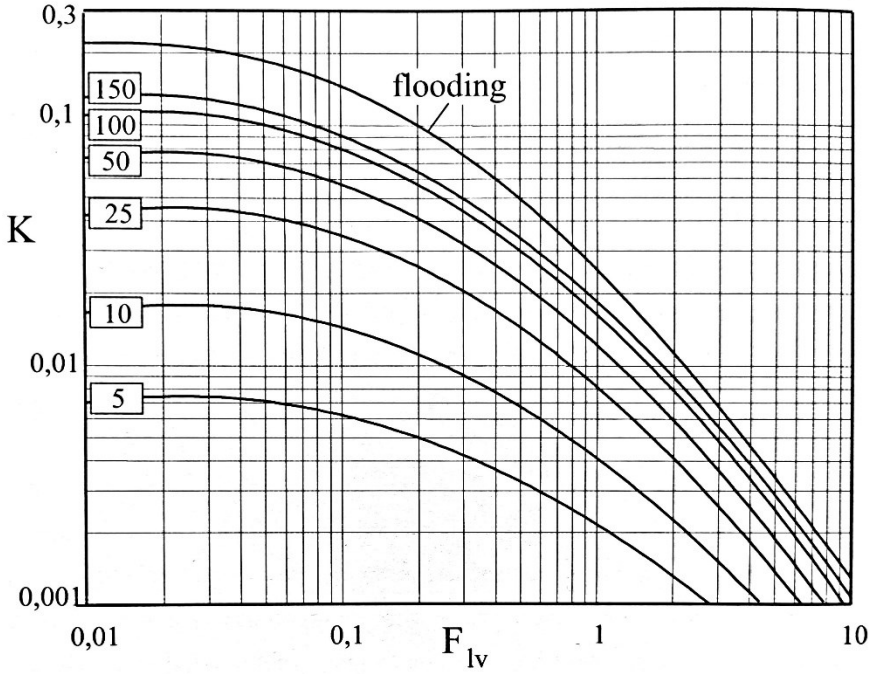

Figure 4.3: Eckert diagram for random packed columns (Bertucco et al., 2023)

$$F_{lv} = \frac{Q_L}{Q_A} \cdot \sqrt{\frac{\rho_L}{\rho_A}} = \frac{3.58\,\frac{m^3}{h}}{1771.25\,\frac{m^3}{h}} \cdot \sqrt{\frac{1391\,\frac{kg}{m^3}}{1.19\,\frac{kg}{m^3}}} = 0.07 \tag{18}$$

$$K = \frac{(\frac{\dot{m}_A}{A})^2 \cdot C_f \cdot \left(\frac{\mu_L}{\mu_{H2O}}\right)^{0.2} \cdot (\frac{\rho_{H2O}}{\rho_L})}{g \cdot \rho_A \cdot \rho_L} \tag{19}$$

Among the several curves reported in Figure 4.3, the flooding represents a condition of rapid increase in pressure drops with simultaneous loss of mass transfer efficiency (Bertucco et al., 2023). Indeed, the channels for the gas flow are so narrow that the gas is forced to bubble into the liquid, becoming a dispersed phase and acting like a bubbling column. Theory suggests correct operations below 80% flooding. Thus, the $K_{flooding}$ obtained from the Eckert diagram is 0.12, leading to a corrected value of 0.10. The area connected to this K is 0.17 m^2, derived through the inversion of Equation 19. The resulting diameter ranges around 0.47 m. However, the design diameter is approximated to 0.50 m for commercial availability, leading to a cross-sectional area close to 0.2 m^2. It is worth noting that the geometrical gas velocity from the ratio between Q_A and A becomes 2.51 m/s, slightly higher than the general *on-field* experience. Finally, Table 4.6 reports the major features designed for each packed column. The design principles outlined in this thesis aim to ease further investigation studies for the full-scale plant realization. Indeed, economic

assessments as cost-benefit analysis may overturn the resulting outcomes, in favour of other more sustainable solutions.

Table 4.6: Features of each packed column

Total Height Z [m]	2
Total Area A [m^2]	0.20
Diameter D [m]	0.50
Liquid Flowrate Q_L [m^3/h]	3.58
Air Flowrate Q_A [m^3/h]	1771.25

Conclusions

This thesis aims to provide useful information on ammonia stripping and absorption technology for the recovery of ammonium sulphate from the liquid fraction of digestate. The pilot plant, composed of around 1 m^3 air bubble reactor for stripping and three scrubbing columns in parallel for the absorption, was fed with the liquid fraction of the OFMSW digestate. The choice of the air bubble reactor relies on the high %TSS content. Air is used as stripping gas, whereas the scrubbing solution consists of a $50\%_{w/w}$ sulphuric acid solution. Several tests were conducted, each with a set of conditions, to evaluate the changes in the removal efficiency. However, the operating variables consideration for both the stripping and absorption process would provide more accurate results but increasing process complexity.

The analysis of the inlet solution samples showed deviations from the expected values. Indeed, the extended storage in the accumulation tank, coupled with the high summer temperatures, led to the digestion process going on. The result was a pH and NH_4 increase (8.00 and 3448.25 $mg_{NH4\text{-}N}/l$ on average) and an enhanced NH_4 and CO_2 volatilization in the tank due to the temperatures. The pH decrease and the NH_4 concentration rise after the new inlet solution refilling contrasted with the expectation but was explained by the milder autumn temperature that made the volatilization effect more contained. However, the continuous feeding of a full-scale plant would limit this problem.

The evaluation of the *on-field* conditions highlighted sharp deviations of air and purge flowrates from set values, changing the working conditions. The reason was mainly attributable to the installed blower. Nevertheless, a variation reduction from -25% to -10% from set values was observed after the blower substitution. Further drops can be barely reached due to plant normal instability. Besides, the increase in purge flowrate reflected positively on the pH rise since the lower CO_2 presence in the gas stream entering the stripping plant.

The average NH_4 removal efficiencies for each test were always higher than 50%. Low HRT (14.17 h) and raised pH (average of 10.32) outlined a beneficial effect on the removal efficiency, with mean values above 70%. Contained HRT values should influence the energy consumed for pumping, but this trend was not visible from the plant energy monitoring. The reason may rely in the small difference between the tested flowrates. On the contrary, the temperature and the energy absorbed by the resistors for the liquid mass heating were directly linked, suggesting T containment.

The Response Surface Methodology application in Minitab allowed the definition of a model to ease data interpretation and offered the possibility to evaluate the combined effects of the operating variables. After the removal of the outliers, connected to plant malfunctions, the model showed an R^2 of 74.85%, higher than the 70% threshold. Further fitting improvements may be reached after the repetition of some specific measurements, mainly due to lab inaccuracies. The p-value indicated the significance of the HRT and the pH (both p-values of 0.00) and their interaction (p-value of 0.00), corroborating the experimental impact of the two factors on the response. Looking at the single operating variables, the model read an efficiency increase by lowering the HRT and the R_{PA}, although more with the first factor. Smaller HRT values at constant volume imply greater inlet flowrates, providing fresh solution and an ammonia load higher than the one already present inside the reactor. This favoured efficiency. In the case of R_{PA}, higher purge flowrates should increase the removal, by cleaning the air in the loop and decreasing the components partial pressure in the rector. This contrast with the model but the problems connected to the blower and the large flowrate instability ask for more investigations. The pH and the temperature positively influenced the removal, with higher impacts in the first case. However, the choice of pH containment becomes paramount in a cost-benefit perspective. The contour plots demonstrate the system complexity, which is largely influenced by HRT values. Indeed, the interaction of each operating variable with the others broke the linearity of the expected tendency in favour of mixed trends. To cope with that, the optimization process led to a target efficiency of 70% with an HRT of 14.17 h, an R_{PA} of 0.39, a T of 60°C, and a pH of 9.13. Another solution resulted in an HRT of 14.00 h, an R_{PA} of 0.30, a T of 55°C, and a pH of 9.13. This second trial would allow for a reduction in the energy consumption of the resistors. However, the lack of experimental tests conducted in this condition forced the choice of the first solution as a base for the up-scaling procedure.

As for the pilot plant, the full-scale reactor relies on the air bubble type likewise. The inlet liquid flowrate of 100 m^3/d and an HRT of 14.17 h led to a liquid volume of 59.02 m^3. The design hinges on an aspect ratio AR of 1.2 to limit pressure drops, with consequent diameter and total height values of 4.00 m and 9.60 m, respectively. The total reactor volume is occupied half by the liquid and half by the air. This configuration is crucial to avoid the liquid entrance in the air ducts and damage to the scrubber unit. A design improvement would result from the use of two reactors in series to match the set HRT with the real *on-field* value. Nevertheless, this point is left out of the thesis. The heat demand of the plant seasonally varies, with estimated winter and summer power consumptions of 140.99 kW and 93.99 kW, respectively. To these, the power to heat the make-up air must be added. Through the application in full-scale of the pilot-scale specific air flowrate of 1.50 $m^3_{air}/(m^3_{liq} \cdot min)$, the air and purge flowrates were 5313.75 m^3/h and 2076 m^3/h, requiring a

further 31.75 kW. In full-scale, the energy may be provided by implementing a photovoltaic system or through other sustainable technologies left outside the thesis for the sake of simplicity.

The application of the McCabe-Thiele graphical method allowed the scrubber height calculation. Two stages resulted in satisfying the process operative needs. The equilibrium and operating lines definition was solved by assuming a scrubbing efficiency of 85% and with balances around the splitter and the mixer. By considering an HETP of 1 m for packed columns, the total height of each of the three scrubber columns accounted for 2 m. A diameter of 0.5 m was found using the Eckert diagram, with a liquid inlet flowrate of 3.58 m^3/h. Higher flowrates would increase the diameter and reduce the height. However, further costs would be added to buy the liquid sulphuric acid solution. Thus, the proposed solution is accepted as a compromise.

In conclusion, the expected performances of the pilot plant were satisfied. The reached average efficiencies often overcome the set threshold of 70%, with peaks of maximum values above 80% with raised pH. Thus, pH and HRT consideration is critical to ensure high removals. Anyway, pH limitations must be followed to contain operative costs for chemicals. The obtained results provided effective information for the up-scaling process, even if further cost-benefit analyses are required to strengthen the outlined outcomes of this thesis. Finally, the production of a sustainable mineral fertiliser reusable in agricultural has still to be assessed, but this starting point can only lead the way to future circular developments.

References

Agnieszka, U., Małgorzata, K.K., 2022. Properties of Flat Ceramic Membranes and Their Application for Municipal Digestate Liquid Fraction Purification. Journal of Membrane Science and Research 9 (2023) 556692. https://doi.org/10.22079/JMSR.2022.556692.1549

Akhiar, A., Guilayn, F., Torrijos, M., Battimelli, A., Shamsuddin, A.H., Carrère, H., 2021. Correlations between the Composition of Liquid Fraction of Full-Scale Digestates and Process Conditions. Energies 2021, 14(4), 971. https://doi.org/10.3390/en14040971

Akhiar, A., Battimelli, A., Torrijos, M., Carrere, H., 2017. Comprehensive characterization of the liquid fraction of digestates from full-scale anaerobic co-digestion. Waste Management Volume 59, January 2017, Pages 118-128. https://doi.org/10.1016/j.wasman.2016.11.005

Baldi, M., Collivignarelli, M.C., Abbà, A., Benigna, I., 2018. The Valorization of Ammonia in Manure Digestate by Means of Alternative Stripping Reactors. Sustainability 2018, 10, 3073. https://doi.org/10.3390/su10093073

Barampouti, E.M., Mai, S., Malamis, D., Moustakas, K., Loizidou, M., 2020. Exploring technological alternatives of nutrient recovery from digestate as a secondary resource. Renewable and Sustainable Energy Reviews Volume 134, December 2020, 110379. https://doi.org/10.1016/j.rser.2020.110379

Barreiro-Vescovo, S., Barbera, E., Bertucco, A., Sforza E., 2020. Integration of Microalgae Cultivation in a Biogas Production Process from Organic Municipal Solid Waste: From Laboratory to Pilot Scale. ChemEngineering 2020, 4(2), 25. https://doi.org/10.3390/chemengineering4020025

Bertucco, A., Barbera, E., Guarise, G. B. (2023). Separation Unit Operation and Process Simulation. Cleup.

Boehler, M.A., Heisele, A., Seyfried, A., Grömping, M., Siegrist, H., 2014. (NH4)2SO4 recovery from liquid side streams. Environmental Science and Pollution Research Volume 22, pages 7295–7305 (2015). https://doi.org/10.1007/s11356-014-3392-8

Bolzonella, D., Fatone, F., Gottardo, M., Frison, N., 2017. Nutrients recovery from anaerobic digestate of agro-waste: Techno-economic assessment of full scale applications. Journal of

Environmental Management Volume 216, 15 June 2018, Pages 111-119. https://doi.org/10.1016/j.jenvman.2017.08.026

Chandrasekhar, K., Raj, Ramanaiah, S.V., Kumar, G., Banu, J.R., Varjani, S., Sharma, P., Pandey, A., Kumar, S., Kim, S.H., 2021. Algae biorefinery: A promising approach to promote microalgae industry and waste utilization. Journal of Biotechnology 345 (2022) 1–16. https://doi.org/10.1016/j.jbiotec.2021.12.008

Chuda, A., Jastrzabek, K., Zieminski, K., 2022. Changes in the Composition of Digestate Liquid Fraction after Ozone and Ultrasonic Post-Treatment. Energies 2022, 15(23), 9183. https://doi.org/10.3390/en15239183

Engineering ToolBox (2023a). Air - Specific Heat vs. Temperature at Constant Pressure. https://www.engineeringtoolbox.com/air-specific-heat-capacity-d_705.html, last visit: 12/11/2023

Engineering ToolBox (2023b). Water - Dynamic (Absolute) and Kinematic Viscosity vs. Temperature and Pressure. https://www.engineeringtoolbox.com/water-dynamic-kinematic-viscosity-d_596.html, last visit: 18/11/2023

ETRA. (n.d.). B-WaterSmart. https://www.etraspa.it/il-gruppo/progetti-europei/corso/b-watersmart, last visit: 31/08/2023

EUR-Lex. (2023). Council Directive of 12 December 1991 concerning the protection of waters against pollution caused by nitrates from agricultural sources (91/676/EEC). https://eur-lex.europa.eu/legal-content/EN/TXT/?qid=1561542776070&uri=CELEX:01991L0676-20081211, last visit: 31/07/2023

European Commission. (2020). Farm to Fork strategy for a fair, healthy and environmentally-friendly food system. https://food.ec.europa.eu/horizontal-topics/farm-fork-strategy_en, last visit: 11/08/2023

Fertilizers Europe. (2018). Fertilizers Basics. https://www.fertilizerseurope.com/wp-content/uploads/2019/08/Fertilizer_Basics.pdf, last visit: 17/07/2023

Fertilizers Europe. (2019). Farming & Air Quality. https://www.fertilizerseurope.com/agriculture-environment/farming-air-quality/, last visit: 17/07/2023

Fertilizers Europe. (2023a). Fertilizer Industry - Facts & Figures 2023. https://www.fertilizerseurope.com/publications/fertilizers-industry-facts-and-figures-2023-edition/, last visit: 17/07/2023

Fertilizers Europe. (2023b). Forecast of food, farming & fertilizer use in the European Union 2022-2032. https://www.fertilizerseurope.com/publications/forecast-of-food-farming-and-fertilizer-use-in-the-european-union-2022-2032/, last visit: 17/07/2023

HandyMath. (2023). The Complete Aqueous Sulfuric Acid Solutions Density-Concentration Calculator. https://www.handymath.com/cgi-bin/sulfurictble11.cgi?submit=Entry, last visit: 17/11/2023

Herbes, C., Roth, U., Wulf, S., Dahlin, J., 2020. Economic assessment of different biogas digestate processing technologies: A scenario-based analysis. Journal of Cleaner Production Volume 255, 10 May 2020, 120282. https://doi.org/10.1016/j.jclepro.2020.120282

Hidalgo, D., Corona, F., Martín-Marroquín, J.M., del Álamo, J., Aguado, A., 2015. Resource recovery from anaerobic digestate: struvite crystallisation versus ammonia stripping. Desalination and Water Treatment 57(6):1-7. https://doi.org/10.1080/19443994.2014.1001794

International Energy Agency. (2021). Ammonia Technology Roadmap. https://www.iea.org/reports/ammonia-technology-roadmap, last visit: 03/08/2023

International Fertilizer Association. (2023-a). Organic and Mineral Fertilizers. https://www.fertilizer.org/about-fertilizers/organic-and-mineral-fertilizers/, last visit: 02/08/2023

International Fertilizer Association. (2023-b). The Ammonia Technology Roadmap: IFA Summary for Policymakers. https://www.fertilizer.org/resource/the-ammonia-technology-roadmap-ifa-summary-for-policymakers/, last visit: 02/08/2023

IRSA. (n.d.-a). 2000 - PARAMETRI FISICI, CHIMICI E CHIMICO-FISICI. Vol.1 - sez. 2000: Parametri fisici, chimici e chimico-fisici, https://www.irsa.cnr.it/wp/?page_id=5435, last visit: 29/09/2023

IRSA. (n.d.-b). Metodi analitici per le acque, Volume Secondo. Vol. 2 - sez. 4000: Organici non metallici, https://www.irsa.cnr.it/wp/?page_id=5435, last visit: 29/09/2023

Jamaludin, Z., Rollings-Scattergood, S., Lutes, K., Vaneeckhaute, C., 2018. Evaluation of Sustainable Scrubbing Agents for Ammonia Recovery from Anaerobic Digestate. Bioresource Technology Volume 270, December 2018, Pages 596-602. https://doi.org/10.1016/j.biortech.2018.09.007

Kang, J., Kwon, G., Nam, J.H., Kim, Y.O., Jahng, D., 2017. Carbon dioxide stripping from anaerobic digestate of food waste using two types of aerators. International Journal of Environmental Science and Technology volume 14, pages1397–1408 (2017). https://doi.org/10.1007/s13762-017-1250-1

Kar, S., Singh, R., Gurian, P.L., Hendricks, A., Kohl, P., McKelvey, S., Spatari, S., 2022. Life cycle assessment and techno-economic analysis of nitrogen recovery by ammonia air-stripping from wastewater treatment. Science of the Total Environment Volume 857, Part 3, 20 January 2023, 159499. https://doi.org/10.1016/j.scitotenv.2022.159499

LabChem (2012). Sulfuric Acid, 50% v/v Safety Data Sheet. https://www.labchem.com/tools/msds/msds/LC25640.pdf , last visit: 18/11/2023

MASAF (n.d.). DECRETO LEGISLATIVO 29 aprile 2010, n.75 - Riordino e revisione della disciplina in materia di fertilizzanti, a norma dell'articolo 13 della legge 7 luglio 2009, n. 88. https://www.politicheagricole.it/flex/cm/pages/ServeBLOB.php/L/IT/IDPagina/10087, last visit: 04/10/2023

Munasinghe-Arachchige, S.P., Nirmalakhandan, N., 2020. Nitrogen-Fertilizer Recovery from the Centrate of Anaerobically Digested Sludge. Environmental Science & Technology Letters, 2020, 7, 450-459. https://dx.doi.org/10.1021/acs.estlett.0c00355

Myers, R.H., Montgomery, D.C., Anderson-Cook, C.M. (2009). Response surface methodology: process and product optimization using designed experiments - 3rd ed. John Wiley & Sons, Inc.

Our World in Data (2023). Electricity production by source, World. https://ourworldindata.org/grapher/electricity-prod-source-stacked, last visit: 09/08/2023

Palakodeti, A., Azman, S., Rossi, B., Dewil, R., Appels, L., 2021. A critical review of ammonia recovery from anaerobic digestate of organic wastes via stripping. Renewable and Sustainable Energy Reviews Volume 143, June 2021, 110903. https://doi.org/10.1016/j.rser.2021.110903

Peng, P., Pivato, A., 2017. Sustainable Management of Digestate from the Organic Fraction of Municipal Solid Waste and Food Waste Under the Concepts of Back to Earth Alternatives and

Circular Economy. Waste and Biomass Valorization volume 10, pages465–481 (2019). https://doi.org/10.1007/s12649-017-0071-2

Provolo, G., Perazzolo, F., Mattachini, G., Finzi, A., Naldi, E., Riva, E., 2017. Nitrogen removal from digested slurries using a simplified ammonia stripping technique. Waste Management Volume 69, November 2017, Pages 154-161. https://doi.org/10.1016/j.wasman.2017.07.047

RISE Foundation. (2016). Nutrient Recovery and Reuse (NRR) in European agriculture: a review of the issues, opportunities and actions. https://www.researchgate.net/publication/299630294_Nutrient_Recovery_and_Reuse_NRR_in_European_agriculture_a_review_of_the_issues_opportunities_and_actions, last visit 31/07/2023

Rosemount. (2022, March 29). How pH Sensors Work [Video]. YouTube. https://www.youtube.com/watch?v=65r7pJpNT34

Sander, R. (2023). Compilation of Henry's law constants (version 5.0.0) for water as solvent. Atmos. Chem. Phys., 23, 10901–12440. https://doi.org/10.5194/acp-23-10901-2023

Shi, L., Simplicio, W.S., Wu, G., Hu, Z., Hu, H., Zhan, X., 2018. Nutrient Recovery from Digestate of Anaerobic Digestion of Livestock Manure: a Review. Curr Pollution Rep 4, 74–83 (2018). https://doi.org/10.1007/s40726-018-0082-z

Sobhi, M., Guo, J., Gaballah, M.S., Li, B., Zheng, J., Cui, X., Sun, H., Dong, R., 2021. Selecting the optimal nutrients recovery application for a biogas slurry based on its characteristics and the local environmental conditions: A critical review. Science of The Total Environment Volume 814, 25 March 2022, 152700. https://doi.org/10.1016/j.scitotenv.2021.152700

Systemic. (n.d.). Liquid fraction digestate. https://systemicproject.eu/wp-content/uploads/Factsheet-product-liquid-fraction-digestate.pdf, last visit: 20/09/2023

UNI (n.d.). UNI 11759:2019. https://store.uni.com/uni-11759-2019, last visit: 04/10/2023

United Nations. (n.d.). GLOBAL ISSUES Population. https://www.un.org/en/global-issues/population, last visit: 01/08/2023

Vaneeckhaute, C., Meers, E., Michels, E., Buysse, J., Tack, F.M.G., 2013. Ecological and economic benefits of the application of bio-based mineral fertilizers in modern agriculture. Biomass and Bioenergy Volume 49, February 2013, Pages 239-248. https://doi.org/10.1016/j.biombioe.2012.12.036

Vaneeckhaute, C., Lebuf, V., Michels, E., Belia, E., Vanrolleghem, P.A., Tack, F.M.G., Meers, E., 2016. Nutrient Recovery from Digestate: Systematic Technology Review and Product Classification. Waste Biomass Valor 8, 21–40 (2017). https://doi.org/10.1007/s12649-016-9642-x

Wikipedia (2023). Densità dell'aria. https://it.wikipedia.org/wiki/Densit%C3%A0_dell%27aria#:~:text=Per%20convenzione%2C%20la%20densit%C3%A0%20dell,a%20circa%201%2C225%20kg%2Fm%C2%B3, last visit: 12/11/2023

Yang, D., Chen, Q., Liu, R., Song, L., Zhang, Y., Dai, X., 2022. Ammonia recovery from anaerobic digestate: State of the art, challenges and prospects. Bioresource Technology Volume 363, November 2022, 127957. https://doi.org/10.1016/j.biortech.2022.127957

Ye, Y., Ngo, H.H., Guo, W., Liu, Y., Chang, S.W., Nguyenb, D.D., Liangc, H., Wang, J., 2018. A critical review on ammonium recovery from wastewater for sustainable wastewater management. Bioresource Technology Volume 268, November 2018, Pages 749-758. https://doi.org/10.1016/j.biortech.2018.07.111

Zhao, Q.B., Ma, J., Zeb, I., Yu, L., Chen, S., Zheng, Y.M., Frear, C., 2015. Ammonia recovery from anaerobic digester effluent through direct aeration. Chemical Engineering Journal Volume 279, 1 November 2015, Pages 31-37. https://doi.org/10.1016/j.cej.2015.04.113

Un ringraziamento ad ETRA per la possibilità offertami di collaborare ad un progetto stimolante. In particolare, ad Omar Gatto e Paolo Franceschetti per avermi seguito e coinvolto durante i mesi di stage. Un grazie anche alla professoressa Elena Barbera, sempre disponibile con professionalità ed interesse a stimolarmi nella risoluzione di problemi talvolta complessi. Un pensiero speciale a mia mamma, senza la quale tutto questo non sarebbe possibile, e Laura, paziente supporter delle mie mille preoccupazioni. Ringrazio infine tutti i professori ed i miei compagni di viaggio di questi anni, per aver reso unico un percorso condito da gioie e soddisfazioni.